Mon. Not. R. Astron. Soc. **000**, 1–40 (2014) Printed 25 February 2015 (MN LATEX style file v2.2)

The soft γ-ray pulsar population: an high-energy overview

L. Kuiper[1⋆] and W. Hermsen [1,2⋆]
[1]*SRON-National Institute for Space Research, Sorbonnelaan 2, 3584 CA, Utrecht, The Netherlands*
[2]*Astronomical Institute "Anton Pannekoek", University of Amsterdam, Science Park 904, 1098 XH Amsterdam, The Netherlands*

arXiv:1502.06769v1 [astro-ph.HE] 24 Feb 2015

Accepted ..... Received 2014 December 11; in original form 2014 December 11

ABSTRACT

At high-energy γ-rays (> 100 MeV) the Large Area Telescope (LAT) on the *Fermi* satellite already detected more than 145 rotation-powered pulsars (RPPs), while the number of pulsars seen at soft γ-rays (20 keV - 30 MeV) remained small. We present a catalogue of 18 non-recycled RPPs from which presently non-thermal pulsed emission has been securely detected at soft γ-rays above 20 keV, and characterize their pulse profiles and energy spectra. For 14 of them we report new results, (re)analysing mainly data from *RXTE*, *INTEGRAL*, *XMM-Newton* and *Chandra*. The soft γ-pulsars are all fast rotators and on average $\sim 9.3\times$ younger and $\sim 43\times$ more energetic than the *Fermi* LAT sample. The majority (11 members) exhibits broad, structured single pulse profiles, and only 6 have double (or even multiple, Vela) pulses. Fifteen soft γ-ray pulsar show hard power-law spectra in the hard X-ray band and reach maximum luminosities typically in the MeV range. For only 7 of the 18 soft γ-ray pulsars pulsed emission has also been detected by the LAT, but 12 have a pulsar wind nebula (PWN) detected at TeV energies. For six pulsars with PWNe, we present also the spectra of the total emissions at hard X-rays, and for IGR J18490-0000, associated with HESS J1849-000 and PSR J1849-0001, we used our *Chandra* data to resolve and characterize the contributions from the point-source and PWN. Finally, we also discuss a sample of 15 pulsars which are candidates for future detection of pulsed soft γ-rays, given their characteristics at other wavelengths.

Key words: radiation mechanisms: non-thermal – stars: neutron – X-rays: general – gamma-rays: general – pulsars: individual: PSR J0205+6449, PSR B0531+21, PSR J0537-6910, PSR B0540-69, PSR B0833-45, IGR J14003-6326, PSR B1509-58, PSR J1617-5055, PSR J1640-4631, PSR J1811-1925, PSR J1813-1246, PSR J1813-1749, AX J1838.0-0655, PSR J1846-0258, IGR J18490-0000, PSR J1930+1852, PSR J2022+3842, PSR J2229+6114, PSR J1119-6127, PSR J1124-5916, PSR J1357-6429, PSR J1833-1034, PSR J1420-6048, PSR J1418-6058, PSR J1023-5746, PSR J1838-0537, PSR J1826-1256, PSR J1301-6305, PSR J1341-6220, PSR J1614-5048, PSR J1803-2137, PSR J1856+0245, IGR J11014-6103

1 INTRODUCTION

Rotation-powered pulsars (RPPs) form a well-established galactic γ-ray source population known to emit steadily from radio frequencies up to high-energy γ-rays. Despite decades of theoretical modeling the origin and nature of the non-thermal high-energy ($\gtrsim 10$ keV) emission are still being debated. The most developed models assume as production site of the high-energy emission either a location in the pulsar magnetosphere near (or starting near) the magnetic pole (polar cap models (Harding et al. 2005); slot gap models (Muslimov & Harding 2004; Dyks & Rudak 2003)) or in vacuum gaps along the last closed field lines in the outer magnetosphere (outer gap models (Cheng et al. 1986; Romani 1996; Cheng et al. 2000)), or even in the stripe of the pulsar wind outside the light cylinder radius (Pétri et al. 2012a). Modeling its emission characteristics (e.g. phase-resolved spectra, pulse morphology and polarization) drives ever-more sophisticated electrodynamic calculations (e.g. Wang & Hirotani 2011; Kalapotharakos et al. 2012a; Li et al. 2012; Pétri et al. 2012b; Hirotani 2015). Simulations have been performed for the different geometrical models to compute beaming patterns and light curves as a function of magnetic inclination angle and viewing direction, resulting in atlasses of gamma-ray profiles and radio lags (e.g. Watters et al. 2009; Romani & Watters 2010; Bai & Spitkovsky 2010a,b; Kalapotharakos et al. 2012b). These recent theoretical developents were driven by the major observational progress achieved by the Large Area Telescope (LAT; 20 MeV - 300 GeV) aboard the *Fermi* Gamma-ray Space Telescope, launched June 11, 2008. After more than four years of operations *Fermi* LAT had detected and characterized the pulsed emission (see e.g. Abdo et al. 2010a; Ray et al. 2011a; Abdo et al. 2013) of about 145 pulsars (status May 8, 2013), a significant fraction of these is γ-ray only i.e. Geminga-like with no obvious counter-

⋆ E-mail: L.M.Kuiper@sron.nl (LK); W.Hermsen@sron.nl (WH)

parts at other (less energetic) wavelengths regimes. This number can be compared with only seven pulsars securely detected above 100 MeV with EGRET on the preceding Compton Gamma-Ray Observatory (*CGRO*; April 5, 1991 – June 4, 2000).

The observational progress at softer γ-rays proceeded much slower. After the *CGRO* mission (till ~ 2005), at soft γ-rays above 20 keV up to ~ 30 MeV the pulsed signals from only four pulsars had been detected, hampered mainly by the intrinsic source weaknesses in this energy band with the relatively poorer sensitivities of the operational instruments. These were the Crab (PSR B0531+21) and the Vela (PSR B0833-45) pulsars, detected up to GeV energies, PSR B1509-58 in MSH 15-52, detected up to ~ 10 MeV, and the twin of the Crab pulsar in the Large Magellanic Cloud (LMC) PSR B0540-69 detected up to ~ 50 keV (see for references section 5).

Significant progress could be achieved in the hard X-ray/soft γ-ray band when the high-resolution imaging (*Chandra*) and large sensitive area X-ray observatories (*RXTE*, *XMM-Newton*, *Suzaku* and recently *NuSTAR*) became available, allowing the detections of weak energetic point-sources at soft/medium X-rays (0.1-10 keV) in young supernova remnants (SNRs), often discovered at radio-frequencies, or in location-error boxes of unidentified *CGRO* EGRET/*Fermi* LAT ($\gtrsim 100$ MeV), *INTEGRAL* ISGRI (20-300 keV) or H.E.S.S./VERITAS/MAGIC ($\gtrsim 30/100$ GeV) sources. In the X-ray band below ~ 10 keV, the instruments aboard these observatories were sufficiently sensitive to allow for the measurements of pulsar ephemerides, when there were no radio ephemerides available (many are radio-weak or even radio-quiet). For energies above 20 keV, the operational instruments were relatively insensitive, and could not detect independently the pulsed signals. But, once these timing solutions were determined at lower energies, phase folding of the event arrival times measured with *RXTE* PCA & HEXTE and *INTEGRAL* ISGRI in the hard X-ray band could be performed to search for and reveal the pulsed signals above 20 keV.

Currently, there are 18 pulsars for which pulsed emission has been detected in the soft γ-ray band above 20 keV up to $\sim 50-150$ keV. In this paper we present the catalogue of soft γ-ray pulsars, and for each entry an overview with the latest observational results. For 14 of them we present in this work new results, mainly from analyses of archival *RXTE* PCA & HEXTE and *INTEGRAL* ISGRI data for energies above 20 keV, but also from analyses of *XMM-Newton*, *Chandra* and *ASCA* data below 10 keV, or *CGRO* COMPTEL and BATSE data at MeV energies. For one pulsar and its nebula, the *INTEGRAL* source IGR J18490-0000/PSR J1849-0001 we present the results from our follow-up *Chandra* observations of this source together with new results from analyses of archival *XMM-Newton*, *RXTE* and *INTEGRAL* data.

The structure of the paper is as follows. Section 2 describes the *Fermi*LAT high-energy γ-ray pulsar population of which the hard non-thermal power-law spectra are expected to extrapolate into the soft gamma-ray band. We will therefore compare the average characteristics of the pulsars in the two catalogues in the discussion. Section 3 presents briefly the properties of the instruments used in this work, and section 4 briefly the timing-analysis methods. In section 5, a status review is given for each of the 18 pulsars with new results for 14 of them. Section 6 presents the observational status for very young ($\lesssim 15$ kyr) and energetic ($L_{sd} \gtrsim 10^{36}$ erg/cm^2 s) pulsars so far not detected at hard X-rays, but that are good candidates for future detections of pulsed soft γ-rays, given their characteristics at other wavelengths. Finally, in section 7 the results are summarized and discussed, including the above-mentioned comparison between the *Fermi*-LAT and soft γ-ray pulsar populations.

2 THE *Fermi*-LAT HIGH-ENERGY (> 100 MEV) GAMMA-RAY PULSAR POPULATION

The launch of *Fermi* heralded a new era in high-energy gamma-ray pulsar research. Analyzing the first three years of observations, Abdo et al. (2013) present the second *Fermi* LAT pulsar catalogue, listing 117 gamma-ray pulsars (an additional 28 were discovered by the LAT collaboration and other groups during the preparation of the catalogue). The 117 pulsars are categorized in three groups: radio-loud pulsars (number 42, obtained through pulse-phase folding using radio-ephemerides), radio-quiet pulsars (number 35, discovered at γ-energies through blind searches) and millisecond (i.e. recycled) pulsars (number 40). All have spin-down powers L_{sd} above 3×10^{33} erg/s, which seems to be a lower-limit for detectability as γ-ray (> 100 MeV) pulsar.

The recycled millisecond γ-ray pulsars are *not* addressed in this work, although some of the most energetic ($L_{sd} > 1 \times 10^{35}$ erg/s) ones like PSR J0218+4232, PSR B1937+21 and PSR B1821-24, have been detected earlier as hard X-ray pulsars with *pulsed* emission detected up to 20–30 keV (Kuiper et al. 2003a, 2004).

Of the 77 $(= 42 + 35)$ young/middle-aged ($\tau_c \lesssim 4 \times 10^6$ y) non-recycled pulsars, 58 ($\sim 75\%$) show at high-energy γ-rays pulse profiles with two strong, well separated, caustic peaks, with often significant bridge emission. The radio phase lag δ between the γ-ray leading pulse and the radio main pulse (often fiducial point) and the γ-ray peak separation Δ show a strong anti-correlation, being a predicted general property of outer-magnetosphere models with caustic pulses (see e.g. Fig. 3 of Romani & Yadigaroglu 1995). On average the γ-ray peak separation is in the 0.4–0.5 range (about half a rotation), while the radio lag distribution reaches its maximum in the 0.15 - 0.25 range.

In the spectral domain the pulsed emission of the young/middle-aged γ-ray pulsars can well be represented by a power law model in combination with a simple exponential cutoff , i.e. $F_\gamma = k \cdot (E_\gamma/E_0)^\Gamma \cdot \exp(-(E_\gamma/E_c)^\beta)$ with $\beta \equiv 1$ and E_γ, the photon energy, E_0, the pivot energy minimizing the co-variance between the parameters, Γ, the photon index, E_c, the cutoff energy and k the normalization.

Outer-gap and slot-gap models predict the production of γ-rays at high altitudes in the magnetosphere with such a simple exponential cut-off ($\beta \sim 1$), while in polar cap models the production occurs near the magnetic poles with a sharp hyper-exponential turn over ($\beta \sim 2$) of the spectrum at high energies. The *Fermi* spectral results thus disfavours the polar-cap models (see e.g. the detailed discussions of the fits to the Vela pulsar spectrum (Abdo et al. 2009c) and the Crab pulsar spectrum (Abdo et al. 2010c)).

The cutoff energies E_c are on average in the 1–3 GeV range, while the photon index distribution peaks in the -1.8 – -1.3 range.

Abdo et al. (2013) also considered the properties of the LAT detected pulsars in the soft X-ray band (0.3–10 keV). Though the X-ray coverage is rather uneven, with the newly discovered LAT pulsars having often only snapshots observations with *Swift* XRT, while deep observations with *Chandra* and/or *XMM-Newton* exist for the well-know gamma-ray pulsars, all LAT pulsars do have X-ray coverage. Of the 77 young/middle-aged LAT pulsars 49 (30 radio-loud; 19 radio-quiet) have an X-ray counterpart with a non-thermal (i.e. flagged with a power law) spectral component obtained through model fitting in terms of a power-law in combination

with one (or even two) blackbody(ies). The X-ray counterpart association was established either through the detection of X-ray pulsations or positional coincidence with accurately determined radio- or LAT timing positions.

For only 21[1] of the young/middle-aged LAT pulsars the *pulsed* fingerprints are detected in the canonical X-ray band (< 10 keV).

3 INSTRUMENTS

In this section we discuss briefly the general characteristics of the instruments aboard *RXTE*, *INTEGRAL*, *XMM-Newton* and *Chandra*, that we extensively used in this work to obtain new results on the (hard) X-ray/soft γ-ray properties of the pulsar sample presented in this paper. For the Vela pulsar (PSR B0833-45) and PSR B1509-58 we obtained new pulse profiles analysing archival *CGRO* COMPTEL 0.75–30 MeV and *CGRO* BATSE 317–1102 keV data, respectively, from observations covering the full *CGRO* mission lifetime. For PSR J2229+6114 archival *ASCA* GIS data were analysed to obtain new pulse profiles and a new spectrum for the pulsed emission. For the latter instruments references are given in those sections where data from these instruments are analysed by us.

3.1 Rossi X-ray Timing Explorer (*RXTE*)

In this work extensive use has been made of data from observations of rotation powered pulsars with the two *non-imaging* X-ray instruments aboard *RXTE*, the Proportional Counter Array (PCA; 2-60 keV) and the High Energy X-ray Timing Experiment (HEXTE; 15-250 keV).

3.1.1 RXTE PCA

The PCA (Jahoda et al. 1996) consisted of five collimated Xenon proportional counter units (PCUs) with a total effective area of $\sim$ 6500 cm^2 over a $\sim 1^\circ$ (FWHM) field of view. Each PCU had a front Propane anti-coincidence layer and three Xenon layers which provided the basic scientific data, and was sensitive to photons with energies in the range 2-60 keV. The energy resolution was about 18% at 6 keV. All PCA data used in this study have been collected from observations in `GoodXenon` mode allowing high-time resolution (0.9μs) analyses in 256 spectral bins. Since the launch of *RXTE* on Dec. 30, 1995 the PCA has experienced high voltage breakdowns for all constituting PCUs at irregular times. To reduce further breakdowns during its mission, which ended on Jan. 5, 2012, not all PCUs were simultaneously operating. The most stable PCU was PCU-2, which was on for almost all of the time. On average one (50%) or two (40%) PCUs was/were operational during a typical observation.

[1] Table 15 of Abdo et al. (2013) labeled 13 LAT pulsars with "P" (Pulsed X-ray emission detected), omitting by mistake this label for PSR B1509-58 (PSR J1513-5908, Seward & Harnden (1982)) and PSR J2021+3651 (Hessels et al. 2004), while pulsed X-ray emission has been detected for 6 LAT pulsars; PSR J1459-6053 (Pancrazi et al. 2012), PSR J2021+4026 (Lin et al. 2013), PSR J1741-2054 (Marelli et al. 2014), PSR J1813-1246 (Marelli et al. 2014b), PSR J1836+5925 (Arumugasamy et al. 2014b; Lin et al. 2014) and PSR B0540-69 (Martin et al. 2014) after the publication of the catalogue.

3.1.2 RXTE HEXTE

The HEXTE instrument (Rothschild et al. 1998) consisted of two independent detector clusters A& B, each containing four Na(Tl)/CsI(Na) scintillation detectors. The HEXTE detectors were mechanically collimated to a $\sim 1^\circ$ (FWHM) field of view and covered the 15-250 keV energy range with an energy resolution of $\sim$ 15% at 60 keV. The collecting area was 1400 cm^2 taking into account the loss of the spectral capabilities of one of the detectors. The maximum time resolution of the tagged events was 7.6μs. In its default operation mode the field of view of each cluster was switched on and off source to provide instantaneous background measurements. However, also HEXTE suffered from aging, and since July 13, 2006 HEXTE cluster-A operated in staring mode at an on-source position, while on March 29, 2010 cluster-B was commanded to stare at an off-source position. Due to the co-alignment of HEXTE and the PCA, celestial targets have been observed simultaneously.

3.2 *INTEGRAL*

The *INTEGRAL* spacecraft (Winkler et al. 2003), launched 17 October 2002, carries two main γ-ray instruments: a high-angular-resolution imager IBIS (Ubertini et al. 2003) and a high-energy-resolution spectrometer SPI (Vedrenne et al. 2003). The payload is further equiped with an X-ray monitoring instrument, the Joint European Monitor for X-rays (JEM-X; Lund et al. 2003) providing complementary observations in the X-ray band. These three high-energy instruments make use of coded aperture masks enabling image reconstruction in the hard X-ray/soft γ-ray band.

In this work, guided by sensitivity considerations, we only used data recorded by the *INTEGRAL* Soft Gamma-Ray Imager ISGRI (Lebrun et al. 2003), the upper detector system of IBIS, sensitive to photons with energies in the range $\sim$15 keV – 1 MeV (effectively about 300 keV).

With an angular resolution of about $12'$ and a source location accuracy of better than $1'$ (for a $> 10\sigma$ source) ISGRI is able to locate and separate high-energy sources in crowded fields within its $19^\circ \times 19^\circ$ field of view (50% partially coded) with an unprecedented sensitivity ($\sim$ 960 cm^2 at 50 keV). Its energy resolution of about 7% at 100 keV is amply sufficient to determine the (continuum) spectral properties of hard X-ray sources in the $\sim$ 20 - 300 keV energy band.

The timing accuracy of the ISGRI time stamps recorded on board is about 61μs. The time alignment between *INTEGRAL* and *RXTE* is better than $\sim 50\mu$s, verified using data from simultaneous *RXTE* and *INTEGRAL* observations of the accretion-powered millisecond pulsars IGR J00291+5934 and IGR J17511-3057 (Falanga et al. 2005, 2011, respectively).

3.3 *XMM-Newton*

XMM-Newton launched Dec. 10, 1999, carries three different Wolter type-1 multi-shell grazing incidence mirrors focusing X-rays to different X-ray instruments. One of the telescopes focusses the X-rays directly on an EPIC pn type CCD camera, while the other two telescopes have reflection grating arrays (RGA) in their light paths dispersing by reflection about 40% of the incoming X-ray radiation to a linear strip of CCDs (RGS detector) at their secondary foci, while about 44% of the incoming X-ray radiation passes to the prime foci onto MOS type CCD cameras. With

the EPIC cameras very sensitive imaging observations can be performed over a $30'$ (diameter) field of view across the 0.15-12 keV band with a spectral resolution ($E/\Delta E$) of 20–50 and angular resolution of $\sim 6\farcs6$ (FWHM).

In this work we only used data collected by the EPIC pn instrument (Strüder et al. 2001), consisting of 12 back-illuminated CCDs, because the operation modes of this CCD camera are well suited for accurate studies of timing phenomena occuring at milli second scales. In particular, the Small window mode offers a fast read-out/frame time of about 5.67 ms, amply sufficient for most of the soft γ-pulsars studied in this work, while imaging information is kept only for the central CCD number 4 in a frame of 63×64 pixels of $4\farcs1 \times 4\farcs1$ size each offering thus a $4\farcm3 \times 4\farcm37$ field of view.

For one pulsar in our sample, PSR J0537-6910, we analyzed the EPIC pn data collected in timing mode, in which the time stamps are registered at a $\sim 30\mu$s resolution, while one-dimensional imaging information is conserved. The other pulsars for which we analyzed *XMM-Newton* EPIC pn data were PSR J0205+6449, PSR B0833-45, PSR J1813-1246, PSR J1813-1749 and IGR J18490-0000, and in these cases the data were taken in Small window mode.

3.4 *Chandra*

The *Chandra* X-ray Observatory CXO (Weisskopf et al. 2000) was launched on July 23, 1999, and combines a sub-arcsecond resolution X-ray telescope with advanced imaging and spectroscopic instruments in the focal plane of the High Resolution Mirror Assembly (HRMA), which is composed of a nested set of four Wolter type-1 grazing-incidence X-ray mirror pairs with an outer diameter of 1.2 m and focal length of 10 m. Within the optical path (between the HRMA and focal plane instruments) two different types of grating assemblies, the High-Energy Transmission Grating (HETG) - comprised of a High Energy Grating (HEG) and Medium Energy Grating (MEG) on a single structure - and the Low Energy Transmission Grating (LETG), can be placed mechanically on command.

The Science Instrument Module (SIM) at the focal plane houses two instruments, the Advanced CCD Imaging Spectrometer (ACIS) and High Resolution Camera (HRC).

The ACIS instrument (Garmire et al. 2003) contains 10 planar, 1024×1024 pixels (pixel scale is $0\farcs4920 \pm 0\farcs0001$) CCDs of which 4 are arranged in a 2×2 array ($16\farcm9 \times 16\farcm9$ field of view) for imaging purposes (ACIS-I) and the other 6 in a 1×6 array ($8\farcm3 \times 50\farcm6$ field of view) serving either as grating readout or as imaging detector (ACIS-S; containing two back-illuminated CCDs).

The energy resolving power ($E/\Delta E$) is moderate and depends on the CCD type (front or back-illuminated), is energy and time (Charge Transfer Inefficiency) dependent, and is in the range $\sim$10–60 for the FI CCDs and $\sim$4–45 for the BI CCDs. The BI type CCDs ($\sim$ 0.18-10 keV) have higher effective area at lower energies than the FI type CCDs ($\sim$0.48-10 keV). The effective area reaches a maximum of about 600 cm^2 at 1.4 keV for the FI CCDs. The nominal frame time in Timed Exposure (TE) mode is 3.2 s with a 40.96 ms read-out time. This relatively long integration time can cause pile-up (more than one event registered in a pixel during a frame time) effects even for moderate count rates.

Although in TE mode other frame times are possible using subarray read-outs, the default TE mode is not suitable for pulsar timing studies at millisecond time scales, but it is very useful to obtain sub-arcsecond (energy resolved) images of the pulsar environment. The other operation mode of the ACIS is Continuous Clocking (CC). In this mode the integration time is 2.85 ms, and this is reached at the expense of spatial information in one direction.

The other focal plane instrument is the HRC (Murray et al. 2000), which is comprised of two multichannel plate imaging detectors: the HRC-I offering wide-field imaging ($30' \times 30'$ field of view with $0\farcs13175$/pixel), and the HRC-S serving mainly as read-out for the LETG. The HRC detectors do not/hardly have energy resolving power. Due to a wiring problem the time resolution of the HRC-I/S detector is governed by the actual count rate and is much worse than the anticipated resolution of about 16 μs. However, the central segment of the HRC-S ($6' \times 30'$ field of view) can be operated in a special mode, designed for accurate timing studies, in which the original 16 μs time resolution can be recovered.

In this work we present (PI-obtained) *Chandra* data for IGR J18490-0000 from two 25 ks observations, one with the HRC-S in timing mode and one with the ACIS-S. Moreover, we have estimated the genuine pulsed fraction of PSR J1617-5055 using *Chandra* HRC-S timing mode data.

4 ANALYSIS METHODS

In the analysis of the high-energy data from the non-imaging *RXTE* instruments PCA and HEXTE, the coded-mask imager ISGRI aboard *INTEGRAL* and the X-ray telescopes aboard *Chandra* and *XMM-Newton* some common analysis procedures exist. To obtain pulsed flux measurements accurate timing models (ephemerides) are required describing every revolution of the neutron star accurately. These so-called phase coherent ephemerides are mainly based, in this work, on Time-of-Arrival (ToA) determinations of a pulse template using *RXTE* PCA data, and are listed in Table 1 for a limited set of soft γ-ray pulsars, for which *RXTE* PCA monitoring observations exist. The method to obtain accurate timing models is extensively described in Sect. 4.1 of Kuiper & Hermsen (2009).

Irrespective of the high-energy instrument with which the data have been collected a typical timing analysis consists of 1) data selection using e.g. the HEASARC browse interface for *RXTE*, *XMM-Newton* and *Chandra* observations fulfilling the source search criteria or the browse facility at the ISDC for *INTEGRAL* data, 2) screening the data by creating good-time intervals (GTI), 3) barycentering the event time tags using the instantaneous spacecraft ephemeris (position and velocity) information, the JPL solar system ephemeris information (DE200/DE405) and an accurate source position to convert the times from Terrestial Time scale (TT or TDT, which differs from Coordinated Universal Time (UTC) by a number of leap seconds and a fixed offset of 32.184 s) into Barycentric Dynamical Time (TDB) scale, a time standard for Solar system ephemerides.

Subsequently, the TDB time tags are converted to pulse phases (see formula (1) in Sect. 3.4 of Kuiper et al. 2010) adopting appropriate timing models (phase folding). Next, the events are sorted on pulse phase and energy to obtain 2d event distributions, storing thus pulse profiles for any energy band covering the passband of the involved instrument. The detection of a pulsed signal is expressed in a number of σ's applying the Z_n^2 test described in Buccheri et al. (1983). Typical timing analyses of *RXTE* PCA, HEXTE, *XMM-Newton* and *INTEGRAL* ISGRI data are described in Sect. 3.1, Sect. 3.7 and Sect. 3.8 of Kuiper et al. (2010) and Sect. 4.3 of Kuiper & Hermsen (2009), respectively. A typical timing analysis for *Chandra* HRC data is given in Sect. 4 of Kuiper et al. (2002) and Sect. 5.15 of this work.

From the pulse-phase distributions per energy band we derived the number of pulsed excess counts by fitting with (a) pulse profile template(s) or a truncated Fourier series. The pulsed fluxes were obtained by applying forward folding spectral fitting procedures taking into account the instrument spectral response, effective area, exposure time and absorption in the interstellar medium. This is explained for example in Sect. 5 of Kuiper & Hermsen (2009) for PCA, HEXTE and ISGRI data. For *XMM-Newton* (see e.g. Sect. 4 of Kuiper et al. 2010) and *Chandra* equivalent procedures exist.

5 THE SOFT γ-RAY PULSAR POPULATION

5.1 PSR J0205+6449

PSR J0205+6449 is a young ($\tau \sim 5.4$ kyr) 65 ms pulsar located near the center of super nova remnant/pulsar wind nebula 3C58 with a spin-down luminosity of 2.7×10^{37} erg/s. Its pulsation was discovered in the X-ray band using *Chandra* data and confirmed using *RXTE* PCA data (Murray et al. 2002), and its weak pulsed signal was later detected at radio frequencies.

At TeV-energies (> 300 GeV) VERITAS did not (yet) detect emission from the sky region including 3C58, yielding a 99% flux upper-limit of about 2% of the Crab nebula (Humensky et al. 2009). However, the upgraded stereoscopic MAGIC telescope detected 3C58 as unresolved source at a 5.7σ level with an integral flux above 1 TeV of about 0.65% of the Crab (Aleksić et al. 2014b).

Detailed timing studies in the X-ray and radio-bands have been performed by both Livingstone et al. (2009) and Kuiper et al. (2010). The X-ray pulse profile shows two sharp peaks separated in phase by 0.488 ± 0.002 with the main peak lagging the single radio pulse by 0.089 in phase. The pulsed X-ray/soft γ-ray spectrum over the energy band 0.56-267.5 keV (based on *XMM-Newton* EPIC-pn, *RXTE* PCA and HEXTE measurements) for the sum of the two pulses is very hard with photon index -1.03 ± 0.02 (Kuiper et al. 2010). No difference in spectral shape is found for the two pulses in the X-ray/soft γ-ray band. High-energy γ-ray pulsations (> 100 MeV) from PSR J0205+6449 have been detected using *Fermi* LAT data (Abdo et al. 2009a). The γ-ray lightcurve (> 100 MeV) shows also two pulses, aligned with the X-ray pulses, but now the strongest γ-ray pulse coincides with the weakest X-ray pulse, indicating different spectral behaviours of the two pulses when considering the full 0.5 keV to 10 GeV band. For more detailed information about the high-energy characteristics of the pulsed emission we refer to Kuiper et al. (2010) and Abdo et al. (2009a).

5.2 The Crab pulsar, PSR B0531+21 / PSR J0534+2200

The 33 ms pulsar, PSR B0531+21 or PSR J0534+2200, in the Crab nebula (3C 144; NGC 1952; CTB 18) was discovered in 1968 by Staelin & Reifenstein (1968). Since its detection at radio-frequencies the pulsed fingerprint of PSR B0531+21 has been detected across the full electro-magnetic spectrum from radio, optical/infra-red, soft X-rays (0.1-2 keV), hard X-rays (2-20 keV), soft γ-rays (20-500 keV), medium-energy γ-rays (0.5 MeV - 30 MeV, see e.g. Kuiper et al. 2001, for a high-energy picture from soft X-rays up to high-energy γ-rays), high-energy γ-rays (30 MeV - 100 GeV, see e.g. Abdo et al. 2010c) and recently even at TeV energies (> 0.1 TeV, see e.g. Aliu et al. 2008; Aleksić et al. 2011, 2014a; Aliu et al. 2011).

An intriguing feature of its pulsed emission is that the double-peaked pulse-profile with a peak separation of about 0.4 (in phase) keeps its identity and preserves its alignment approximately (the X-ray/γ-ray main pulse preceeds the radio main pulse by about 300μs) across the electro-magnetic spectrum (see e.g. Fig. 6 of Kuiper et al. 2003), though the relative intensities of the two pulses vary.

The total emission of the Crab (nebula and pulsar) has long time served as flux/spectral calibration target for various instruments because of its detectability across the 'full' electro-magnetic spectrum and its stability over time. The latter property has been abandoned recently by the discovery of considerable variations in the hard X-ray/soft γ-ray band (Wilson-Hodge et al. 2011) and flaring activity at high-energy γ-rays (Tavani et al. 2011; Abdo et al. 2011). Contrarily, the pulsed emission of PSR B0531+21 as seen by *RXTE* PCA (3.2-35 keV) seems rather stable and decreases steadily consistent with the pulsar spin-down (Wilson-Hodge et al. 2011).

The high-energy spectrum of the pulsed emission of PSR B0531+21 across 8 decades in energy from soft X-rays up to high-energy γ-rays is shown in the multi-source spectral compilation depicted in Fig. 28 as red-coloured datapoints. Data from *CGRO* OSSE, COMPTEL and EGRET, *BeppoSAX* LECS, MECS and PDS and the balloon-borne GRIS instruments are included (see Kuiper et al. 2001, for more details), supplemented by *RXTE* PCA (5-50 keV, `E_250us_128M_14_1s` event mode; this work) and HEXTE ($\sim$ 13-235 keV; this work) pulsed flux measurements. The HEXTE data have been collected during observation run 40805 covering the time periods March 17–31, 1999 and December 18–19, 1999, for an effective deadtime corrected ON source time of 22.7 ks and 23.8 ks for cluster A and B, respectively. Also included in Fig. 28 is the model spectrum of the pulsed emission (100 MeV – 10 GeV) as obtained by Abdo et al. (2010c) using *Fermi* LAT data. Maximum pulsed flux is reached near 100 keV, while beyond 30 MeV a flattening occurs, followed beyond $\sim$ 10 GeV by a power-law like decay, detected up to about 400 GeV by the VERITAS TeV telescope (Aliu et al. 2011).

The (unabsorbed; using a N_H of 3.61×10^{21} cm^{-2}) 2–10 keV, 20–100 keV, 1–10 MeV and 0.1–1 GeV pulsed fluxes for the Crab pulsar are $(1.948 \pm 0.005) \cdot 10^{-9}$, $(2.766 \pm 0.008) \cdot 10^{-9}$, $(1.36 \pm 0.05) \cdot 10^{-9}$ and $(7.87 \pm 0.28) \cdot 10^{-10}$ erg/cm^{2}s, respectively, derived from *RXTE* PCA/HEXTE data (2–10 and 20–100 keV, this work), *CGRO* COMPTEL (see e.g. Kuiper et al. 2001, from the pulsed flux measurements reported in that work we derived the 1–10 MeV pulsed flux value) and *Fermi* LAT (flux value derived from the spectral parameters and their 1σ statistical errors as given in Sect. 4.3 of Abdo et al. 2010c).

5.3 PSR J0537-6910

Marshall et al. (1998a,b) reported the discovery of a young ($\tau \sim 4.9$ kyr) fast 16 ms pulsar in LMC supernova remnant N157B (NGC 2060) using *RXTE* PCA data taken from 2 observation runs in 1996 centered on the nearby SN 1987A and archival *ASCA* GIS observations to pin down its location and derive its spin-down. So far, PSR J0537-6910 is the fastest and most energetic ($\dot{E} \sim 4.9 \times 10^{39}$ erg/s) non-recycled spin-down powered pulsar. The pulsed signal was also found in archival *BeppoSAX* MECS (2–10 keV; Cusumano et al. 1998a,b) and *ROSAT* HRI data (0.1–2.4 keV; Wang & Gotthelf 1998), and in follow-up *Chandra* HRC-S data (Wang et al. 2001).

On January 19, 1999 an intensive *RXTE* monitoring (observation id. 40139) of PSR J0537-6910 commenced, which ended with

Table 1. Phase-coherent ephemerides, derived in this work, for the subset of soft γ-ray pulsars for which *RXTE* PCA monitoring data exist.

Pulsar #	Start [MJD]	End [MJD]	t_0, Epoch [MJD,TDB]	ν [Hz]	$\dot{\nu}$ $\times 10^{-11}$ Hz/s	$\ddot{\nu}$ $\times 10^{-22}$ Hz/s^2	Validity range (days)
PSR J0537-6910	51197	51263	51237.0	62.0402460583(64)	-19.9221(2)	99(40)	67
PSR J0537-6910	51294	51423	51366.0	62.0380675984(19)	-19.92497(3)	84(5)	130
PSR J0537-6910	51422	51547	51480.0	62.0361053238(9)	-19.92024(2)	46(6)	126
PSR J0537-6910	51576	51706	51628.0	62.0335856000(14)	-19.92746(3)	72(3)	131
PSR J0537-6910	51715	51786	51761.0	62.0313152172(24)	-19.9279(1)	248(16)	72
PSR J0537-6910	51795	51818	51795.0	62.03072978(2)	-19.920(2)	0.0	24
PSR J0537-6910	51833	51875	51833.0	62.0300843300(32)	-19.9294(2)	0.0	43
PSR J0537-6910	51886	51955	51886.0	62.02918045(1)	-19.9357(8)	276(30)	70
PSR J0537-6910	51964	51996	51964.0	62.0278657375(87)	-19.9354(7)	0.0	33
PSR J0537-6910	51997	52145	52049.0	62.0264019706(14)	-19.92818(3)	63(2)	149
PSR J0537-6910	52132	52166	52132.0	62.0249729876(73)	-19.9153(6)	0.0	35
PSR J0537-6910	52175	52230	52175.0	62.0242443562(98)	-19.9364(9)	167(38)	56
PSR J0537-6910†	52252	52368	52252.0	62.0229447197(59)	-19.9342(2)	68(5)	117
PSR J0537-6910	52389	52446	52389.0	62.02059598(1)	-19.936(1)	134(56)	58
PSR J0537-6910	52459	52540	52459.0	62.019403934(12)	-19.9359(7)	103(22)	82
PSR J0537-6910	52551	52648	52551.0	62.0178456346(56)	-19.9374(3)	94(7)	98
PSR J0537-6910	52647	52718	52647.0	62.016192268(14)	-19.9327(9)	148(29)	72
PSR J0537-6910	52745	52792	52745.0	62.0145138255(43)	-19.9360(3)	0.0	48
PSR J0537-6910	52822	52884	52822.0	62.013203356(14)	-19.9401(9)	141(36)	63
PSR J0537-6910	52889	53008	52889.0	62.0120638182(43)	-19.9409(2)	132(3)	120
PSR J0537-6910	53019	53122	53019.0	62.0098457965(56)	-19.9405(3)	95(7)	104
PSR J0537-6910	53128	53143	53128.0	62.007969319(34)	-19.939(6)	0.0	16
PSR J0537-6910	53147	53285	53147.0	62.0076662548(52)	-19.9426(2)	95(3)	139
PSR J0537-6910	53290	53366	53290.0	62.005227527(14)	-19.9488(8)	240(29)	77
PSR J0537-6910	53365	53444	53365.0	62.003935314(18)	-19.9404(9)	192(30)	80
PSR J0537-6910	53446	53549	53446.0	62.002556305(10)	-19.9471(4)	165(10)	104
PSR J0537-6910	53551	53682	53609.0	61.9997679030(28)	-19.94013(3)	106(5)	132
PSR J0537-6910	53710	53860	53792.0	61.9966405925(17)	-19.93914(2)	83(3)	151
PSR J0537-6910	53862	53947	53862.0	61.995449381(11)	-19.9510(5)	230(17)	86
PSR J0537-6910	53952	53996	53952.0	61.993899826(27)	-19.945(3)	531(154)	45
PSR J1811-1925	52341	52541	52341.0	15.4612089999(14)	-1.056106(19)	0.0	201
PSR J1811-1925	52595	52904	52595.0	15.4609772117(10)	-1.056411(9)	0.0	310
PSR J1811-1925	52904	53333	52904.0	15.4606951476(22)	-1.056670(25)	-2.03(15)	430
AX J1838.0-0655	54513	55002	54513.0	14.1847581888(11)	-0.992954(11)	1.95(6)	488
AX J1838.0-0655	55038	55537	55136.0	14.1842449934(1)	-0.999054(6)	3.8(1.2)	497
IGR J18490-0000	55525	55545	55526.0	25.961259794(16)	-0.961(2)	0.0	19
PSR J1930+1852	52529	52633	52529.0	7.30613850(9)	-4.008(2)	0.0	104
PSR J2022+3842	55223	55232	55223.0	20.58651709(2)	-3.649(6)	0.0	10

†This entry has been used for *XMM-Newton* EPIC-pn observation 0113020201 in timing mode

cessation of the *RXTE* mission in early January 2012, aimed at following its timing behaviour with time. Analyzing the first 2.6 years of this monitoring campaign resulted in a glitch rate of 2.3 per year, the highest seen for any pulsar (Marshall et al. 2004). An update on this work was provided by Middleditch et al. (2006) analyzing 7.6 years of *RXTE* monitoring data, and finding 23 glitches at a rate of 3.3 per year. The latter authors found a correlation between the time interval between two glitches and the amplitude of the first glitch (of the interval), yielding a prediction of these intervals with an accuracy of a few days.

While its timing characteristics have been studied intensively, the high-energy spectral characteristics of PSR J0537-6910 are poorly determined. Therefore, we invoked the huge *RXTE* data archive on PSR J0537-6910 to establish its high-energy spectral characteristics. For this purpose we used a (slightly larger) dataset than Middleditch et al. (2006) and revisited their analyses to obtain the alignment for each of the 24 timing segments enabling us to co-add the pulse profiles for each of the 24 timing segments directly (Note: this alignment information is not given in Middleditch et al. 2006)[2].

We started with the derivation of ToA's for all observations between Jan. 19, 1999 and Oct. 5, 2006 (time span MJD 51197 – 53996; 7.7 years). From these ToA's we determined in a consistent way phase coherent timing models, which are in good agreement with those obtained by Middleditch et al. (2006) and are listed in Table 1. Across this period we found 24 glitches of which 23 have been reported on by Middleditch et al. (2006), resulting in 24 timing segments for which phase coherent solutions (all with proper alignment) have been derived.

[2] Analyzing the full *RXTE* database on PSR J0537-6910 is outside the scope of this paper, but work on this, in particular to derive the characteristics for all the glitches across the full *RXTE* data period, is in progress.

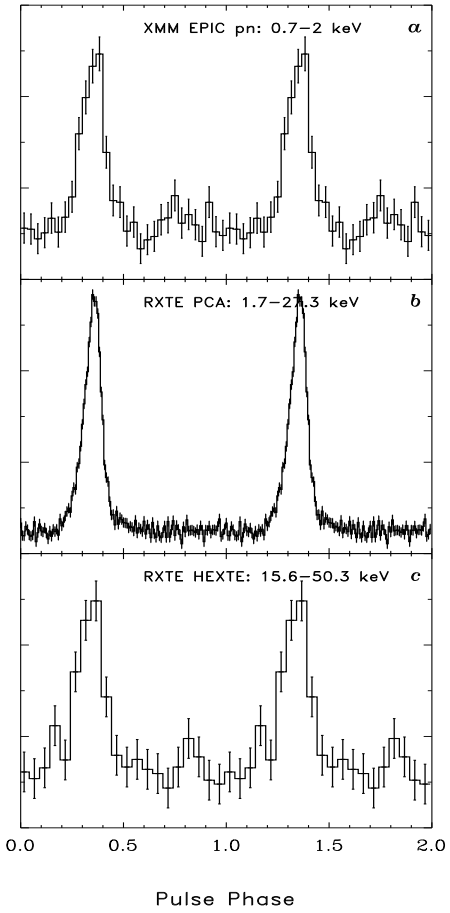

Figure 1. PSR J0537-6910; pulse profiles for *XMM-Newton* EPIC pn (0.7-2 keV; panel a), *RXTE* PCA (1.7-27.3 keV; panel b) and *RXTE* HEXTE (15.6-50.3 keV; panel c). Pulsed emission has been significantly detected up to ~ 50 keV.

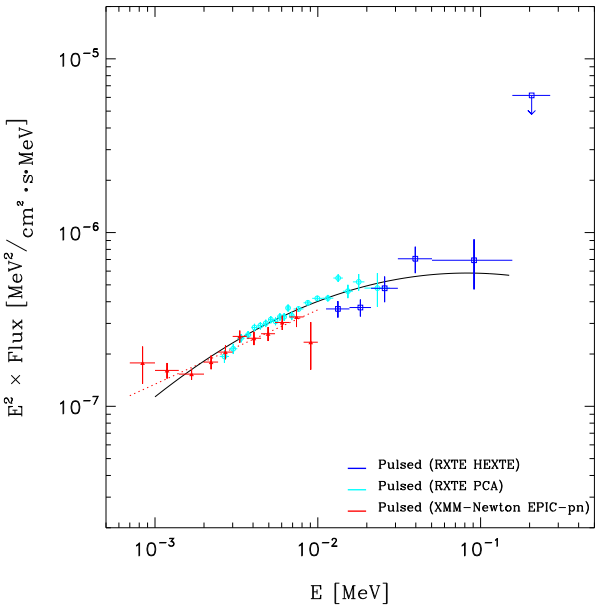

Figure 2. PSR J0537-6910; high-energy (0.7-250 keV) unabsorbed pulsed spectrum as derived from measurements by *XMM-Newton* EPIC-pn (0.7-10 keV; red), *RXTE* PCA (2.5-30 keV; aqua) and *RXTE* HEXTE (15-250 keV; blue). The best fit model ("curved" power-law) to all these pulsed flux measurements is superposed as solid black line. The red dotted line represents the best power-law fit model to solely EPIC-pn flux measurements.

Subsequent pulse-phase folding of PCA events (from all detector layers), screened according to standard criteria and removing break-down periods of the detector units, yielded high-statistics 2 dimensional event distributions sorted on pulse-phase and energy (PHA). In Fig. 1 panel b the 120 bin 1.7–27.3 keV profile is shown, analyzing PCA data from time segments 1–18, which provides us already with very high pulsed-signal statistics. Similar procedures for HEXTE yielded, now analyzing all 24 segments given the poor pulsed-signal statistics contrary to the PCA case, a $\sim 10\sigma$ pulsed signal for the 15.6-50.3 keV band (see Fig. 1 panel c), and even a 5.2σ signal for the 31.0-50.3 keV band, establishing PSR J0537-6910 as a soft γ-ray pulsar. Indications for pulsed emission were found for energies above 50 keV.

In order to determine the timing characteristics of PSR J0537-6910 below ~ 2 keV we also analyzed EPIC pn timing mode data from a 35.9 ks *XMM-Newton* observation (obs. id. 0113020201) performed on November 19, 2001 (data period MJD 52232.949 - 52233.366). Default screening and optimizing on the RAWX event parameter by allowing only events with RAWX in the range $[26, 42]$ yielded highly significant pulse profiles after phase folding using the PSR J0537-6910 ephemeris entry with epoch MJD 52252 (see Table 1)[3]. The resulting 0.7-2 keV *XMM-Newton* EPIC pn pulse profile is shown in Fig.1 panel a, and the deviation from uniformity is about 16.4σ applying a Z_5^2-test.

In order to derive the pulsed spectrum of PSR J0537-6910 we fitted a model composed of a (flat) background component and a component describing the shape of the single pulse, as derived from the high-statistics *RXTE* PCA profile, to the pulse profiles of any of the energy bands in the band width of *XMM-Newton* EPIC pn, *RXTE* PCA and HEXTE. The resulting pulsed excess counts are converted to pulsed fluxes in a forward folding procedure assuming an underlying (photon) power-law model and adopting interstellar absorption under a column of N_H of 7×10^{21} cm^{-2} (see e.g. Table 4 of Townsley et al. 2006, for X-ray spectroscopic information of some sources in the 30 Doradus region, including PSR J0537-6910 and SNR N157B, using *Chandra* ACIS data).

In Fig. 2 the pulsed flux measurements across the 0.7-250 keV band are shown for *XMM-Newton* EPIC pn (red data points), *RXTE* PCA (aqua) and *RXTE* HEXTE (blue) along with fits to solely EPIC-pn data (power-law model; red dotted line; 0.7-10 keV) and to all data ("curved" power-law; black solid line; 0.7-250 keV). The later model provides a 4.3σ improvement over a simple power-law model fit considering the full dataset, and thus proves the necessity of a gradually breaking spectrum. The unabsorbed pulsed flux in the 2–10 keV band for the "curved" PL-model is $(7.42 \pm 0.26) \times 10^{-13}$ erg/cm^{2}s, about 10% higher than the 2–10 keV flux of $(6.72 \pm 0.38) \times 10^{-13}$ erg/cm^{2}s derived from the PL-fit using solely EPIC-pn data (the photon index was -1.57 ± 0.03 in this case). Both values are, however, consistent with the value of

[3] Middleditch et al. (2006) reported a glitch (#8 in their table 4) occuring at MJD 52241.6 ± 7.8, however, the *XMM-Newton* data can still be correctly described by the post-glitch ephemeris entry and *not* with the pre-glitch ephemeris, indicating that the glitch must have occured somewhere between MJD 52230 (the end time of the pre-glitch ephemeris) and MJD 52232.949, the start time of the *XMM-Newton* observation.

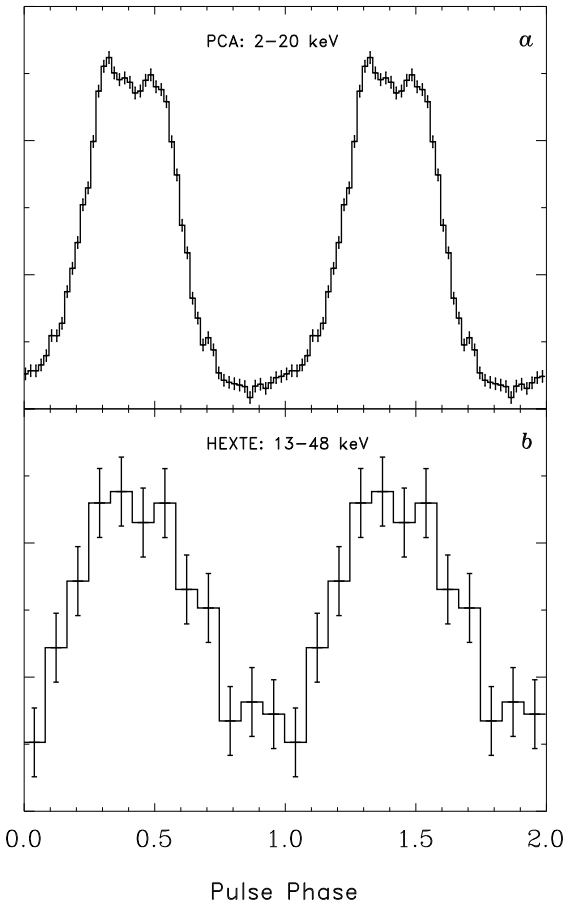

Figure 3. PSR B0540-69; pulse profile (broad single-pulse with a dip in the middle) for the 2–20 keV band as measured by *RXTE* PCA (upper panel) combining about 700 ks of effective exposure time (see de Plaa et al. 2003). In the lower panel the *RXTE* HEXTE lightcurve of PSR B0540-69 is shown for the $\sim$ 13-48 keV band ($Z_1^2 \simeq 8.3\sigma$) using about 250 ks of dead-time and off-axis corrected exposure time for clusters A and B.

$(6.7 \pm 0.6) \times 10^{-13}$ erg/cm^{2}s given by Marshall et al. (1998b). Comparing the unabsorbed pulsed flux in the 2–8 keV band of $(6.04 \pm 0.24) \times 10^{-13}$ erg/cm^{2}s (this work) with the unabsorbed flux value of 3.09×10^{-12} erg/cm^{2}s as given by Townsley et al. (2006) for the total emission of PSR J0537-6910 indicates that about 18% of the emission is pulsed in this band, similar to what has been found for the Crab pulsar/nebula system.

Noteworthy is the recent detection of PSR J0537-6910 by *INTEGRAL* ISGRI in the 20–60 keV band, at a flux of 0.44 ± 0.08 mCrab (total emission), resulting from a very deep survey of the LMC region (Grebenev et al. 2013).

On the other hand no pulsed radio and high-energy γ-ray emissions have been detected so far from PSR J0537-6910 (see Crawford et al. 1998; Abdo et al. 2013, for the radio and high-energy γ-ray band, respectively). In the TeV domain, however, the H.E.S.S. collaboration reported recently on the detection, at a 14σ level, of a point source positionally consistent with N157B/PSR J0537-6910 making this the first extragalactic PWN association (H.E.S.S. Collaboration et al. 2012).

5.4 PSR B0540-69 / PSR J0540-6919

PSR B0540-69 was discovered at X-rays by Seward et al. (1984) using *Einstein* X-ray observatory data, soon followed by a detection in the optical band (Middleditch et al. 1985) and a weak radio detection (Manchester et al. 1993) about a decade later. It is a young Crab-like pulsar located in the Large Magellanic cloud, and it is one of the few known spin-down powered pulsars resident outside our own galaxy (see Ridley et al. 2013, for an update on the spin-down powered pulsar content of the LMC, now 23 members, and SMC, 5 members).

Since its discovery PSR B0540-69 has been a primary target for many different X-ray instruments e.g. *Ginga* (Nagase et al. 1990; Deeter et al. 1999), *ROSAT* (Finley et al. 1993), *ASCA* (Hirayama et al. 2002), *BeppoSAX* (Mineo et al. 1999; Cusumano et al. 2003), *Chandra* (Gotthelf & Wang 2000; Kaaret et al. 2001) and *RXTE* (de Plaa et al. 2003; Livingstone et al. 2005; Campana et al. 2008).

de Plaa et al. (2003) reported for the first time the detection of pulsed emission from PSR B0540-69 in the hard X-ray band up to $\sim$ 50 keV using *RXTE* PCA and HEXTE data. Figure 3 shows the pulse profiles of PSR B0540-69 for the $\sim$ 2–20 and 13–48 keV bands, as measured by *RXTE* PCA (panel a) and HEXTE (panel b), respectively, using the same data as in de Plaa et al. (2003). Moreover, these authors found that the pulsed spectrum softens towards higher energies. An update of the findings by de Plaa et al. (2003) was presented by Campana et al. (2008) using about 3 times more *RXTE* PCA and 5 times more HEXTE exposure time. In general, these authors reached similar conclusions, namely that the pulsed spectrum softens towards higher energies, but obtained a difference in flux normalization of about 30% and a somewhat different spectral shape. The first discrepancy can be traced back almost completely to improper response functions for the PCA units (i.e the sensitive areas) used by de Plaa et al. (2003) at the time of the production of their paper, thereby overshooting the normalization by more than 20%, while the shape discrepancy can be traced back by the different Hydrogen column densities used by the different authors, i.e. 4.6×10^{21} cm^{-2} by de Plaa et al. (2003) (see e.g. Kaaret et al. 2001), while Campana et al. (2008) derived/used a slightly lower value of 3.7×10^{21} cm^{-2}. We prefer the higher valued number, which finds support in the work of Serafimovich et al. (2004).

The softening of the pulsed spectrum explains also the non-detections by *CGRO* BATSE $\gtrsim$ 20 keV and *CGRO* OSSE (in the 80-210 keV band) (see Wilson et al. 1993b; Hertz et al. 1995, respectively). The unabsorbed pulsed fluxes of PSR B0540-69 for the 2–10 and 20–100 keV bands are $(6.7^{+0.4}_{-0.7}) \cdot 10^{-12}$ and $(6.1^{+0.6}_{-2.1}) \cdot 10^{-12}$ erg/cm^{2}s, respectively (see Campana et al. 2008). The former flux value was derived from the absorbed flux value of $(6.5^{+0.4}_{-0.7}) \cdot 10^{-12}$ erg/cm^{2}s given by Campana et al. (2008) adopting their estimated Hydrogen column density N_H of 3.7×10^{21} cm^{-2}.

A comparison of the spectral energy distributions of PSR B0540-69 and its PWN for the $\sim$ 1–100 keV band using *Swift* XRT (WT mode), *RXTE* PCA and HEXTE for the pulsed emission, and *Swift* XRT (PC mode) and *INTEGRAL* ISGRI for the total (=pulsar plus PWN) emission is given in Campana et al. (2008), and shows that about 25% of the total emission is pulsed. Noteworthy is also the work presented by Grebenev et al. (2013) on a deep hard X-ray survey of the LMC using *INTEGRAL* ISGRI (4.8 Ms effective exposure; PSR B0540-69 (plus PWN) was detected at a 22.0σ significance level in the 20-60 keV band with a 20-60 keV

flux of 1.68 ± 0.08 mCrab) and *INTEGRAL* JEM-X (1.8 Ms effective exposure; 3-20 keV flux of 1.28 ± 0.07 mCrab ($\sim 18\sigma$)).

At GeV energies recently the pulsed fingerprint of PSR B0540-69 has been detected at a 6.8σ level using a *RXTE* based ephemeris covering a time span of $\sim$3.5 years (Martin et al. 2014). The GeV pulse profile exhibits a single broad pulse and the GeV spectrum of the pulsed emission is soft and properly described by a cutoff power-law model connecting smoothly to the soft γ-ray part of the spectrum.

So far, (pulsed) emission has not been detected from PSR B0540-69 at TeV energies (Komin et al. 2012).

5.5 The Vela pulsar, PSR B0833-45 / PSR J0835-4510

Targeting the Vela Supernova remnant at radio-frequencies Large et al. (1968) discovered short period pulsations with $P \sim 89$ ms from a young (11 kyr) and energetic ($L_{sd} \sim 6.9 \times 10^{36}$ erg/s) neutron star, known since as PSR B0833-45. Since then the Vela pulsar has been monitored intensively at radio-frequencies, and it turns out to be a frequent glitcher, e.g. nine major glitches occured in the time period 1969 – 1994. Detailed single-pulse studies showed that the radio pulse (single; see e.g. Fig. 4 panel *a*) could be described as a composite of four (Gaussian) components (Krishnamohan & Downs 1983) covering a phase extent of ~ 0.055. Morphology changes of the radio pulse as a function of frequency (1.4-24 GHz) can be described by merely intensity variations of the constituting four Gaussian pulses, while maintaining their widths and positions (Keith et al. 2011). Further single pulse studies (Johnston et al. 2001) reveal the presence of giant micropulses in the leading edge of the radio pulse and on the trailing edge a large Gaussian component.

In the optical domain pulsations from PSR B0833-45 were detected by Wallace et al. (1977) from a sky region including the candidate proposed by Lasker (1976). The statistics of the (double pulsed) optical profile has increased significantly since the first detection (see e.g Manchester et al. 1980) with a most accurate characterisation of the profile given by Gouiffes, C. (1998) using fast-photometry observations performed at the ESO 3.6 m telescope in 1993 and 1994. The latter observations revealed a third narrow pulse coinciding with the radio pulse (see e.g. Fig. 4 panel *b*), the presence of which was confirmed at smaller wavelengths by *HST* STIS NUV and FUV observations (see e.g. Fig. 4 panels *c* and *d*, Romani et al. 2005). The latter observations revealed even a narrow fourth pulse preceding the radio-pulse.

Multi-band optical photometry with ESO NTT (Nasuti et al. 1997), ESO VLT (ISAAC, J_s and *H* bands, Shibanov et al. 2003), *HST* STIS (NUV and FUV, Romani et al. 2005; Kargaltsev et al. 2007) and Gemini GeMS (K_s-band, Zyuzin et al. 2013) along with spectroscopy observations (VLT *FORS2*; 4000- 11000 Å, Mignani et al. 2007) yielded a detailed spectral picture from near-IR to FUV of the Vela pulsar revealing a very flat spectrum with index $\alpha = -0.01 \pm 0.01$ (Zyuzin et al. 2013) across this range confirming, inline with its high pulsed fraction of about 80%, the non-thermal magnetospheric nature of the near-IR to FUV emission.

Optical astrometry with (initially) the ESO 3.5 m NTT (Nasuti et al. 1997), *HST* WFC/WFPC2 (de Luca et al. 2000; Caraveo et al. 2001) made accurate proper motion and even parallax measurements of the Vela pulsar possible, yielding a distance of 294^{+76}_{-50} pc, consistent with the more accurate distance estimate of 287^{+19}_{-17} pc derived somewhat later from VLBI (radio) observations (Dodson et al. 2003).

In the soft X-ray band (0.1-4 keV) the first detailed imaging studies of the Vela pulsar environment have been performed with the IPC ($\sim 1'$ spatial resolution) and HRI ($\sim 2''$ resolution) instruments aboard the *Einstein* satellite (Nov. 12, 1978 - April 1981). Structures at four different spatial scales could be discerned from the images (Harnden et al. 1985), in particular a) a pointlike object coincident with the pulsar, b) a relatively bright $\sim 4'$ diffuse nebula about the pulsar, c) diffuse hard emission at $\sim 1^\circ$ scale between the pulsar and the radio object Vela X and finally d) thermal emission from the entire $\sim 5^\circ$ Vela SNR. No evidence for X-ray pulsations could be found from the pointlike object associated with PSR B0833-45, indicating a rather low pulsed fraction of $\lesssim 9\%$ (see also, Ögelman & Zimmermann 1989, using *EXOSAT* 0.03-2.4 keV imaging observations).

The first unambiguous detection of pulsed X-ray emission from PSR B0833-45 was reported by Ögelman et al. (1993) using *ROSAT* PSPC (0.1-2.4 keV) data. This was confirmed by *ROSAT* HRI monitoring observations of PSR B0833-45 yielding a pulsed fraction of about 12% (Seward et al. 2000). The soft X-ray (0.1-2.4 keV) pulse shape turned out to be composed of one broad and two narrower pulses.

In the meantime *Chandra* and *XMM-Newton* observations considerably improved the overall soft X-ray picture of the Vela pulsar and its PWN. The subarcsecond angular resolution of *Chandra* made it possible to separate the pulsar from its bright PWN, and to determine the genuine underlying pulsar spectrum. The featureless phase-averaged pulsar spectrum (see Pavlov et al. 2001a, using a combination of HRC-S/LETG and ACIS-S/HETG in CC-mode data) could best be described in terms of a two component model composed of a Hydrogen NS atmosphere model (to describe the soft part) and a power-law model with best fit photon-index of -1.5 ± 0.3, nicely connecting to both the optical part and high-energy part of the Vela pulsar spectrum.

Monitoring observations of the Vela PWN with the ACIS-S show a highly dynamical system with a complex variability and morphological changes of structures (e.g. inner/outer and counter jets; inner/outer arcs; shell) in the PWN (Pavlov et al. 2001b, 2003; Durant et al. 2013).

In the timing domain *Chandra* observations with the HRC-I instrument showed the tripled peaked (energy integrated) soft X-ray profile in detail and aligned according to a contemporaneous radio ephemeris (Helfand et al. 2001). These authors derived a pulsed fraction of 7.1 ± 1.1 across the 0.1-10 keV band (gravity point near 1 keV) not diluted by PWN emission.

The Vela pulsar/PWN region was also observed (early in the mission on Dec. 1–2, 2000[4]) by the (large collecting area) *XMM-Newton* satellite with the EPIC pn operating in Small Window mode at a temporal resolution of 5.7 ms, amply sufficient to study the energy dependency of the pulse morphology (see e.g. Manzali et al. 2007, for phase-resolved spectroscopy; however, the moderate angular resolution of about $6\farcs6$ FWHM and $10''$ extraction radius used, imply a severe (not accounted for) PWN nebula contribution at every phase slice making their published (phase-resolved) spectral results unreliable).

We also analysed the *XMM-Newton* Vela observation of Dec. 2, 2000 (obs. id. 0111080201; 58.6 ks pn time) to study the energy dependency of the pulse profile. The radio-aligned profiles for the 0.2-0.8 and 0.8-2 keV ranges are shown in Fig. 4 panels *e–f* (the 2–8 keV band pn profile is statistically equivalent to the *RXTE* PCA

[4] Since April 27, 2006 there is a yearly monitoring of the Vela pulsar region

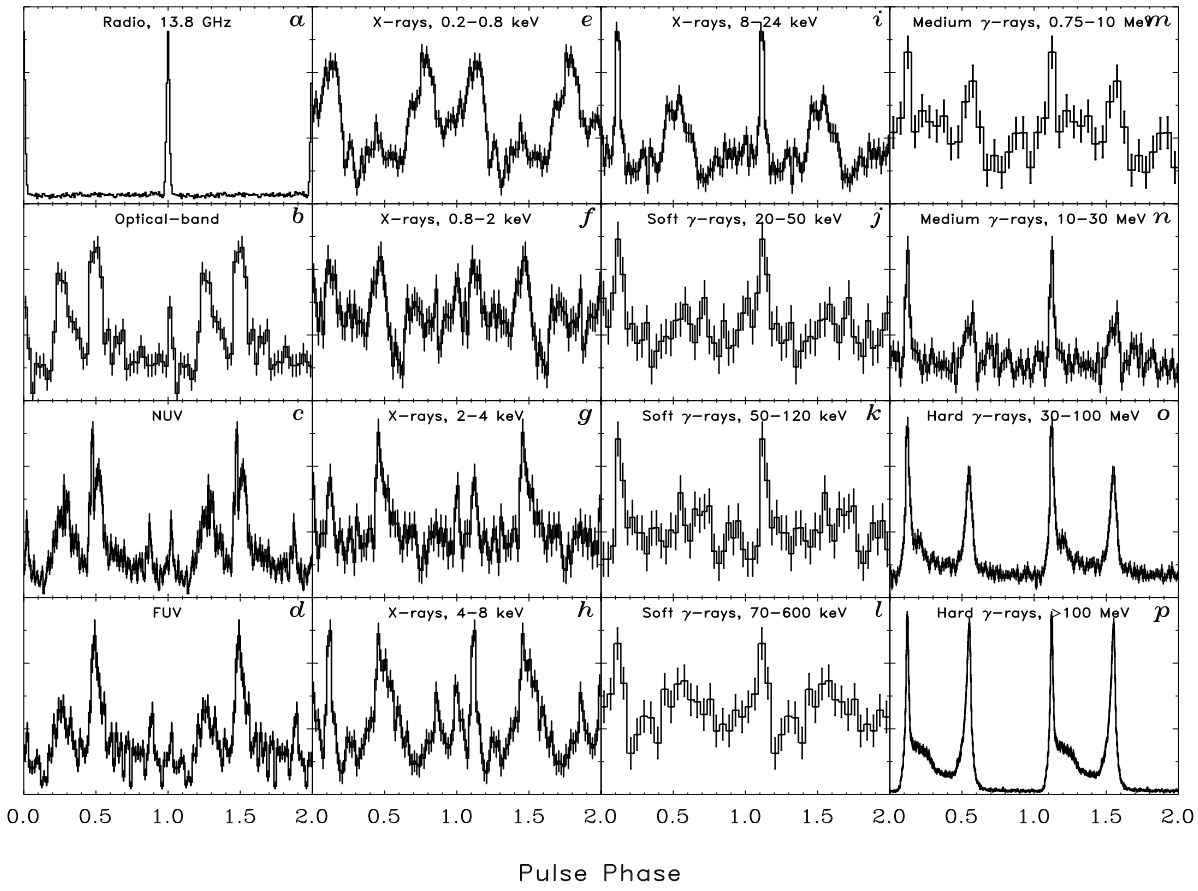

Figure 4. PSR B0833-45; multi-wavelength radio-phase aligned pulse-profile collage from radio-frequencies up to high-energy γ-rays. The left 4 panels (*a*–*d*) show the 'low' energy profiles: *a*) radio profile at 13.8 GHz, *b*) optical profile (Gouiffes, C. 1998) and *c*–*d*) NUV (1400-3270 Å) & FUV (1140-1730 Å) profiles (Romani et al. 2005). Panels *e*–*i* show the soft-hard X-ray pulse-profiles as obtained from XMM EPIC pn (panels *e*–*f*) and *RXTE* PCA (panels *g*–*i*) data. In panels *j*–*l* the soft γ-ray profiles are displayed obtained from multi-year *INTEGRAL* ISGRI (panels *j*–*k*) and *CGRO* OSSE (panel *l*, Strickman et al. 1996) data. Finally, the right hand panels *m*–*p* show the medium- and high-energy γ-ray pulse profiles as obtained by analyzing multi-year *CGRO* COMPTEL (panels *m*–*n*, this work), *CGRO* EGRET (panel *o*) and *Fermi* LAT (panel *p*) data. Notice the dramatic morphology changes as function of energy from single peaked (radio) to double peaked with bridge emission at high-energy γ-rays, with at intermediate energies very complex shapes with a plethora of pulses at optical, X-rays and soft/medium energy γ-rays.

2–8 profile and therefore is not shown here). Drastic changes can be discerned between the two - soft and intermediate (transition to the non-thermal regime) - bands.

At medium energy X-rays (*RXTE* PCA; $\sim 2-30$ keV) the morphology of the lightcurve drastically changed with two (narrow) peaks roughly aligned in phase with the high-energy γ-pulses (Strickman et al. 1999, 93 ks obs. performed during Jan 12–23, 1997). Much deeper *RXTE* PCA observations (274 ks exposure collected during April–May and July-August 1998), yielding much-improved statistics, showed the presence of several (narrow) emission components (Harding et al. 2002). In this work we reanalyzed *all* available *RXTE* PCA data on PSR B0833-45, totaling 360 ks screened exposure time (for PCA unit-2). The resulting lightcurves for the 2-4, 4-8 and 8-24 keV bands are shown in Fig. 4 panels *g*–*i*. Notice the presence of at least 5 (narrow) pulse components, one coincident with the radio and narrow optical/NUV/FUV pulse at phase zero, rendering the Vela pulsar as the most complex pulsar at X-ray energies.

Preceded by non-detections (Knight et al. 1982, *HEAO 1*; 15 keV - 11 MeV) and controversial (short duration) balloon flight results (e.g. Harnden et al. 1972; Tümer et al. 1984; Sacco et al. 1990), the first unambiguous detection (4.6σ in the 70-600 keV band) of the Vela pulsar at soft γ-rays was made by the OSSE instrument aboard *CGRO* (Strickman et al. 1996). The pulse profile (see Fig. 4 panel *l*; 70-600 keV) showed two peaks - a narrow and a more structured broad one - coincident with the pulses seen at high-energy γ-rays.

The ISGRI instrument ($\sim$ 20-300 keV) aboard the *INTEGRAL* satellite offered a new look at the Vela pulsar at soft γ-rays. In this work a timing analysis of 2244 *INTEGRAL* ISGRI observations of the Vela region, spread over the period June 12, 2003 – Oct. 13, 2010 (*INTEGRAL* Revolution period 81–976), has been performed to shed light on the pulse morphology in the so far poorly explored soft γ-ray band. The combined ISGRI dataset represents an effective on-axis exposure time of 6.12 Ms. The pulse profiles of PSR B0833-45, generated through folding upon proper radio- or *Fermi* LAT based timing models, are shown in Fig. 4 panels *j*–*k* for the 20-50 and 50-120 keV bands, yielding non-uniformity significances of 5σ and 4.9σ, respectively, adopting a Z^2_{11} test. The 20–300 keV pulse profile represents even a 7.9σ significance, with one prominent narrow first pulse and a structured second broader pulse.

At medium γ-ray energies ($\sim$ 1–30 MeV), using data from the COMPTEL telescope aboard *CGRO* (Schönfelder et al. 1993), secure detections of the Vela pulsar have been reported by Hermsen et al. (1993, 1994) and Kuiper et al. (1998). In the latter work phase-resolved spectra were shown combining COMPTEL MeV data collected from the first four observation cycli of *CGRO*. In this work we present some new, unpublished so far, COMPTEL Vela pulsar results based on observations performed over the full *CGRO* mission lifetime, spanning nine observation cycli and covering the period May 10, 1991–March 21, 2000 (23 viewing periods, typically lasting 2 weeks, with PSR B0833-45 within 30° from the pointing axis).

Applying event selections using optimized parameter windows on Time of Flight (TOF), Pulse Shape Discrimination (PSD) and $\phi_{\rm arm}$ (see e.g. sections 2 & 3 of Kuiper et al. 2001, and references therein) and sorting the barycentered timetags on pulse phase and energy resulted in pulse-phase distributions as shown in Fig. 4 panels m–n, for the 0.75-10 and 10-30 MeV bands, respectively. The Z^2_9-test significances represent a 6.2σ and 12.7σ deviation from uniformity for both ranges, respectively. Clearly visible are emission peaks coincident with the two high-energy γ-ray pulses, P1 and P2, with in between bridge emission (most notably in the 0.75-10 MeV band). Indications for emission structures in the off-pulse region exist for energies above 3 MeV.

PSR B0833-45 was the *first* pulsar recognized in high-energy γ-ray data from the SAS-2 satellite (Thompson et al. 1975, 1977), followed by more detailed studies with COS-B (Bennett et al. 1977; Kanbach et al. 1980; Grenier et al. 1988) and later with *CGRO* EGRET (Kanbach et al. 1994; Fierro et al. 1998). The γ-ray pulse profile shows two pulses with clear bridge emission with the main pulse trailing the radio-pulse ~ 0.12 in phase (see e.g. Fig. 4 panel *p* for a > 100 MeV *Fermi* LAT profile). *Fermi* LAT made high-statistics (phase-resolved) studies at high-energy γ-rays possible, revealing a third component in the bridge region, which moves towards higher phase with increasing energy. The two γ-ray pulses become narrower the higher the energy (Abdo et al. 2009c, 2010d) with an even vanishing first (main) pulse component. This has been confirmed now by the upgraded TeV telescope systeem H.E.S.S. (phase II, including a fifth 28m telescope at the center location; energy threshold about 30 GeV), yielding a $\sim 11.0\sigma$ pulsed signal (H-test) at a mean energy of 40 GeV (Stegmann et al. 2014).

Considering the full pulse-profile collage shown in Fig. 4 it is clear that PSR B0833-45 shows extremely complex emission patterns, which change drastically as a function of energy. Therefore, it will be a major theoretical challenge to understand the multi-beam emission structures of PSR B0833-45 and so to unveil the topology and plasma filling of its magnetosphere.

In Fig. 28 the total pulsed flux of PSR B0833-45 across the $\sim$ 2 keV – 10 GeV band (thermal part excluded) is shown in blue color as solid curves and data symbols. Published data and spectral fit results from *CGRO* OSSE (Strickman et al. 1996) and Fermi LAT (Abdo et al. 2009c) are shown as well as newly derived pulsed fluxes for the $\sim$ 2– 30 keV (*RXTE* PCA), 20–175 keV (*INTEGRAL* ISGRI) and 0.75-30 MeV (*CGRO* COMPTEL) bands.

Given the complexity of the Vela lightcurve at X-rays (see e.g. Fig. 4 panel *h*) it is rather difficult to define the unpulsed or DC level. For the *RXTE* data we have used the phase stretch 0.68-0.78 to determine this level. A spectral analysis adopting a power-law model with N_H fixed to 3.3×10^{20} cm^{-2} (see e.g. Pavlov et al. 2001a, Table 1) yielded a photon index of -1.06 ± 0.05 across the 2.2–28.1 keV band. Pulsed fluxes (unabsorbed) are: 2–10 keV $(8.0 \pm 1.0) \cdot 10^{-13}$ erg/cm^{2}s (*RXTE* PCA); 20–100 keV $(1.1 \pm 0.4) \cdot 10^{-11}$ erg/cm^{2}s (*INTEGRAL* ISGRI[5]); 1–10 MeV $(6.2 \pm 0.8) \cdot 10^{-10}$ erg/cm^{2}s (*CGRO* COMPTEL; systematic errors are of the order of 30% because of uncertainties in the unpulsed level); 0.1–1 GeV $(3.92 \pm 0.49) \cdot 10^{-9}$ erg/cm^{2}s (*Fermi* LAT).

The Vela pulsar is often considered as the canonical high-energy γ-ray pulsar reaching maximum luminosity at GeV energies. Note, however, that the detection at hard X-rays/soft γ-rays is just possible because the pulsar is relatively nearby. Would PSR B0833-45 be placed at 2 kpc, as the Crab pulsar, then the pulsed hard X-ray/soft γ-ray emission would reach flux levels below the detection limits of current instrumentation.

5.6 PSR J1400-6325 / IGR J14003-6326

IGR J14003-6326 was discovered by Keek et al. (2006) in a deep 1.9 Ms *INTEGRAL* ISGRI mosaic image of the Circinus region for the 20–60 keV band using *INTEGRAL* observations performed between Febr. 28, 2003 and Mar. 3, 2005. A 20–60 keV flux of 0.97 ± 0.15 mCrab and a positional error of $3\farcm6$ at 90% confidence were derived.

A $\sim$ 5 ks follow up observation with *Chandra* on June 29, 2008 revealed the presence of an extended X-ray source, nearly circular with a $1\farcm5$ radius, within the ISGRI error region (Tomsick et al. 2009). Its morphology with at the center region a PWN surrounding a so-far undetected pulsar made a SNR identification plausible. Tomsick et al. (2009) derived spectral characteristics for the composite emission region within $1\farcm5$ from the central source by fitting an absorbed power-law model over the 0.3-10 keV range, and obtained an absorbing Hydrogen column N_H of $(3.1 \pm 0.3) \times 10^{22}$ cm^{-2}, a photon index of -1.83 ± 0.13 and an unabsorbed 2–10 keV flux of 1.9×10^{-11} erg/cm^{2}s ($\sim$ 1 mCrab).

Renaud et al. (2010) reanalyzed the *Chandra* data and decomposed the emission into 3 components: 1) a point-source, extracted for a circular region of $1\farcs5$ centered on source with background taken from an annulus with radii $1\farcs5$ and $2''$, 2) a PWN-region extracted from an annulus with radii $1\farcs5$ and $39''$ and 3) the SNR-region extracted from an annulus with radii $0\farcm98$ and $1\farcm27$. Assuming absorbed power-law models they found the following photon-indices and unabsorbed 2–10 keV fluxes for an absorbing column of $(2.09 \pm 0.12) \times 10^{22}$ cm^{-2}: -1.22 ± 0.15, -1.83 ± 0.09 and -2.56 ± 0.18, and $(1.95 \pm 0.5) \times 10^{-12}$, $(1.51 \pm 0.2) \times 10^{-11}$ and $(1.1 \pm 0.2) \times 10^{-12}$ erg/cm^{2}s for the 3 components, respectively. The PWN is thus by far the most dominant source, and about 8 times brighter than the hard point-source.

The detection of pulsed X-ray emission of IGR J14003-6326 was also reported by Renaud et al. (2010) using 2 sets of *RXTE* PCA observations of 44 ks each, taken one year apart on Sept. 29, 2008 and Sept. 30, 2009. They found an energetic ($\dot{E} = 5.1 \times 10^{37}$ erg/s) pulsar spinning with a 31.2 ms pulse period and an estimated age of 12.7 kyr. This period was later confirmed at radio-frequencies with the Parkes telescope, resulting furthermore in a (very) high DM value of 563 ± 4 cm^{-3} pc and flux densities of 250 and 110 μJy at 1.374 and 3.1 GHz, respectively.

Renaud et al. (2010) also derived the pulsed spectrum of IGR J14003-6326, through an on-off method, for the 2–10 keV band using only the top detection layer of each involved PCU. They

[5] Because of the complexity of the lightcurve we fitted the 20-100 keV profile in terms of a constant and 7 harmonics to estimate the unpulsed level, and so the number of pulsed excess counts. Varying the number of harmonics, 5, 7, 9, 11, yielded consistent results.

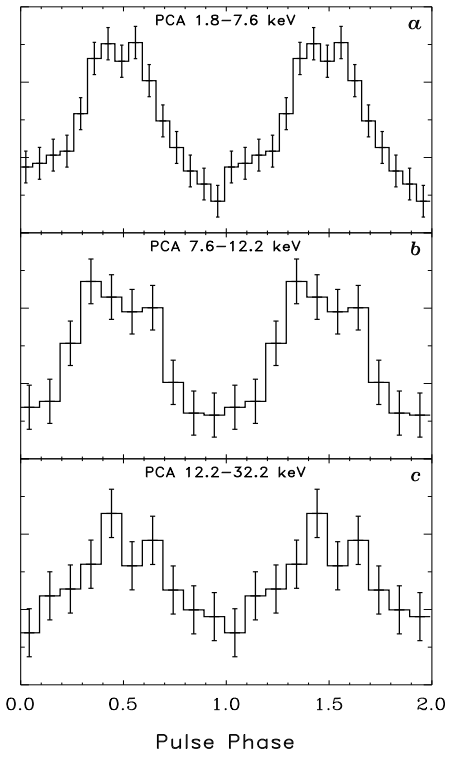

Figure 5. IGR J14003-6326; pulse profiles for *RXTE* PCA in different energy bands. The significance in the 12.2-32.2 keV band is 3.7σ (panel c).

found an absorbed 2–10 keV pulsed flux of 3.0×10^{-13} erg/cm^{2}s and a (*soft*) photon index of $-2.0^{+0.5}_{-0.3}$.

We reanalyzed the PCA data including now all PCU detector layers to be more sensitive to the hard X-ray photons with energies in excess of 10 keV. Pulse profiles for three PCA bands are shown in Fig. 5. Significant pulsed emission at $\sim 3.7\sigma$ is found for the 12.2– 32.2 keV band. Pulsed excess counts have been derived through pulse template fitting using as extractor the 3 harmonics fit to the lightcurve of the 4–87 PHA band. These excess counts have been converted to pulsed fluxes adopting an absorbing Hydrogen column of 2.09×10^{22} cm^{-2} (Renaud et al. 2010) and assuming an underlying (absorbed) power-law model for the photon flux. We obtained a photon index of -1.95 ± 0.04, consistent with Renaud et al. (2010), and an unabsorbed 2–10 keV flux of $(1.3 \pm 0.1) \times 10^{-12}$ erg/cm^{2}s, about ~ 4 times larger than found by Renaud et al. (2010). Our pulsed flux represents $\sim 67\%$ of the total 2–10 keV flux, while Renaud et al. (2010) found a pulsed fraction of only $\sim 18\%$. The pulsed flux measurements of IGR J14003-6326 for $\sim 2 - 32$ keV band are shown in Fig. 28 (left panel) as yellow data points.

We also analyzed HEXTE data. As expected, we could not find evidence for pulsed emission for energies in excess of ~ 15 keV.

In the TeV domain no point-like source has been detected above 5σ in the latest map of the H.E.S.S. Galactic Plane Survey (Chaves et al. 2008, 2009). Also at the GeV energies neither a point-like source is found in *Fermi* LAT data (Nolan et al. 2012) at the location of IGR J14003-6326 nor pulsed emission has been detected (Abdo et al. 2013).

5.7 PSR B1509-58 / PSR J1513-5908

PSR B1509-58 was discovered at X-rays as a 150 ms pulsar in *Einstein* HRI and IPC (0.2-4 keV) data by Seward & Harnden (1982), and later confirmed at radio-wavelengths by Manchester et al. (1982). Its characteristic age of only 1570 years and spin-down luminosity of 1.8×10^{37} erg/s, as inferred from its timing parameters, qualifies PSR B1509-58 as a very young and energetic spin-down powered pulsar. Its derived surface polar magnetic field strength of 3.1×10^{13} G is close to the quantum critical field strength of 4.413×10^{13} G, above which exotic quantum electrodynamic effects play an important role in the high-energy pulsar emission mechanisms.

PSR B1509-58 is associated with supernova remnant MSH 15-52 (G320.4-1.2), and various detailed studies using X-ray data have been performed since the early eighties to disentangle the complex morphology of MSH 15-52 with at the north western rim an excess near Hα nebula RCW 89 and near the centre a clump containing a diffuse synchrotron nebula surrounding the pulsar (its PWN). Using the superb X-ray imaging quality of *Chandra* Gaensler et al. (2002) showed that, while the overall PWN shows a clear symmetry axis, the PWN also reveals several new components. Extended TeV emission (> 280 GeV) from MSH 15-52 was detected at a 25σ confidence level by H.E.S.S. (Aharonian et al. 2005b), and later at higher TeV γ-rays (> 810 GeV) by CANGAROO-III at a 7σ level (Nakamori et al. 2008). In the GeV band extended γ-ray emission has been detected by the *Fermi* LAT (Abdo et al. 2010b).

Pulsed emission in the medium/hard X-ray band was detected by Kawai et al. (1991) using *Ginga* (2-60 keV) data. These authors also found that, using contemporaneous X-ray (*Ginga*) and radio (Parkes) data, the radio pulse leads the asymmetric X-ray pulse by 0.25 ± 0.02 in phase. Soon after the launch of the Compton Gamma-Ray Observatory (*CGRO*) on April 16, 1991, pulsed hard X-ray/soft γ-ray emission above ~ 60 keV was detected by BATSE using data collected in the folded-on-board data mode (Wilson et al. 1993a,b), confirmed later by Ulmer et al. (1993) and Matz et al. (1994) using *CGRO* OSSE (0.05-10 MeV) data. The radio- soft γ-ray pulse lag found by Ulmer et al. (1993) combining BATSE and OSSE data was 0.32 ± 0.02, somewhat larger than the lag found at lower energies. In the spectral domain Matz et al. (1994) derived for the pulsed spectrum from 50 keV to 5 MeV, fitting a power-law model, a photon index of -1.68 ± 0.09, significantly softer than the value of -1.30 ± 0.05 obtained for the 2-60 keV band by Kawai et al. (1991) analyzing *Ginga* data, strongly indicating a softening towards higher energies.

Pulsed emission was also detected in the medium energy γ-ray band by Kuiper et al. (1999) using *CGRO* COMPTEL (0.75-30 MeV) data. They found a 5.4σ pulsed signal, a broad asymmetric pulse, for the 0.75-30 MeV band analyzing COMPTEL data collected over 6 *CGRO* observation cycli. The pulse reaches its maximum at phase 0.38 ± 0.03 with respect to the radio pulse. The apparent shift of the pulse maxima from soft X-rays to medium energy γ-rays can be explained by different spectral behaviours of two Gaussian shaped pulses comprising the broad asymmetric pulse with one pulse peaking at 0.250 ± 0.008 and the other at 0.386 ± 0.012 as derived from high-statistics *RXTE* PCA data. The first (narrower) pulse seems to vanish towards higher energies (Kuiper et al. 1999). The spectrum of the pulsed emission clearly breaks above ~ 10 MeV, though there were weak indications for pulsed emission beyond 10 MeV in both COMPTEL and *CGRO* EGRET data (also in the spatial domain).

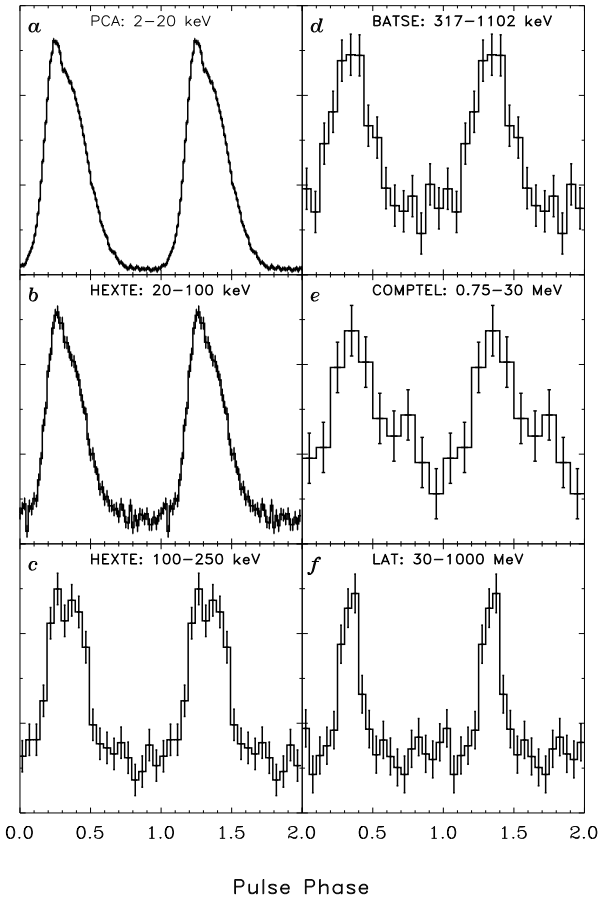

Figure 6. PSR B1509-58 (the prototype soft γ-pulsar); pulse profiles from 2 keV up to 1 GeV using multi-year *RXTE* PCA & HEXTE data (panels *a*–*c*), *CGRO* BATSE (Cycli I-IX; panel *d*) & COMPTEL (Cycli I-VI; panel *e*) and *Fermi* LAT (covering 3.4 years; panel *f*).

At high-energy γ-rays (> 100 MeV) significant progress has been made analyzing *Fermi* LAT data (Abdo et al. 2010b) and *AGILE* data (Pellizzoni et al. 2009; Pilia et al. 2010) by detecting pulsed emission from PSR B1509-58 well above 100 MeV. In den Hartog et al. (2014) the *Fermi* LAT results are presented analyzing $\sim$ 5 years of data detecting pulsed emission from PSR B1509-58 at a 18.2σ level across the $\sim$ 30 - 1000 MeV band, enabling detailed studies of the morphology of the lightcurve and the breaking part of the spectrum at these energies.

To achieve pulse profile morphology comparisons across the $\sim$ 2 keV - 1 GeV range at a high statistics level we analyzed and processed multi-year data from *RXTE* PCA (2-30 keV; April 25, 2002 - Oct. 9, 2003), *RXTE* HEXTE (15-250 keV; Feb. 10, 1999 - Jan. 1, 2012), *CGRO* BATSE (22 - 4000 keV; Oct. 31, 1991 - May 9, 2000; MJD 48560–51673; *CGRO* Cycli I-IX), *CGRO* COMPTEL (0.75-30 MeV; Oct. 17, 1991 - Nov. 3, 1997; MJD 48546.6–50755.6; *CGRO* Cycli I-VI) and *Fermi* LAT (30-1000 MeV; Aug. 4 18:00:00 - Jan. 1, 2012; MJD 54682.75–55927).

RXTE PCA data (in *goodXenon* mode) were collected during observation run 70701 and part of 80803. The time intervals are fully covered by the validity interval of an ephemeris from the ATNF archive ensuring proper timing information. Subsequent screening adopting default criteria rendered for PCU-2 an effective exposure of 74.53 ks. This yielded ample statistics to study its timing characteristics in great detail, because PSR B1509-58 is a relatively strong pulsar at medium/hard X-ray energies. To determine the pulsed spectrum across the 15-250 keV band we used *RXTE* HEXTE data collected over a much longer time period than used for the PCA. We combined all available HEXTE data on PSR B1509-58 taken during observation cycli P40704 – 96803 (Feb. 10, 1999 – Jan. 1, 2012) to obtain the highest possible statistics. For more information on these *RXTE* PCA and HEXTE data we refer to the section on *RXTE* in den Hartog et al. (2014). The resulting pulse profiles for the PCA (2-20 keV) and HEXTE (20-100 and 100-250 keV) are shown in panels a–c of Fig. 6. The Z_2^2-test significance of the 100-250 keV profile is about 17.1σ.

To study the pulse profile of PSR B1509-58 at soft/medium energy γ-rays we analyzed BATSE (see e.g. Fishman et al. 1993, and references therein) LAD folded-on-board data types collected during the *full* duration of the *CGRO* mission yielding a net screened exposure of about 10.6 Ms (integrated sum for all 8 LADs) for the time period Oct. 31, 1991 - May 9, 2000. The processing of these data is analoguous to that in Kuiper et al. (2001) for the Crab pulsar (see Section 5.3 of that paper). The resulting 317-1102 keV BATSE profile of PSR B1509-58 is shown in panel d of Fig. 6. The deviation from a statistically uniform distribution is about 10.4σ adopting a Z_2^2-test. Panel e of Fig. 6 shows the COMPTEL 0.75-30 MeV profile as obtained by Kuiper et al. (1999).

Finally, panel f of Fig. 6 shows the *Fermi* LAT 30-1000 MeV lightcurve using data from a 5° aperture around PSR B1509-58 collected during Aug. 4, 2008 18:00:00 and Jan. 1, 2012 (about 3.4 years) obtained after folding the SSB corrected arrival times with *RXTE* PCA based timing models. The Z_2^2-test significance of the 30-1000 MeV profile is about 10.2σ, and a single Gaussian can describe the measured distribution accurately. Pulse maximum occurs at phase 0.342 ± 0.007 and the width (Gaussian σ) is 0.064 ± 0.007. This indicates that the first pulse indeed vanishes, while the second pulse becomes somewhat narrower, when the energy increases.

Equiped with the multi-year *RXTE* PCA/HEXTE data covering at high statistics the $\sim$ 2 – 250 keV band, the multi-year *Fermi* LAT (30-1000 MeV) data (den Hartog et al. 2014), supplemented by the (archival) COMPTEL (0.75-30 MeV) data (Kuiper et al. 1999) and *INTEGRAL* ISGRI (20-175 keV; 550 ks of dedicated PSR B1509-58 observation during *INTEGRAL* AO2; this work), we attempted a broad-band spectral fit of the *pulsed* emission across the $\sim$ 2 keV - 1 GeV range adopting a photon flux model (a kind of power-law with a (modified) exponential cutoff) F_γ with the following E_γ dependency:

$$F_\gamma = k \cdot (E_\gamma/E_0)^\Gamma \cdot \exp(-(E_\gamma/E_c)^\beta)$$

Interstellar absorption effects, only applicable to *RXTE* PCA data, are modeled out adopting an absorbing Hydrogen column N_H of 9.5×10^{21} cm^{-2} (Gaensler et al. 2002). For our spectral dataset the normalization energy E_0, which minimizes the correlation between the 4 fit parameters, was 0.100518 MeV, while the best fit ($\chi^2_{r,59-4} = 1.35$ i.e. acceptable) yielded the following fit parameters, $k = (1.574 \pm 0.012) \cdot 10^{-2}$ ph/cm^{2}s MeV; $\Gamma = -1.233 \pm 0.005$; $E_c = 0.078 \pm 0.003$ MeV and $\beta = 0.286 \pm 0.005$. The broad-band $\sim$ 2 keV - 1 GeV pulsed spectrum of PSR B1509-58 is shown in Fig. 7 along with the best fit model. Maximum luminosity per energy decade is reached at $\sim$ 2.5 MeV and therefore PSR B1509-58 can be considered as the "canonical" soft γ-ray pulsar.

Pulsed fluxes (unabsorbed), obtained from the best fit model, in the 2–10 keV, 20–100 keV, 1–10 MeV and 0.1–1 GeV are, $(2.52 \pm 0.05) \cdot 10^{-11}$, $(9.59 \pm 0.13) \cdot 10^{-11}$, $(4.4 \pm 0.3) \cdot 10^{-10}$ and $(1.2 \pm 0.4) \cdot 10^{-11}$ erg/cm^{2}s, respectively.

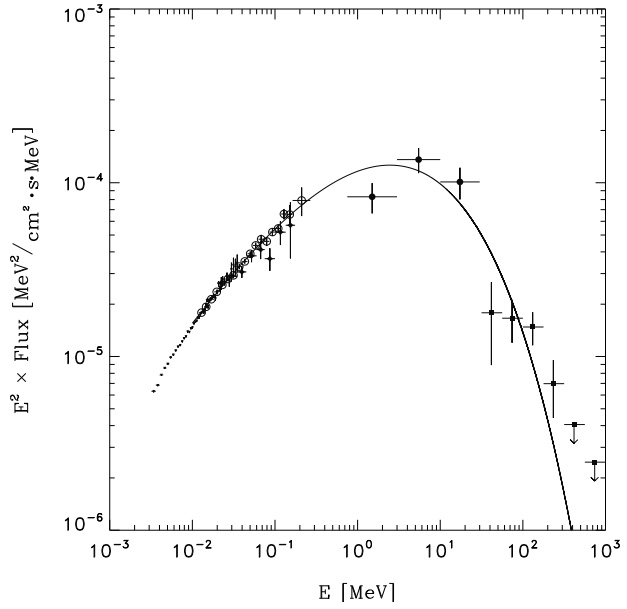

Figure 7. PSR B1509-58; unabsorbed high-energy spectrum of the pulsed emission across the $\sim$ 2 keV - 1 GeV range, combining *RXTE* PCA, HEXTE, *INTEGRAL* ISGRI, *CGRO* COMPTEL and Fermi LAT measurements (see text). Maximum luminosity is reached at about 2.5 MeV making PSR B1509-58 an archetypal soft γ-ray pulsar.

5.8 PSR J1617-5055

Torii et al. (1998) discovered an energetic 69 ms pulsar, PSR J1617-5055, $\sim 7'$ from SN-remnant RCW 103, analysing X-ray data obtained with the *ASCA* GIS instrument. It is noteworthy that Aoki et al. (1992) already detected pulsed emission from the RCW 103 region with the *Ginga* large area counters in data taken in March 1989.

Weak (~ 0.5 mJy at 1.4 GHz) radio pulsations were detected by Kaspi et al. (1998) using the Parkes radio telescope. Combining more pulse period measurements from X-ray observations a characteristic age of about 8 kyr could be derived as well as strong indications for a giant glitch (Torii et al. 2000) that occured between August 1993 and September 1997.

RXTE had the sky region containing PSR J1617-5055 several times in its field of view: on Jan. 2, 1998 and during March 5–6, 1999 in observation run 30210 with prime target 1E 161348-5055 (the point source in the middle of RCW 103), on Jan. 22, 2001 during run 50428 with prime target RCW 103, and finally in a dedicated observation run, 80090, performed during September 20–21, 2003 for about 80 ks. We combined *RXTE* PCA (total screened PCU-2 exposure 146.53 ks) and HEXTE (dead-time and off-axis corrected cluster-0/1 exposures of 47.7 and 49.3 ks, respectively) data from these 3 observation runs and significantly detected pulsed X-ray emission up to ~ 64 keV. Pulse profiles in differential energy bands, all single peaked with a sharper rise than fall, are shown in Fig. 8. The HEXTE profile for energies in excess of 35.3 keV (Fig. 8f) has a Z_1^2 significance of 3.8σ.

We estimated the pulsed excess counts through pulse-profile model fitting with a truncated Fourier series (fundamental plus 2 harmonics) and converted these to photon flux values, adopting an absorbed power-law model with a fixed column density N_H of 3.2×10^{22} cm^{-2} (Becker & Aschenbach 2002). This yielded for the pulsed emission in the 2.5-30 keV PCA band a hard photon index of -1.42 ± 0.02 and a 2–10 keV unabsorbed flux of

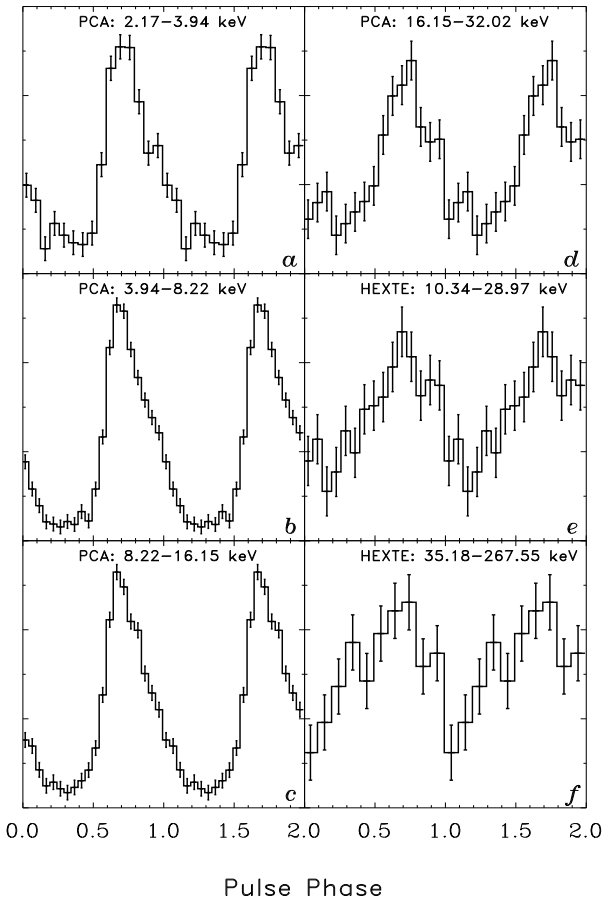

Figure 8. PSR J1617-5055; pulse profiles in various energy bands for *RXTE* PCA (panels a–d) and *RXTE* HEXTE (panels e–f). Pulsed emission has been detected up to ~ 64 keV.

$(3.30 \pm 0.16) \times 10^{-12}$ erg/cm^{2}s. We used all PCA detection layers to be more sensitive to hard X-ray photons. The reconstructed *RXTE* PCA pulsed flux values are shown in Fig. 9 as aqua colored points along with the best fit. HEXTE pulsed flux measurements are also shown (blue squares).

Unfortunately, neither X-ray monitoring- nor regular radio observations (too weak, requiring long exposure times) have been performed on this pulsar, that would have enabled us to construct phase coherent timing models over long time stretches. Therefore, we could not do a timing analysis for the soft γ-band using the low-countrate *INTEGRAL* ISGRI data. However, Landi et al. (2007) demonstrated in a spatial analysis in ISGRI maps the presence of a hard X-ray source coincident with PSR J1617-5055 with a significance in the 18-60 keV band of $\sim 7.4\sigma$, combining data collected since the beginning of the mission (November 2002) up to April 2006. Our own spectral analysis of ISGRI data (Revs. 46-411; March 2, 2003 - Feb. 24, 2006) yielded for the *total* emission in the 20-300 keV band a photon index of -1.93 ± 0.28 and a 20-100 keV flux of $(1.25 \pm 0.18) \times 10^{-11}$ erg/cm^{2}s, consistent with the values obtained by Landi et al. (2007). The ISGRI total flux measurements in the 20–300 keV band are indicated in Fig. 9 as purple datapoints along with the best power-law fit.

The total emission spectrum of PSR J1617-5055 below 10 keV was already derived by Torii et al. (2000); Becker & Aschenbach (2002); Landi et al. (2007); Kargaltsev et al. (2009) using X-ray instruments on different spacecrafts – *ASCA*, *XMM-Newton*,

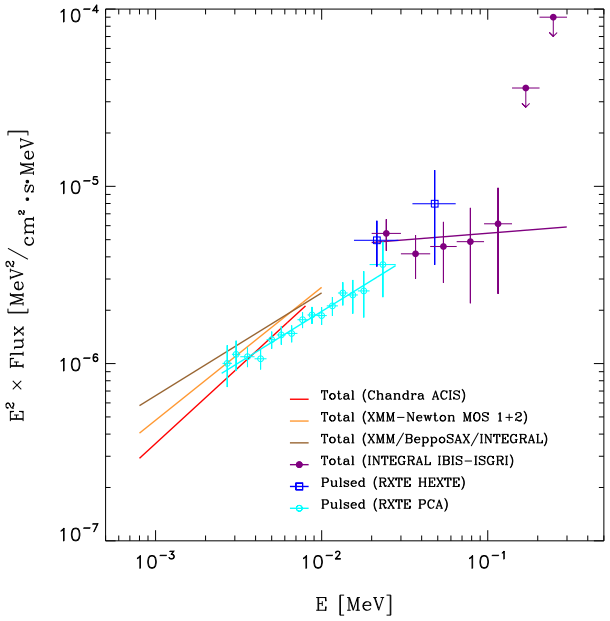

Figure 9. PSR J1617-5055; high-energy (0.8-300 keV) total and pulsed spectra as derived from measurements by *Chandra* ACIS (total pulsar 0.8-8 keV; solid red; Kargaltsev et al. (2009)), *XMM-Newton* MOS (total, including compact PWN, 0.8-10 keV; solid orange; Becker & Aschenbach (2002)), joint fit *XMM-Newton*/*BeppoSAX*/ISGRI (total, including compact PWN, 0.8-10 keV; solid brown; Landi et al. (2007)), *RXTE* PCA (pulsed 2.5-30 keV; aqua; this work), *RXTE* HEXTE (pulsed 15-150 keV; blue; this work) and *INTEGRAL* ISGRI (total 20-300 keV; purple; this work).

BeppoSAX and *Chandra*. The most recent determination by Kargaltsev et al. (2009), using *Chandra* ACIS-I data, resolves the emission around PSR J1617-5055 in a point-like component, associated with the pulsar, an inner compact pulsar wind nebula component of $\sim 1''$ size within $0\farcs5$ and $1\farcs5$ from the pulsar and an outer nebula extending up to $\sim 1'$ from the pulsar. Fitting a power-law to the spectral data extracted from a circular aperture of $0\farcs5$ centered on PSR J1617-5055, Kargaltsev et al. (2009) derived a power-law index of -1.14 ± 0.06 and a 0.5–8 keV (unabsorbed) flux of $(3.6 \pm 0.1) \times 10^{-12}$ erg/cm^{2}s for the total (=pulsed+pulsar DC) emission of the pulsar. This converts to a 2–10 keV (unabsorbed) flux of $\sim 3.58 \times 10^{-12}$ erg/cm^{2}s. The flux of the inner compact PWN is about 10–15 % of the total pulsar flux, and its combination is consistent with the total emission spectra derived using the X-ray instruments with much less spatial resolution: Landi et al. (2007) find a 2–10 keV flux of 4.2×10^{-12} erg/cm^{2}s using *BeppoSAX* MECS, *XMM-Newton* MOS 1+2 and *INTEGRAL* ISGRI in combination, while the 2–10 keV flux, estimated from the best fit values given by Becker & Aschenbach (2002), amounts 4.0×10^{-12} erg/cm^{2}s. The best fit models derived by Becker & Aschenbach (2002); Landi et al. (2007); Kargaltsev et al. (2009) are shown as solid orange, brown and red, respectively, lines in Fig. 9.

Comparing the pulsed (*RXTE* PCA; this work) and total 2–10 keV flux values (*Chandra*; MOS 1+2; *BeppoSAX*) yields a (high) pulsed fraction in the range 79-92 %. This value is consistent with the value, derived in this work, using data from merely *Chandra* HRC-S in timing mode. During a 78.2 ks exposure of 1E 161348-5055 on July 2, 2007 (obs.id. 7619) with the HRC-S PSR J1617-5055 was observed $7\farcm3$ off-axis. Using a $8''$ extraction radius, because of the strongly degraded PSF, and using an annulus centered on the pulsar with inner and outer radii of $12''$ and $16''$, respectively, to determine the local background, we derived a genuine pulsed fraction (0.2-10 keV) of $78 \pm 2\% \pm 10\%$ taking into account the 10-15 % contribution of the inner PWN to the total emission from the $8''$ circular (source) extraction region, which could not be resolved in this observation. The first error is related to the uncertainty in the inner PWN contribution and the second one to the uncertainty in the number of pulsed counts, derived through the method outlined by Swanepoel et al. (1996).

Also, above 20 keV there is very little room for pulsar DC and/or PWN emission. At GeV energies no pulsed high-energy γ-ray emission has been detected so far for PSR J1617-5055 (Abdo et al. 2013).

At TeV energies ($>$ 200 GeV) a bright source, HESS J1616-508, has been detected in the neighbourhood of PSR J1617-5055 (Aharonian et al. 2006). However, due to (severe) misalignment a convincing identification at lower energies is lacking (see e.g. Matsumoto et al. 2007; Kargaltsev et al. 2009).

5.9 PSR J1640-4631 in SNR G338.3-0.0/HESS J1640-465

HESS J1640-465 was discovered during the Galactic plane survey with H.E.S.S. performed during May-July 2004 (Aharonian et al. 2005, 2006). The source is marginally extended at TeV energies and its location is consistent with the $8'$diameter broken-shell SNR G338.3-0.0, which lies near the boundary of a bright H II region. At the center of SNR G338.3-0.0 an X-ray source, AX J1640.7-4632, was detected during the *ASCA* Galactic plane survey (Sugizaki et al. 2001).

HESS J1640-465 was observed by *XMM-Newton* for 21.8 ks on August 20, 2005 with the EPIC-pn and MOS camera's operating in full-frame mode (Funk et al. 2007b). This observation was strongly affected by soft proton flares reducing the effective exposure to only 7.3 ks. Three sources were detected in this observation of which XMM J164045.4-463131 is coincident with AX J1640.7-4632, and is extended in nature with a compact core and a faint tail, resembling morphologically a typical PWN. A spectral analysis of XMM J164045.4-463131, fitting an absorbed power-law model, yielded a rather strong absorbing Hydrogen column N_H of $(6.1^{+2.1}_{-0.6}) \times 10^{22}$ cm^{-2} and a photon index of -1.74 ± 0.12. No shell-like X-ray emission was apparent in the XMM-observation.

The extended nature of XMM J164045.4-463131 was confirmed by Lemiere et al. (2009), who analysed a *Chandra* ACIS observation of HESS J1640-465 taken in May 2007 with an effective exposure time of 26.4 ks. Employing the sub-arcsecond scale spatial resolution of *Chandra* Lemiere et al. (2009) performed a spatially resolved spectral analysis of the near field of XMM J164045.4-463131 and found that the putative pulsar spectrum is very hard with photon index -1.1 ± 0.4 heavily absorbed through a Hydrogen column N_H of 1.4×10^{23} cm^{-2}. The unabsorbed 2–10 keV flux of the putative pulsar was 1.5×10^{-13} erg/cm^{2}s. The compact PWN has a softer photon index of -2.5 ± 0.3 and unabsorbed 2–10 keV flux of 4.2×10^{-13} erg/cm^{2}s, while the extended PWN is somewhat steeper with index -2.7 ± 0.5 and has an unabsorbed 2–10 keV flux of 4.6×10^{-13} erg/cm^{2}s.

Observations with *NuSTAR* (3-79 keV) of HESS J1640-465 on June 22, 2013 and Sept. 29, 2013 for 48.6 and 89.9 ks, respectively, revealed eventually the pulsed nature of XMM J164045.4-463131 (Gotthelf et al. 2014). An energetic, $\dot{E} \simeq 4.4 \times 10^{36}$ erg/s, 206 ms pulsar was found with a characteristic age of 3.35 kyr. The pulsar shows a single pulse - relatively sharp compared to a sinusoid - profile in the 3-25 keV band (see Gotthelf et al. 2014, and also Fig. 27 panel q), and thus can be considered as a soft γ-ray

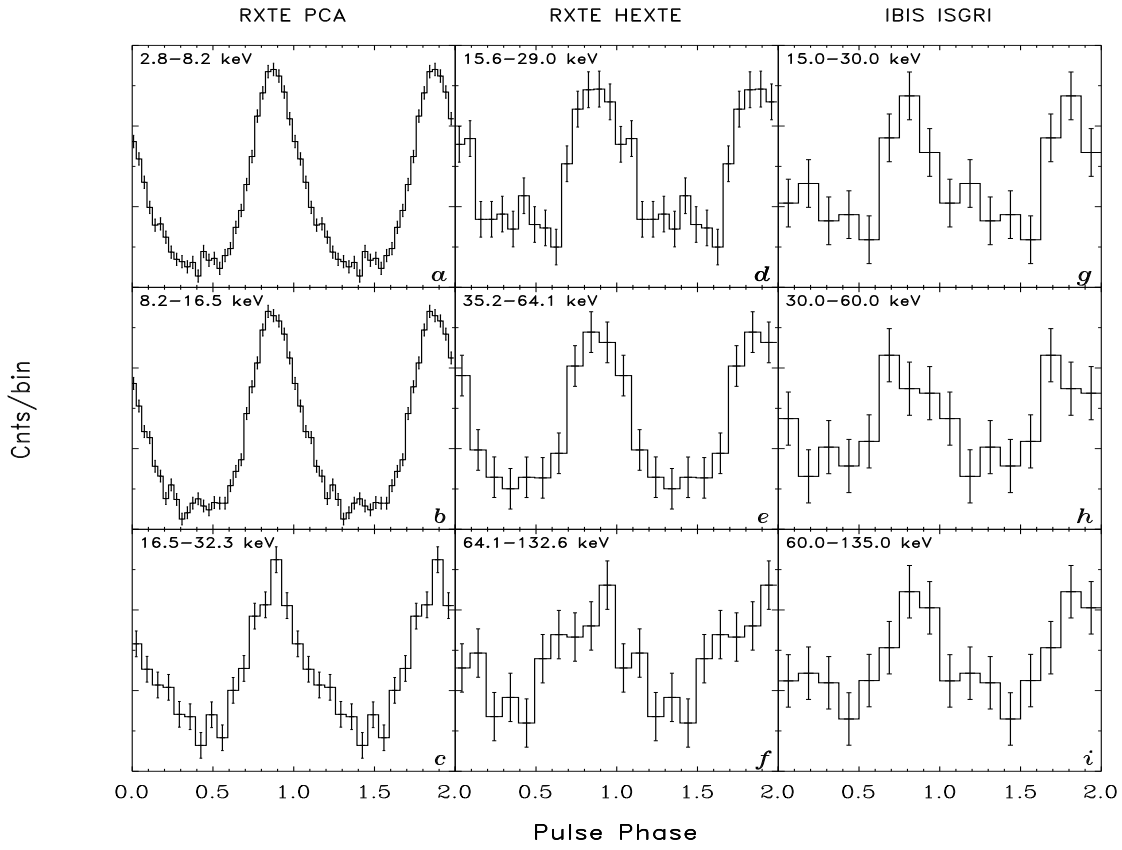

Figure 10. PSR J1811-1925; pulse profiles in various energy bands for *RXTE* PCA (panels a–c), *RXTE* HEXTE (panels d–f) and *INTEGRAL* ISGRI (panels g–i). Pulsed emission has been detected up to ~ 135 keV.

pulsar. The pulsed fraction can be as high as $\sim 82\%$ taking into account both the 'normal' background and PWN contamination. The (total) pulsar spectrum combining *Chandra* and *NuSTAR* data, adopting an absorbed power-law model, has a hard photon index of $-1.3^{+0.9}_{-0.5}$ and an absorbed 2–10 keV flux of $(1.8 \pm 0.4) \times 10^{-13}$ erg/cm^{2}s, which translates to an unabsorbed 2–10 keV flux of $(3.63 \pm 0.81) \times 10^{-13}$ erg/cm^{2}s taking into account the very high Hydrogen column density N_H of $(1.8 \pm 0.6) \times 10^{23}$ cm^{-2}.

Gotthelf et al. (2014) also searched for pulsed high-energy γ-ray emission (> 100 MeV) using *Fermi* LAT data collected over a more than 5 years time period, but found no significant pulsed signal. In the spatial domain, however, the *Fermi* LAT data (first reported on by Slane et al. 2010) do show two distinct sources above 100 MeV in the region containing HESS J1640-465 (Lemoine-Goumard et al. 2014). In light of the new/updated findings of H.E.S.S. TeV measurements on HESS J1640-465 using all data collected between May 2004 and Sept. 2011 (H.E.S.S. Collaboration et al. 2014) and on the recently discovered (hard) nearby HESS J1641-463 (coincident with radio SNR G338.5+0.1), unnoticed using default detection techniques, but detected using much higher energy thresholds (Abramowski et al. 2014), Lemoine-Goumard et al. (2014) revisited the *Fermi* LAT data and reported a power-law spectrum with index $-1.99 \pm 0.04 \pm 0.07$ for HESS J1640-465, which smoothly connects to the TeV data points, and a soft power-law spectrum with index $-2.47 \pm 0.05 \pm 0.06$ for HESS J1641-463, requiring a significant hardening towards TeV energies. The new GeV/TeV data suggest that a significant part of the high-energy γ-ray emission from HESS J1640-465 originates from proton acceleration in the supernova remnant shell (H.E.S.S. Collaboration et al. 2014).

Castelletti et al. (2011) presented a high-resolution imaging study of the G338.3-0.0 supernova remnant at radio frequencies acquired by the Giant Metrewave Radio Telescope GMRT (235, 610 and 1280 MHz) and ATCA (1290 and 2300 MHz), and searched for a radio pulsar at 610 and 1280 MHz in a beam covering the XMM J164045.4-463131 location (coincident with PSR J1640-4631). This search yielded no radio pulsar counterparts and resulted in flux density upper limits of 2 and 1 mJy for 610 and 1280 MHz, respectively, at 8σ confidence level.

5.10 PSR J1811-1925

PSR J1811-1925 was discovered by Torii et al. (1997) during *ASCA* (0.5-10 keV) observations of G11.2-0.3, known to be a composite supernova remnant, proposed to be associated with the historical supernova of A.D. 386 (Vasisht et al. 1996). They found a 65 ms pulsar exhibiting a hard X-ray spectrum. Subsequent *ASCA* and *BeppoSAX* observations (Torii et al. 1999) allowed the measurement of the spin-down and yielded a characteristic age of 2.4×10^4 yr. No pulsed radio emission has so far been detected from the sky region containing the pulsar (Crawford et al. 1998). A high precision *Chandra* X-ray imaging observation (Kaspi et al. 2001) re-

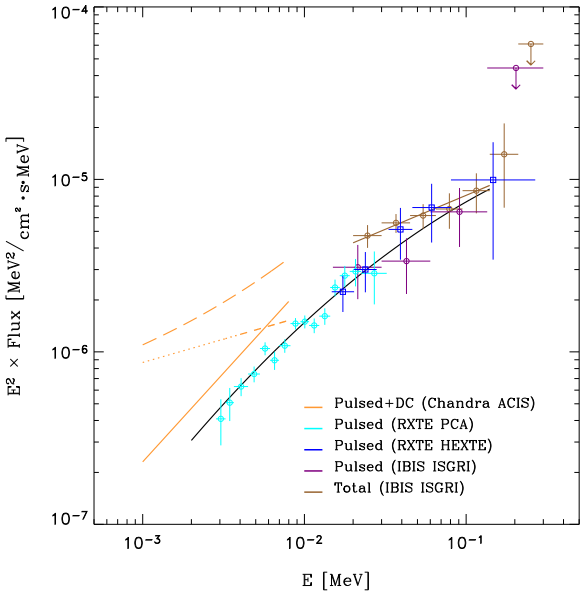

Figure 11. PSR J1811-1925; high-energy (1-300 keV; unabsorbed) total and pulsed spectra as derived from measurements by *Chandra* ACIS (1-7 keV; pulsar Pulsed plus DC (=total; orange solid); PWN (orange dotted); PWN plus pulsar (orange long dashed)), *RXTE* PCA (aqua) and HEXTE (blue; both pulsed) and *INTEGRAL* ISGRI (total (brown) / pulsed (purple)). The ISGRI total flux measurements still contain contributions from the PWN. The spectral measurements are generally consistent with reaching a pulsed fraction of 100% near 50 keV.

vealed at the very center of the SN-remnant the pulsar counterpart at R.A. $18^{\rm h}11^{\rm m}29\overset{\rm s}{.}22$, Decl. $-19^\circ25'27\overset{''}{.}6$ (Epoch J2000), embedded in a diffuse nebula (PWN). This provided strong evidence that the system is much younger than the characteristic age suggests. Assuming conventional spin-down with a constant magnetic field and breaking index *n* (from the assumed spin-down law: $\dot{\nu} \propto \nu^n$) both ages can only be reconciled if the pulsar was initially born with a spin period of ~ 62 ms unless the breaking index is unusally large.

Subsequent *RXTE* PCA X-ray monitoring over 992 days (March 8, 2002 – November 24, 2004; MJD 52341 – 53333) allowed us to generate phase coherent timing models (see Table 1) and using these to detect the pulsed signal up to $\sim$ 100 keV in *RXTE* HEXTE data (see also Roberts et al. 2004). A second *RXTE* PCA monitoring campaign was initiated on August 25, 2007 and ended on October 31, 2011 near the cessation of the *RXTE* mission. The data from this latter campaign are not included in this study.

We performed a timing analysis of *INTEGRAL* ISGRI data for the time span covering *INTEGRAL* revolutions 46-249 (February 28, 2003 – October 28, 2004; MJD 52698 – 53306), for which we derived accurate ephemerides (see Table 1). We found a 6.5σ signal for the 15-135 keV energy band showing a morphology consistent with that derived from *RXTE* PCA and HEXTE data. Pulse profiles in differential energy bands for *RXTE* PCA & HEXTE and *INTEGRAL* ISGRI are shown in Fig. 10. The significances (adopting Z_1^2-statistics) for a deviation from a uniform distribution are: $35.6\sigma, 35.9\sigma$ and 15.9σ for the *RXTE* PCA ranges 2.8-8.2, 8.2-16.5 and 16.5-32.3 keV (panels a–c), respectively; $11.2\sigma, 8.6\sigma$ and 4.4σ for the *RXTE* HEXTE ranges 15.6-29.0, 35.2-64.1 and 64.1-132.6 keV (panels d–f), respectively, and finally, $3.7\sigma, 3.6\sigma$ and 3.4σ for the *INTEGRAL* ISGRI ranges 15.0-30.0, 30.0-60.0 and 60.0-135.0 keV (panels g–i), respectively. We derived the pulsed excess counts in differential energy bands with pulse-profile fitting, which subsequently have been converted to photon fluxes taking into account the energy responses of the involved instruments. These (unabsorbed) pulsed flux measurements are shown in Fig. 11 as aqua (PCA), blue (HEXTE) and purple (ISGRI) data points, along with the best-fit "curved" power-law model (black) resulting from a combined fit. Pulsed fluxes derived from this fit for the 1–10 and 20–100 keV energy bands are $(2.21 \pm 0.47) \times 10^{-12}$ and $(1.22 \pm 0.21) \times 10^{-11}$ erg/cm^{2}s, respectively.

Roberts et al. (2003) presented detailed results from spatially resolved spectral analysis for the point-source (=pulsar) in G11.2-0.3, its PWN and other structures in its near environment using *Chandra* ACIS data. The power-law model fits to the spectral data of the pulsar (=total emission), PWN and their combination are shown in Fig. 11 for the 1–8 keV band. The listed absorbed (private communication M. Roberts) energy flux of the pulsar in the 1–10 keV band, $(2.82 \pm 0.12) \times 10^{-12}$ erg/cm^{2}s has been converted to its unabsorbed value of $(3.48 \pm 0.15) \times 10^{-12}$ erg/cm^{2}s using the estimated column density N_H of 2.22×10^{22} cm^{-2} . Using our value for the pulsed flux, the pulsed fraction in the 1–10 keV band becomes 0.64 ± 0.14.

In the imaging domain we detected soft γ-ray emission up to $\sim$ 150 keV using archival data (*INTEGRAL* revolutions 46-495; February 28, 2003 – October 5, 2006, 11.35 Ms GTI exposure; this work; see also e.g. Bird et al. 2007; Dean et al. 2008). The total (= pulsed plus unpulsed from PSR J1811-1925 and DC from the PWN and SN-remnant) emission spectrum of this source for energies above 20 keV can be described by a power-law model with a (hard) index of -1.61 ± 0.15 and a 20-100 keV flux of $(1.54 \pm 0.12) \times 10^{-11}$ erg/cm^{2}s (see Fig. 11; brown data points). This is consistent with the index and flux derived by Dean et al. (2008), who used slightly less *INTEGRAL* exposure on the source. The pulsed fraction in the 20–100 keV band is 0.79 ± 0.15, and above $\sim$ 50 keV the pulsed PCA/HEXTE/ISGRI spectrum is consistent with the total ISGRI spectrum, thus the pulsed fraction becoming consistent with 100% for energies beyond. Therefore, the spectrum of the PWN (and SN-remnant) above $\sim$ 50 keV has to bend down.

At GeV energies and in the TeV domain no (pulsed) source with a plausible association has been detected in the vicinity of PSR J1811-1925 (Aharonian et al. 2007; Nolan et al. 2012; Abdo et al. 2013).

5.11 PSR J1813-1246

PSR J1813-1246 was detected in blind frequency searches using *Fermi* LAT data by Abdo et al. (2009d). With a pulse period of 48.1 ms and characteristic age of 43 kyr it is the second most energetic ($L_{sd} = 6.3 \times 10^{36}$ erg/s) (radio-quiet) blind-search pulsar. It showed a double peaked γ-ray (> 100 MeV) pulse profile with a peak separation of $0.485(3)$ and with bridge emission between the peaks. Two timing glitches have been detected in the γ-ray data (Ray et al. 2011b; Marelli et al. 2014b). A plausible X-ray counterpart to PSR J1813-1246 was found in a short *Swift* XRT observation (Abdo et al. 2009d; Ray et al. 2011b).

In a deep 108.9 ks *XMM-Newton* observation performed on March 10, 2013 with the EPIC-pn operated in small window mode highly significant pulsations were found with a lightcurve consisting of two peaks separated ~ 0.5 in phase lagging the γ-ray one by ~ 0.25 in phase (Marelli et al. 2014b). The pulsed emission is

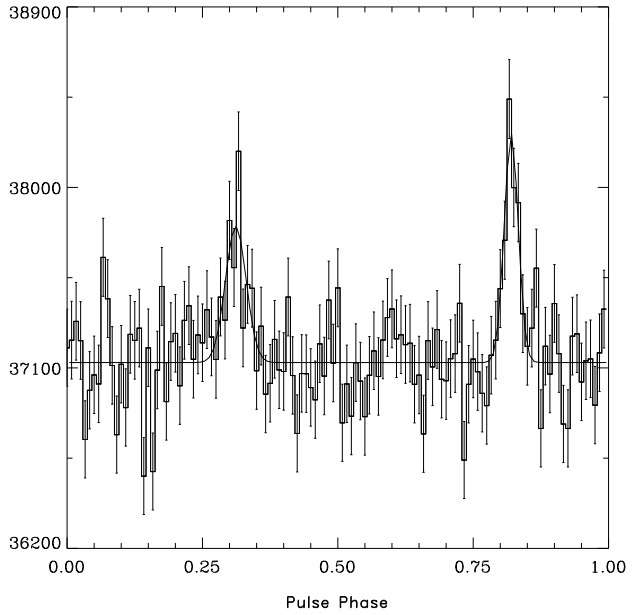

Figure 12. PSR J1813-1246; *RXTE* PCA 120 bins pulse profile for the 1.9-29.3 keV band. A double Gaussian plus background fit is superposed, yielding a 10.5σ improvement with respect to a flat background description.

very hard with a photon index of -0.85(3) and the pulsed fraction is very high, $96 \pm 3\%$. We re-analysed the *XMM-Newton* EPIC-pn data and confirmed the findings of Marelli et al. (2014b). The unabsorbed 2–10 keV pulsed flux is $(0.96 \pm 0.015) \times 10^{-12}$ erg/cm^{2}s. The 8-12 keV EPIC-pn pulse profile of PSR J1813-1246 is shown in Fig. 27 panel r. We verified that very significant (12.1σ) pulsed emission is detected above 10 keV.

In the on-line version of the *INTEGRAL* IBIS 9-year Galactic hard X-ray survey (Krivonos et al. 2012, see also *http://hea.iki.rssi.ru/integral/nine-years-galactic-survey*) the 35-80 keV map of the Galactic bulge region (6.78 Ms exposure time) shows a 3.1σ excess at the location of PSR J1813-1246 representing a (total) flux of 0.43 ± 0.14 mCrab, which corresponds to $(1.05 \pm 0.34) \times 10^{-6}$ ph/cm^{2}s keV.

The hardness of the pulsed spectrum in the *XMM-Newton* bandpass and the detection of a point-source in the 35-80 keV *INTEGRAL* ISGRI band makes it very plausible that PSR J1813-1246 shows pulsed emission at detectable levels in the hard X-ray/soft γ-ray band. In the X-ray archives we found a 26.8 ks *RXTE* PCA observation (obs. id. 20090; taken in *E_125us_64M_0_1s* event mode with a $\sim$ 122.07μs time resolution, and all PCU's operational) performed on Nov. 7, 1997 targeting at GRO J1814-12, which has PSR J1813-1246 in the field of view at an off-axis angle of $23.'7$. Also, the much stronger LMXB 4U 1812-12 was in the field of view at an off-axis angle of $24.'3$ yielding increased (non-Gaussian) background levels in timing searches of PSR J1813-1246 in PCA data. In spite of the more than 11 years time lapse between the detection as (blind search) γ-ray pulsar and the *RXTE* observation a restricted period search (Z^2_8 test, which turned out to be optimal for the EPIC-pn data, for each trial frequency) around the predicted pulse period adopting the timing parameters as given in supplementary material provided by Abdo et al. (2013) yielded a highly significant pulsed signal, 8.5σ single trial, at 20.8047193(8) Hz (epoch MJD 50759) for the 1.9-29.3 keV band. Taken into account the number of scan steps of $\sim$ 830 independent Fourier steps the detected signal remains still very significant.

The 1.9-29.3 keV PCA pulse profile with superposed the best fit double Gaussian model is shown in Fig. 12. The phase separation between the peaks (peak 2 is the most dominant pulse at phase $\sim$ 0.82 in Fig. 12) $\Delta\Phi_{2-1}$ is 0.509 ± 0.004, consistent with the *XMM-Newton* value of 0.5043 ± 0.0009 (see Marelli et al. 2014b). The X-ray pulses, however, are much narrower, $\sigma_1 = 0.019 \pm 0.005$ and $\sigma_2 = 0.013 \pm 0.002$, than observed by XMM EPIC-pn with $\sigma_1 = 0.0330 \pm 0.0008$ and $\sigma_2 = 0.0305 \pm 0.0005$, because of the much better time resolution of the PCA observation with repect to the *XMM-Newton* observation, i.e. ~ 122.07 μs versus ~ 5.7 ms.

For the differential PCA energy bands, 3.9-7.9, 7.9-15.1 and 15.1-33.5 keV, we obtained the following Z^2_8-test significances, $5.3\sigma, 4.3\sigma$ and 3.3σ, respectively, proving PSR J1813-1246 to be a soft γ-ray pulsar. Unfortunately, the statistics are too poor to derive reliable pulsed flux estimates for these PCA energy bands.

The spectrum of the pulsed emission of PSR J1813-1246 is shown in the right panel of Fig. 28 (red-red orange). The X-ray data points are derived in this work from the EPIC-pn data (template fitting per energy band, followed by a spectral fit adopting a power-law photon flux model), while the high-energy γ-ray spectral points and fit are adopted from Abdo et al. (2013). This figure also includes the 35-80 keV total flux measurement of *INTEGRAL* ISGRI. The latter flux is a good estimate of the pulsed flux, because the pulsed fraction is consistent with 100%.

No TeV counterpart has been detected so far for PSR J1813-1246.

5.12 PSR J1813-1749: The pulsar associated with HESS J1813-178/SNR G12.82-0.02/IGR J18135-1751

Aharonian et al. (2005) announced the detection of eight unknown VHE sources during scans of the inner galactic plane with the H.E.S.S. telescope from May to July 2004. One of these new sources is the compact TeV source HESS J1813-178 embedded in a highly obscured region, which lacked at the time of discovery plausible counterparts at other wavelength and was classified as a "dark" particle accelerator. Soon after its detection as TeV source a soft γ-ray counterpart, IGR J18135-1751 (Ubertini et al. 2005), of HESS J1813-178 was discovered. Moreover, radio observations revealed the presence of non-thermal radio emission from a young shell-type SNR G12.82-0.02 with a diameter of $\sim 2.'5$ (Brogan et al. 2005). These properties do conjecture that we are dealing with a PWN powered by a so far undetected energetic pulsar.

Follow-up X-ray observations with *Chandra* (Helfand et al. 2007) and *XMM-Newton* (Funk et al. 2007) indeed revealed the putative pulsar and its nebula, although pulsations still had to be detected, because the operation modes of the involved X-ray instruments had insufficient time resolution to detect pulsations at time scales of 10–100 milli-second.

A 30 ks *Chandra* ACIS-I image of the near environment of G12.82-0.02 is presented in Fig. 13 and shows the extraction regions used in Helfand et al. (2007) to derive the spectra of the (putative) pulsar (circular aperture of $2''$ in radius centered on the point source), the inner pulsar wind nebula ($6'' \times 8''$ elliptical region excluding the point source region) and the outer pulsar wind nebula encompassing the bulk of the nebula extent (a $80''$ radius circular region offset from the point source excluding the point source and the inner nebula). Fitting absorbed power-law models to the various components (Helfand et al. 2007) yielded for the outer PWN a Hydrogen column density N_H of $(9.8 \pm 1.2) \times 10^{22}$ cm^{-2} (90% confidence), consistent with the *XMM-Newton* findings (Funk et al.

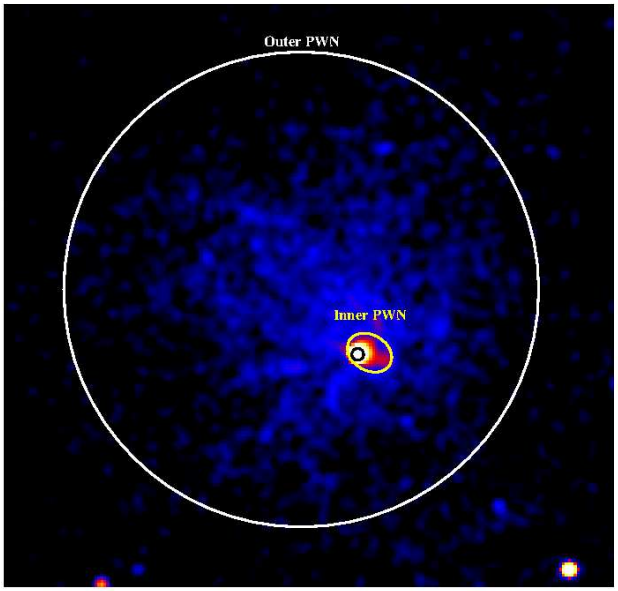

Figure 13. *Chandra* ACIS-I image (30 ks) of G12.82-0.02 showing clearly the point-source, the (putative) pulsar PSR J1813-1749 (black $2''$ circle), the inner PWN confined within a $6'' \times 8''$ (yellow) elliptical region and the outer PWN confined to a $80''$ circular region offset from the point source (large white circle).

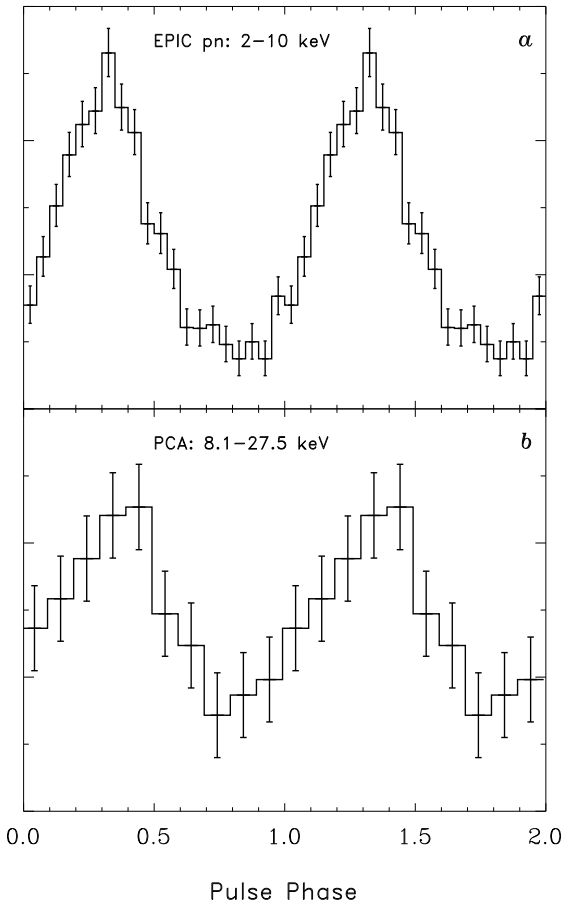

Figure 14. PSR J1813-1749; the upper panel shows the pulse profile for the 2–10 keV band as measured by *XMM-Newton* EPIC pn during a 98 ks observation performed in small-window mode. In the lower panel the *RXTE* PCA lightcurve of PSR J1813-1749 is shown for the 8.1-27.5 keV band ($Z_1^2 = 4.8\sigma$) obtained from dedicated HESS J1813-178 observations performed about 500 days before the discovery of its pulsed nature.

2007), indicating highly absorbed emission. Both the pulsar and the outer PWN show hard power-law indices of about -1.3, while the inner nebula has even a harder index of -0.4 (see e.g. the spectral compilation in Fig. 16 for the fits of the inner PWN, total pulsar emission and its combination as dotted, solid and dashed orange lines, respectively), a clear manifestion of Synchrotron cooling effects. The total flux in the nebula is about 4.3 times larger than that measured for the point-source.

Targeting at the central point source in G12.82-0.02 Gotthelf et al. (2009) finally discovered 44.7 ms pulsations analysing a 98 ks *XMM-Newton* observation performed on March 27, 2009, with the EPIC pn operating in small-window mode providing a time resolution sufficient to detect timing signals up to $\sim$ 125 Hz. Follow-up observations with *Chandra* (ACIS-S3 Continuous Clocking; Feb. 12, 2012) and *XMM-Newton* EPIC pn (small-window mode; March 13, 2011) made it possible to derive a reliable period derivative estimate of PSR J1813-1749, yielding a characteristic age of 5.6 kyr and a spin-down power of 5.6×10^{37} erg/s (Halpern et al. 2012).

We re-analyzed the EPIC pn data of the 98 ks *XMM-Newton* observation (obs. id. 0552790101), performed in small-window mode, with as main goal to derive the pulsed spectrum (not published so far) and from this the pulsed fraction. The pulsed signal was clearly visible at the predicted frequency (Gotthelf et al. 2009) and the pulse profile for the 2–10 keV energy band is shown in the upper panel of Fig. 14. Below $\sim$ 2 keV no pulsed signal can be detected. The 21.1σ 2–10 pulse profile was fitted with a truncated Fourier-series using the fundamental and one harmonic, and the model has subsequently been used in the extraction process of pulsed excess counts. These pulsed excess counts have been converted to pulsed flux values adopting an absorbed power-law model in a forward folding fit procedure using response information taking into account the $15''$ extraction radius.

For comparison purposes with the spectral results determined by Helfand et al. (2007) for the total point source emission we fixed the Hydrogen column density N_H to 9.8×10^{22} cm^{-2}. We derived a photon index of -1.30 ± 0.03 and an unabsorbed/absorbed 2–10 keV pulsed flux of $(9.2 \pm 0.45) \times 10^{-13}/(5.8 \pm 0.82) \times 10^{-13}$ erg/cm^{2}s. This translates, using the absorbed total 2–10 keV flux value of 1.3×10^{-12} erg/cm^{2}s as derived by Helfand et al. (2007), to a (2–10 keV) pulsed fraction of 0.45 ± 0.06, consistent with that estimated by Gotthelf et al. (2009); Halpern et al. (2012). The EPIC pn pulsed flux measurements and its best fit are shown in the spectral compilation depicted in Fig. 16 as dark-orange/red datapoints and solid line, respectively.

We also performed a spatial analysis of the EPIC pn small-window mode data by fitting (adopting Poissonian statistics) a model composed of the EPIC pn PSF, centered on the pulsar's X-ray counterpart, and a (locally) flat background model to the measured 2d-event distribution (extraction radius $30''$) for every required energy band. Because the EPIC pn PSF is worse than that of *Chandra* ACIS-I the extracted total counts are composed of the total emission component of the pulsar and a contribution from the inner pulsar wind nebula, which can not be resolved by XMM.

Initially, we fitted the measured count spectrum with an absorbed power-law model with N_H fixed to 9.8×10^{22} cm^{-2}. However, this rendered a rather poor fit ($\chi^2_{r,17-2} = 28.90/15 = 1.93$;

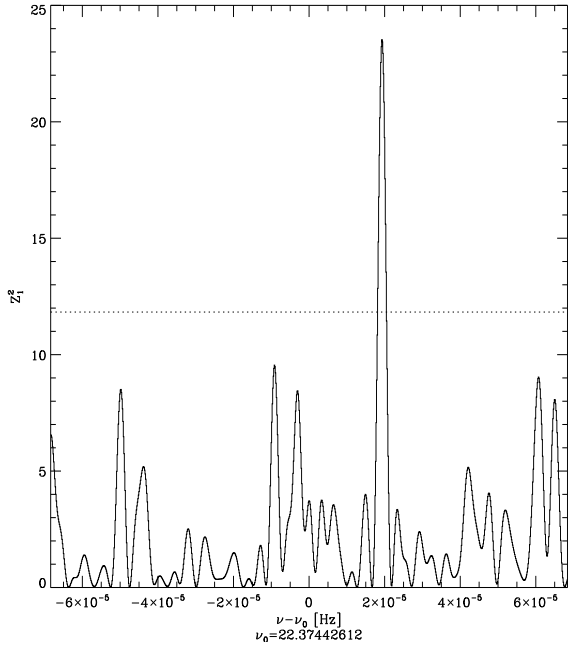

Figure 15. PSR J1813-1749; periodogram showing Z_1^2 versus trial frequency in a 50 IFS window around the predicted frequency ν_0 using events from PCU-2 with PHA in the range 5–50 and employing all detection layers. A 4.6σ single trial peak maximum is found 6.8 IFS shifted from the prediction, resulting in an overall detection significance of 3.7σ. The dotted line indicates the 3σ confidence level for a single trial.

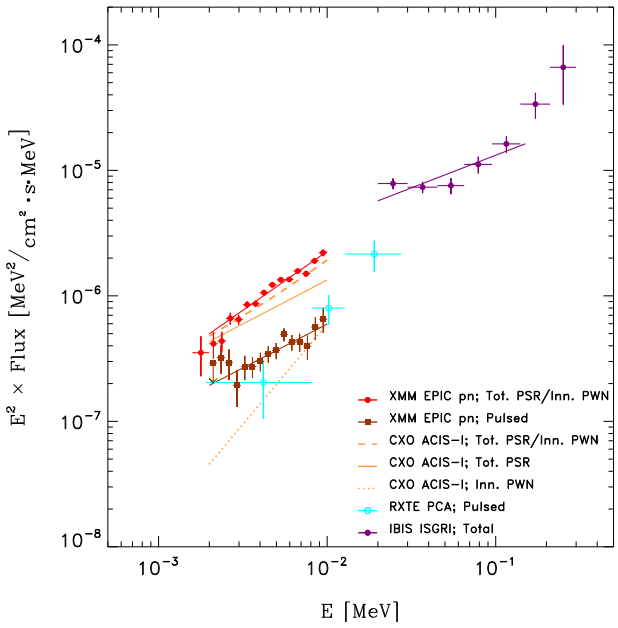

Figure 16. PSR J1813-1749; unabsorbed high-energy spectrum of the pulsed emission along with that of its inner PWN as obtained by CXO ACIS-I (2–10 keV; inner PWN, total pulsar and its combined emission; Helfand et al. 2007), *XMM-Newton* EPIC pn (2–10 keV; pulsed, total pulsar plus inner PWN; this work), *RXTE* PCA (2–30 keV; pulsed; this work) and *INTEGRAL* ISGRI (20–300 keV; total=total pulsar plus inner PWN and whole PWN; this work). An absorbing Hydrogen column density of 9.8×10^{22} cm^{-2} has been assumed for all X-ray measurements to facilitate the comparison of CXO ACIS-I and *XMM-Newton* EPIC pn spectral results.

1.5% probability that a good model gives such a χ^2). The flux measurements and its best fit, adopting $N_H \equiv 9.8 \times 10^{22}$ cm^{-2}, are shown in Fig. 16 as red datapoints and solid line, respectively. We also left N_H free in the absorbed power-law fit and obtained a good fit with $\chi^2_{r,17-3} = 18.34/14 = 1.31$ yielding a N_H of $(11.7 \pm 0.35) \times 10^{22}$ cm^{-2}, slightly higher, but still consistent with the value derived by Helfand et al. (2007) using *Chandra* ACIS-I data. The unabsorbed / absorbed 2–10 keV flux was $(3.30 \pm 0.05) \times 10^{-12}/(1.94 \pm 0.11) \times 10^{-12}$ erg/cm^{2}s and the photon-index -1.31 ± 0.01. The absorbed 2–10 keV flux value is comparable with the sum of the point source - and inner nebula flux of $\sim 1.7 \times 10^{-12}$ erg/cm^{2}s as given in Helfand et al. (2007).

We also revisited PCA/HEXTE data from a dedicated *RXTE* observation of HESS J1813-178 (observation identifier 93022) performed during Nov. 16–20, 2007 (about 500 days before the detection of the pulsed nature) with only one operational PCU and at a $28\farcm3$ offset angle from PSR J1813-1749, thereby considerably reducing the PCA overall sensitivity. The availability of an (incoherent) ephemeris (Halpern et al. 2012) with a sufficiently accurate period derivative made a restricted period search around the predicted (backwards extrapolated) pulse frequency value feasible.

Selecting PCA events with PHA values in the range 5–50 ($\sim 2-20$ keV) using all detection layers from PCU-2, the only operating unit during the 4-days covering observation (MJD 54420.101-54424.332) of about 125 ks, this search yielded a 4.6σ single trial peak shifted 6.8 Independent Fourier Steps (IFS$= 1/\tau$, in which τ is the full time stretch of the observation) from the prediction. Taking into account the number of search steps (50 IFS) this results in an overall detection significance of 3.7σ. The periodogram covering 50 IFS and showing Z_1^2 versus trial frequency near the predicted frequency, is depicted in Fig. 15. We oversampled, for display purposes, one IFS by a factor of 20 to follow the peak structure in detail. This detection of pulsed emission by the PCA at a frequency shifted marginally[6] from the prediction is very plausible, because (W3)PIMMS[7] predicts for the PCA with *one* operational PCU at an offset of about $30'$, reducing the source count rate by $\sim 50\%$, an observation time of 111 ks to reach a 5σ signal in the 0-49 PHA range given the 2–10 keV pulsed flux measured by XMM EPIC pn.

We derived pulsed excess counts for three broad PCA energy bands (see e.g. panel b of Fig.14 for the 8.1-27.5 keV lightcurve) by (XMM EPIC pn) template fitting and converted these to flux values (see Fig. 16; aqua data points) using proper response information and adopting an absorbed power-law model with N_H fixed to 9.8×10^{22} cm^{-2}. In HEXTE ($\gtrsim 15$ keV) data the pulsed emission could not be detected.

In the soft γ-ray band we obtained spectral information on the total emission of PSR J1813-1749 from the *INTEGRAL* ISGRI skymaps produced in seven differential energy bands. These skymaps were centered on PSR J1811-1925 (see Section 5.10), which is only $1\fdg7$ away from PSR J1813-1749. The flux measurements are shown as purple data points in Fig. 16. Fitting a power-law model we derived a photon index of -1.48 ± 0.08 and a 20–100

[6] The *incoherent* ephemeris given by Halpern et al. (2012) does not contain a $\ddot{\nu}$ value, and young pulsars often show glitches making precise predictions impossible given the 500 days back extrapolation.

[7] Portable, Interactive Multi-Mission Simulator; a HEASARC tool to convert count rates/fluxes observed for one high-energy instrument into that for another one, adopting a (photon) spectral model and absorbing Hydrogen column. Online documentation can be found at *http://heasarc.gsfc.nasa.gov/docs/software/tools/pimms.html*.

keV flux of $(2.30 \pm 0.13) \times 10^{-11}$ erg/cm^{2}s, consistent with the value given by Ubertini et al. (2005). Note, that the ISGRI fluxes, due to the lack of resolving power at arcsecond scales, represent the combined emission from the pulsar (pulsed and unpulsed), the inner PWN and outer PWN.

In the hard γ-ray band no pulsed emission from PSR J1813-1749 has been detected by the *Fermi* LAT instrument (Abdo et al. 2013).

Finally, in the radio-band no pulsed emission has been detected so far at 1374 MHz (Helfand et al. 2007) using the ATNF Parkes telescope and at 2 GHz (Halpern et al. 2012) using the NRAO Green Bank Telescope (GBT) telescope, rendering one of the deepest flux upper limits obtained so far for a young radio pulsar (< 0.006 mJy at 2 GHz, equivalent to < 0.01 mJy at 1.4 GHz).

5.13 PSR J1838-0655 / AX J1838.0-0655

The detection of soft γ-ray emission up to ~ 300 keV from the *ASCA* source AX J1838.0-0655 has been reported by Malizia et al. (2005) using *INTEGRAL* ISGRI data. Its location made an association with TeV source HESS J1837-069 (Aharonian et al. 2005) plausible, and thus suggests a pulsar/PWN origin. This was indeed confirmed by Gotthelf et al. (2008), who detected a young (23 kyr) 70.5 ms pulsar in the *INTEGRAL* ISGRI error circle using *RXTE* PCA data. Its spin-down rate, energetics and spectra were reported by Kuiper et al. (2008). So far, no radio emission associated with the pulsar in AX J1838.0-0655 has been reported (see e.g. Sect. 5 of Malizia et al. 2005, who report a flux limit of 1-2 mJy at 1.4 GHz).

Since its identification as a pulsar early 2008 with *RXTE* AX J1838.0-0655 has been monitored up to December 6, 2010. We have made accurate phase-coherent timing models (see Table 1) for the period February 17, 2008 – December 6, 2010, during which a large timing glitch has been detected, occuring somewhere between MJD 55002 and MJD 55018 (June 20 – July 6, 2009) with a fractional frequency ($\Delta\nu/\nu$) jump size of $(1.55 \pm 0.07) \times 10^{-6}$ (Kuiper & Hermsen 2010).

Applying these ephemerides in a timing study of *RXTE* PCA and HEXTE data collected during observation programs P93429 and P94303 (February 17, 2008 – December 5, 2009; MJD 54513 – 55170) resulted in the pulse phase diagrams shown in Fig. 17a–f. The screened (and PCU-detector break-down cleaned) exposure times for units 0–4 are: 60.34, 69.24, 256.60, 45.45 and 72.21 ks, respectively. For HEXTE the deadtime-corrected on-exposure times for the same period are 163.13 and 85.51 ks, for cluster-0 (staring on-source) and cluster-1 (rocking), respectively. Below ~ 16 keV a structured broad pulse is apparent.

Application of the same timing models in a timing analysis of ISGRI data, spanning *INTEGRAL* revolutions 592 - 910 (August 19, 2007 – March 29, 2010; MJD 54331 – 55284[8]; 3.3 Ms of screened vignetting corrected effective on-axis exposure), revealed a 12.1σ pulsed signal in the 15-150 keV band. The significance of the pulsed signal above 50 keV is still 7.2σ (see Fig. 17h).

[8] For the period August 19, 2007 – February 17, 2008 (MJD 54331-54513) the first *RXTE* PCA ephemeris of AX J1838.0-0655 (see Table 1) is used for ISGRI data taken before the monitoring of AX J1838.0-0655 commenced with *RXTE* (thus in backwards extrapolation). The pulsed signal (with proper alignment) could easily be recognized in the ISGRI data during this period not covered by the validity interval of the first ephemeris. This proves that the ephemeris is also valid across a larger (backwards extended) time period.

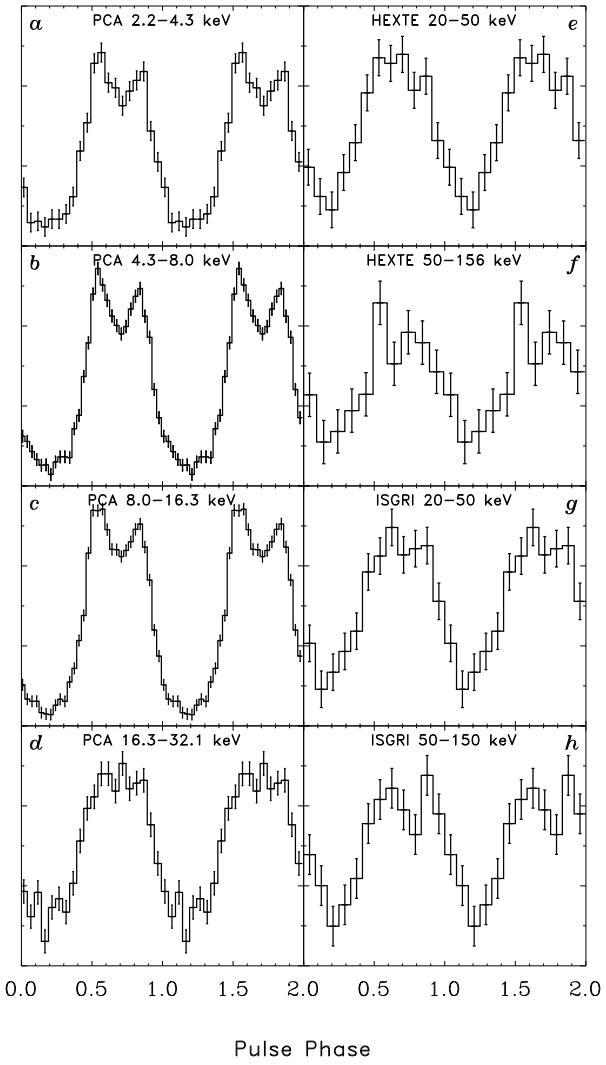

Figure 17. AX J1838.0-0655; pulse profiles in various energy bands for *RXTE* PCA (panels a–d), *RXTE* HEXTE (panels e–f) and *INTEGRAL* ISGRI (panels g–h). Pulsed emission has been detected up to ~ 150 keV.

From the *RXTE* PCA/HEXTE and *INTEGRAL* ISGRI pulse-phase histograms, we have extracted the pulsed excess counts through template fitting, and converted these to photon-flux values adopting (for the PCA range) an absorbing Hydrogen column N_H of 5.4×10^{22} cm^{-2} (see e.g. Anada et al. 2009; Kargaltsev et al. 2012). These pulsed flux measurements are shown in Fig. 18. The combined *RXTE* PCA/HEXTE and *INTEGRAL* ISGRI pulsed flux measurements could be accurately fitted across the 3-150 keV band by a "curved" power-law model (a parabola in a $(\log(\nu F_\nu)$ vs. $\log(\nu))$ spectral representation) with a photon-index of $1.36(2)$ at 14.2 keV (this model is indicated by a black solid line in Fig.18). Pulsed flux estimates (unabsorbed) are $(6.00 \pm 0.33) \times 10^{-12}$ erg/cm^{2}s for the 2–10 keV, and $(2.53 \pm 0.18) \times 10^{-11}$ erg/cm^{2}s for the 20–100 keV band, respectively.

Our derived value for the 2–10 keV unabsorbed flux for the pulsed emission is significantly less than the value of 9.00×10^{-12} erg/cm^2 determined by Gotthelf et al. (2008), who analysed much less *RXTE* PCA data. However, the spectral shape the latter authors derived for the PCA band is compatible with our "curved" spectral model in the overlapping region.

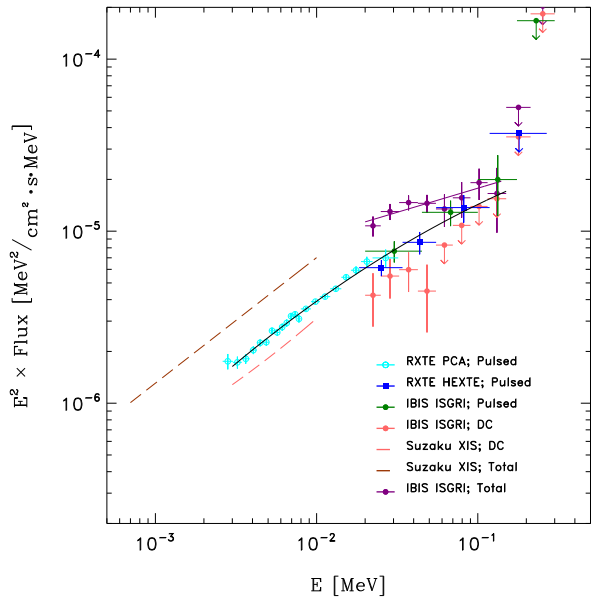

Figure 18. AX J1838.0-0655; high-energy (0.7-300 keV) total and pulsed spectra as derived from measurements by *Suzaku* XIS (total 0.7-10 keV; dashed brown), *RXTE* PCA (pulsed 2-30 keV; aqua), *RXTE* HEXTE (pulsed 15-150 keV; blue) and *INTEGRAL* ISGRI (20-300 keV; total (purple) / pulsed (green)). The best fit model to the pulsed flux measurements is superposed as solid black line. The red dashed line and data points are flux estimates for the underlying PWN, which suggest a break/bend near 50 keV.

We also derived total flux measurements of AX J1838.0-0655 for energies above 20 keV from an *INTEGRAL* ISGRI imaging analysis of the Scutum region (AX J1838.0-0655 was in the field of view of PSR J1846-0258 (see Sect. 5.14) for which we reported the details in Kuiper & Hermsen (2009)), combining observations performed between *INTEGRAL* revolutions 49 and 441 (March 10, 2003 – May 27, 2006; covering a considerably longer time span than Malizia et al. (2005), who used data from Revs 46 to 186). Note that for this period no valid ephemerides exist and thus timing results are lacking. The ISGRI total flux measurements (see Fig.18 for data points and best fit) can be described by a power-law with a photon-index of -1.72 ± 0.07, consistent with the value of -1.66 ± 0.23 obtained by Malizia et al. (2005), and a 20–100 keV (unabsorbed) energy flux of $(3.69 \pm 0.21) \times 10^{-11}$ erg/cm^{2}s. The 20–300 keV flux is $(7.35 \pm 0.39) \times 10^{-11}$ erg/cm^{2}s, slightly less than the value of 9×10^{-11} erg/cm^{2}s from Malizia et al. (2005). The pulsed fraction in the 20–100 keV band is $69 \pm 6\%$.

In the soft X-ray band (< 10 keV) spectral information for AX J1838.0-0655 and its PWN has been derived from *Chandra* ACIS (Gotthelf et al. 2008), *Suzaku* XIS (Anada et al. 2009) and *XMM-Newton* EPIC MOS-2 (Kargaltsev et al. 2012) data. The *Suzaku* XIS spectral analysis of the pulsar plus its surrounding PWN used an extraction radius of $3'$ encompassing $\sim 90\%$ of the source photons, while the *XMM-Newton* EPIC MOS-2 spectral analysis utilized a $40''$ extraction radius centered on the source. Both (unabsorbed) flux measurements in the 2–10 keV band, converted from the 0.7–10 keV flux value of $(13.2^{+0.8}_{-0.6}) \times 10^{-12}$ erg/cm^{2}s for the XIS and from the 1–11 keV flux of $(12.4 \pm 2) \times 10^{-12}$ erg/cm^{2}s for the EPIC MOS-2, are consistent within uncertainties, $(10.7^{+0.6}_{-0.5}) \times 10^{-12}$ erg/cm^{2}s and $(9.7 \pm 1.6) \times 10^{-12}$ erg/cm^{2}s, respectively. Moreover, the derived photon indices for the XIS and MOS-2 measurements of -1.27 ± 0.11 and $-1.25^{+0.30}_{-0.14}$, respectively, and absorbing Hydrogen column densities of $(5.4 \pm 0.5) \times 10^{22}$ cm^{-2} and $(5.2^{+1.0}_{-0.8}) \times 10^{22}$ cm^{-2}, respectively, are consistent.

In a 20 ks *Chandra* ACIS-I observation of HESS J1837-069, as reported by Gotthelf et al. (2008), AX J1838.0-0655 and its PWN were detected $5'.25$ off-axis (from I3 aim-point) degrading considerably the image quality. These authors performed spatially resolved spectral analyses for the compact central source - the pulsar - selecting events from a $5'' \times 7''$ elliptical aperture centered on the source peak, and the PWN selecting events from a $1'$ radius aperture centered at a location slightly offset from the compact source, while excluding a $7'' \times 9''$ elliptical aperture around the compact source. They obtained an *extremely* hard spectrum for the compact source with a photon index of -0.5 ± 0.2 and unabsorbed 2–10 keV flux of 8.8×10^{-12} erg/cm^{2}s, and for the PWN a photon index of -1.6 ± 0.4 and unabsorbed 2–10 keV flux of 1.0×10^{-12} erg/cm^{2}s, both absorbed through a Hydrogen column of $(4.5 \pm 0.8) \times 10^{22}$ cm^{-2}. While the combined compact source and PWN unabsorbed flux of 9.8×10^{-12} erg/cm^{2}s is consistent with that derived by both *Suzaku* XIS and *XMM-Newton* EPIC MOS-2, the spectral shape does not! The cause of this discrepancy is not yet clear.

The spectral model of the total (pulsed plus DC) emission from AX J1838.0-0655 *and* its PWN, as derived by Anada et al. (2009), using *Suzaku* XIS data for energies below 10 keV (=consistent with *XMM-Newton* result) is shown in Fig.18 as a dashed brown line. The pulsed fraction in the 2–10 keV band is 0.56 ± 0.04, including the PWN contribution in the total emission. Thus the genuine pulsed fraction of AX J1838.0-0655 is larger than 56%.

We can estimate the spectrum of the underlying DC-component (0.7-150 keV), which (mainly) originates from the PWN, by subtracting the flux of the pulsed component from that of the total emission. These DC-component flux estimates are also shown in Fig. 18 as red line (< 10 keV) and data points (> 20 keV), and suggest that the PWN spectrum breaks/bends near 50 keV, providing clues on the magnetic field in the PWN (e.g. its averaged strength).

At GeV energies (> 100 MeV) no pulsed γ-ray emission has been detected so far from AX J1838.0-0655 in Fermi LAT data (Abdo et al. 2013). Lande et al. (2012), however, reported recently the detection of spatially extended emission in the 10-100 GeV band from a location positionally consistent with HESS J1837-069.

5.14 PSR J1846-0258

Gotthelf et al. (2000) reported the discovery of PSR J1846-0258 in *ASCA* and *RXTE* data. It is a "slow" radio-quiet pulsar, $P \sim 324$ ms, but it has the smallest characteristic age, $\tau \sim 723$ y, of all known pulsars. Its surface magnetic field strength of 4.9×10^{13} G is above the quantum critical field strength of 4.413×10^{13} G and this classifies the pulsar as a high-B-field pulsar. It is located at the centre of SN-remnant Kes 75 (Helfand et al. 2003) and shows up as a bright hard X-ray source surrounded by a diffuse PWN, also emitting hard X-rays. From *RXTE* monitoring data it was found that PSR J1846-0258 behaves as a very stable rotator (Livingstone et al. 2006). With *INTEGRAL* point-source emission has been detected up to ~ 200 keV (McBride et al. 2008; Kuiper & Hermsen 2009). Pulsed emission has been detected up to ~ 150 keV (Kuiper & Hermsen 2009). For details about the pulsed and total high-energy spectrum across the $\sim$ 2-300 keV band we refer to Kuiper & Hermsen (2009).

Kumar & Safi-Harb (2008) reported the detection of a dra-

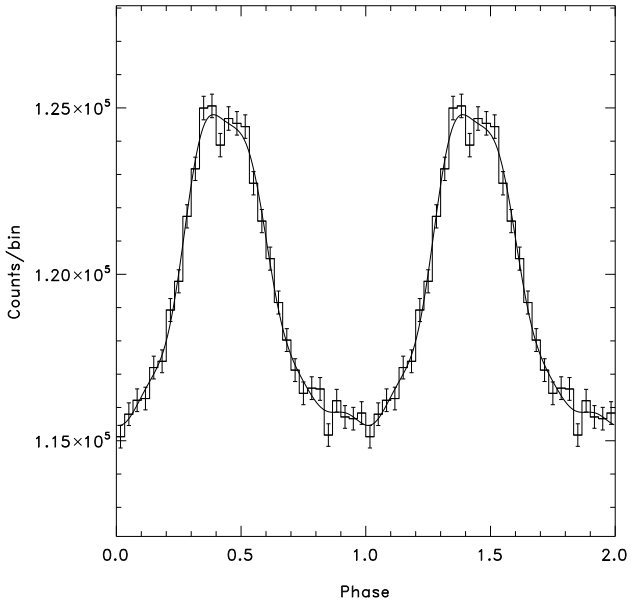

Figure 19. PSR J1849-0001; *RXTE* PCA 30 bins pulse profile for the $\sim 2-28$ keV band (PHA 5–65). Two cycli are shown for clarity. A truncated Fourier-series fit adopting 5 harmonics is superposed.

matic brightening of the pulsar in *Chandra* observations of Kes 75 during June, 7-12, 2006. The pulsar's spectrum softened considerably from a power-law spectrum with index $\Gamma \sim 1.32$ to 1.97. Gavriil et al. (2008) showed that during this radiative event, lasting for about 55 days, phase coherence in pulsar timing was lost due to an unprecedented increase of the timing noise. They also discovered five short magnetar-like bursts during the outburst. Kuiper & Hermsen (2009) discovered that the onset of the radiative event was accompanied by a strong glitch in the rotation behaviour of the pulsar probably triggering the sudden release of magnetic energy. Thus, this over many years very stably behaving source, both temporally and spectrally, exhibited suddenly magnetar-like behaviour during the outburst, after which it continued again as a young energetic rotation-powered pulsar. Therefore, this high-B-field pulsar PSR J1846-0258 might play a crucial role in revealing the connection between rotation-powered and magnetically powered pulsars (magnetars).

So far, the coherent signal from PSR J1846-0258 remains undetected at radio-frequencies with a 4σ upper-limit at 1.95 GHz ranging between 4.9 and 43 μJy, depending on the assumed duty cycle, and at 1400 MHz 27 μJy around the time of the X-ray bursts (Archibald et al. 2008). Also, Parent et al. (2011) have not detected the pulsed signal of PSR J1846-0258 for energies above 100 MeV, analyzing about 20 months of *Fermi* LAT data. However, the source HESS J1846-029 has been detected at TeV energies positionally consistent with Kes 75 with a (post-trial) significance of 8.3σ (Djannati-Ataï et al. 2008). Its TeV flux is at the level of $\sim 2\%$ of that of the Crab nebula, and its intrinsic extension is compatible with a point-like source.

5.15 PSR J1849-0001 / IGR J18490-0000

IGR J18490-0000 was discovered by Molkov et al. (2004) in a survey of the Scutum region, followed somewhat later by the detection of a faint TeV source, HESS J1849-000, coincident with the hard X-ray source (Terrier et al. 2008), suggesting the source to be a PWN powered by an energetic pulsar. *Swift*-XRT (Rodriguez et al. 2008, 12.3 ks) and *XMM-Newton* (Terrier et al. 2008, 10 ks) observations, both performed early 2006, revealed the X-ray counterpart of IGR J18490-0000 at soft X-rays and spectral analysis indicated a (very) hard spectrum from the somewhat blurred counterpart. Ratti et al. (2010) nailed down the location of IGR J18490-0000 to sub-arcsecond level by analyzing a 1.2 ks *Chandra* HRC observation performed on February 16, 2006. No obvious counterparts have been found at lower-energies in the *i'* and K_s bands (Ratti et al. 2010). Also, no radio counterpart could be detected in the 610 MHz band of the GMRT in a systematic follow-up on *INTEGRAL* sources, resulting in an upper-limit of 3.5 mJy (Pandey et al. 2006).

The true nature of IGR J18490-0000 was found by Gotthelf et al. (2011), who detected, pointing at the *Chandra* location, a young and energetic 38.5 ms pulsar using 112.3 ks of *RXTE* PCA exposure time, collected during dedicated observations spanning Nov. 25 - Dec. 15, 2010. Analysing also *XMM-Newton* EPIC pn and MOS data from an 11 ks observation performed on April 3, 2006 these authors estimated a pulsed fraction of $\sim 25\%$ for the 2–10 keV band. Gotthelf et al. (2011) found also evidence for extended emission around IGR J18490-0000 between $20''$ and $150''$ radius. The spectrum of this diffuse component was much softer, with photon index of -2.1 ± 0.3, than that of the point-source emission, with photon index of -1.1 ± 0.2, while it represents about 25% of the point source emission. Given the large Hydrogen column density N_H of $(4.3 \pm 0.6) \times 10^{22}$ cm^{-2} (Gotthelf et al. 2011) the diffuse emission could also be interpreted as a dust-scattered halo around a bright point source.

We (re)analysed the *RXTE* PCA/HEXTE data, collected during the dedicated observations, to obtain a phase coherent timing model and to derive the pulsed emission spectrum over the $\sim 3-150$ keV band. Through template cross-correlation we derived pulse arrival times (ToA's) and from these we determined a phase coherent timing solution, which is shown in Table 1. We produced pulse profiles of IGR J18490-0000 for all 255 PHA channels of the PCA, allowing contrary to Gotthelf et al. (2011) all detector layers, by phase folding (using the coherent timing model) the barycentered event arrival times that passed our selection criteria, and subsequently sort these on PHA. The pulse profile for the PHA band 5-65 in 30 bins ($\sim 2-27$ keV; $Z_1^2 = 2791.9 \equiv 35.2\sigma$) is shown in Fig. 19 and consists of one broad (somewhat structured) single pulse. A smoothed version of this profile (a truncated Fourier series adopting 5 harmonics; shown in Fig. 19 as solid line) has been used in the extraction procedure of the pulsed excess counts, because we do not see pulse morphology changes as a function of energy. The pulsed excess counts have subsequently been converted to pulsed fluxes in a forward folding procedure assuming an underlying power-law model absorbed through a column density N_H of 4.5×10^{22} cm^{-2} (see further in this section) yielding as best fit parameters an unabsorbed 2–10 keV pulsed flux of $(4.21 \pm 0.08) \times 10^{-12}$ erg/cm^{-2}s and a photon index of -1.37 ± 0.01. While the latter value is consistent with that derived by Gotthelf et al. (2011), our derived flux value is about 4 times larger than the value quoted by Gotthelf et al. (2011).

The HEXTE data from the (only active) staring cluster-A detectors have been screened adopting default screening conditions. The barycentered events have subsequently been folded using the coherent timing model to yield pulse profiles for all HEXTE PHA channels. Pulsed emission has been detected significantly up to ~ 60 keV (HEXTE band 31.0–60.1 keV; 4.8σ). Pulsed excess counts in various energy bands have been determined through tem-

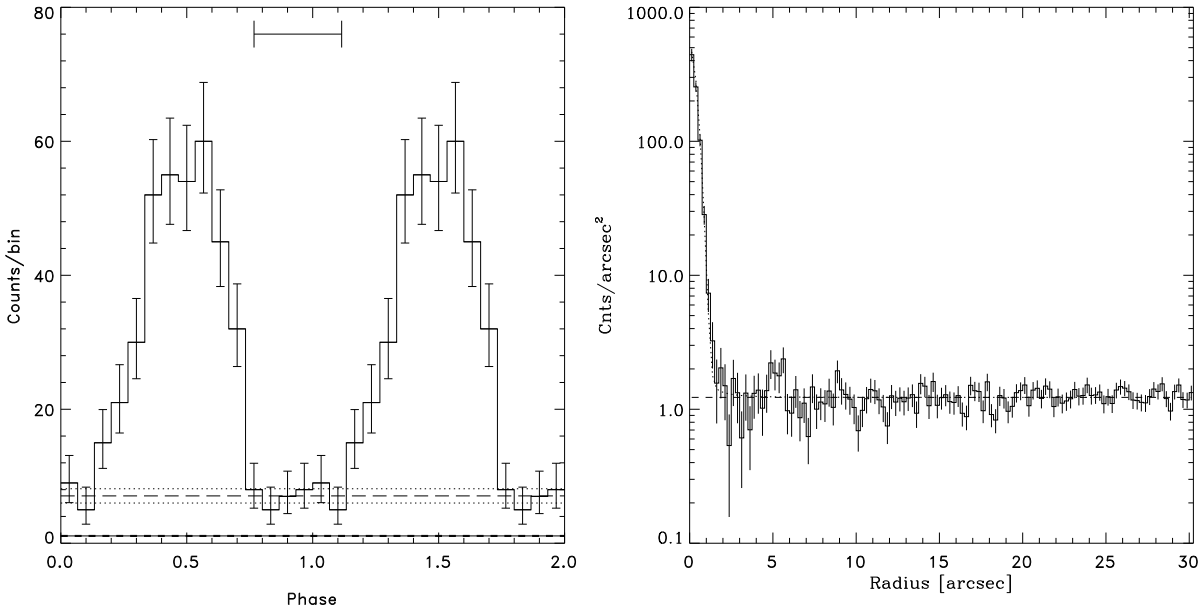

Figure 20. PSR J1849-0001; the left panel shows the (15 bins) HRC-S pulse profile (0.06–10 keV), selecting events within a 2″ aperture around its centroid. The background level at 1.1 counts/bin and its 1σ uncertainty levels are indicated by the horizontal solid and dashed lines, respectively. The unpulsed (DC) level and its 1σ uncertainty levels, as derived from the bootstrap method outlined by Swanepoel et al. (1996), are represented by the long dashed and dotted lines, respectively. The solid horizontal line segment given at the top indicates the unpulsed "region" as estimated by this bootstrap method. The intrinsic pulsed fraction is 0.77 ± 0.04. The right panel shows the radial distribution of HRC-S events centered on IGR J18490-0000 up to 30″ along with a model (dotted line) composed of a flat background (dashed horizontal line) and a point source with 406 counts. No indication for structured extended emission is found in the near vicinity of IGR J18490-0000.

plate fitting. These counts have been converted to flux values using proper HEXTE cluster-A response information and the deadtime corrected exposure for cluster-A, adopting the photon power-law model derived from PCA data. The PCA and HEXTE pulsed flux values are shown in the spectral compilation depicted in Fig. 22 as aqua (PCA) and blue (HEXTE) data points.

Because our own analysis of the pulsed X-ray spectrum of IGR J18490-0000 using *RXTE* PCA data yielded a $\sim 4\times$ larger pulsed flux than that given by Gotthelf et al. (2011), we obtained also a higher pulsed fraction of 88 ± 8 %. To shed light on this discrepancy and on the extended emission around IGR J18490-0000 we proposed 2 *Chandra* observations of 25 ks each, one with the HRC-SI (timing) and one with the ACIS-S (spatially resolved spectral analysis). Our aim was to determine the genuine intrinsic pulsed fraction in the X-ray band and to perform accurate spatially resolved spectral analysis at arcsec scales.

The HRC-S observation in timing mode ($6' \times 30'$ field of view; time resolution 16μs) was performed on Nov. 20, 2011 for an effective exposure time of 25.1 ks (CXO observation id. 13292). An imaging analysis using Maximum Likelihood (ML) techniques for Poissonian distributed pixel content (see e.g. the Supplementary Material of Hermsen et al. 2013, for a similar approach) of the HRC-S data showed a clear point-source at $(\alpha_{2000}, \delta_{2000})$ =(18 49 1$^{\rm s}$.632,-00 01 17″.45) with a formal systematic uncertainty of 0″.6 (in radius; 90%) and a negligible statistical uncertainty of 0″.02 (1σ) in each coordinate. Selecting (barycentered) events within 2″ from the centroid location of IGR J18490-0000 yielded a number of 406 events of which 16.4 ± 1.2 events are expected to be background events as estimated in an annulus of 4″ inner radius and 8″ outer radius centered on IGR J18490-0000.

A restricted period search around the predicted value using the Z_2^2-test statistic yielded a very significant signal at $\nu_{\rm max} = 25.9609614(25)$ Hz, exactly at the extrapolated value from the (*RXTE* PCA based) coherent ephemeris (this work) as given in Table 1. Subsequent phase folding yielded the CXO HRC-S pulse profile (energy integrated; 15 bins) of IGR J18490-0000 as shown in the left panel of Fig. 20. The pulsed fraction, not corrected for (the small) background, is 0.74 ± 0.04, which translates in a (background corrected) intrinsic pulsed fraction of 0.77 ± 0.04, inconsistent with the value of ~ 0.25 derived by Gotthelf et al. (2011), but consistent with the value of 0.88 ± 0.08 we derived earlier from our own *RXTE* PCA spectral analysis of the pulsed emission and the *XMM-Newton* total source flux of IGR J18490-0000 as reported by Gotthelf et al. (2011).

To study the extended emission in the vicinity of IGR J18490-0000 we applied a (deep) Gaussian smoothing to the central part of the raw image centered on IGR J18490-0000 and displayed the image on a log scale to emphasize possibly extended emission. The resulting map (PHA integrated) did not show evidence for the presence of diffuse emission near IGR J18490-0000. It should be noted, however, that given the response of the HRC-S with maximum sensitivity between 1 – 2 keV (strongly reduced beyond 2 keV) this image mainly shows the spatial information at soft X-rays (0.1-2 keV). Moreover, the genuine underlying emission around IGR J18490-0000 is strongly suppressed by the highly absorbing intervening Hydrogen column.

Analyzing the HRC-S data, the more quantitative ML-imaging approach of the near environment of IGR J18490-0000 (in this case a region with a radial extent of 10″ centered on the centroid scanned at 0″.2 scale) also yielded no evidence for structured diffuse emission. This method assigns 406 ± 21 counts to the point source at a background rate of 1.224 ± 0.066 counts/arcsec^2. The

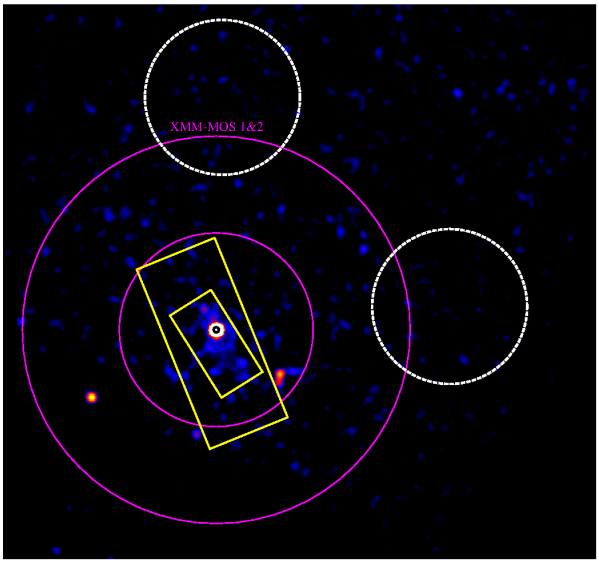

Figure 21. PSR J1849-0001; ACIS-S3 2–10 keV image of the near environment of IGR J18490-0000 (black circle). The image is Gaussian smoothed and scaled logarithmically to emphasize diffuse emission, which is clearly visible in a "rectangular" region of size $75''\times 37\farcs5$ (small yellow box) around IGR J18490-0000. Just outside the larger yellow box of size $150''\times 65''$, used for the determination of the X-ray spectrum of the extended emission, a cluster of three point sources are popping-up at about $60''$ from IGR J18490-0000 (reddish spot). The two circular apertures (white dashed circles) each with a $60''$ radius indicate sky regions used to estimate the background. The purple annulus with radii at $75''$ and $150''$ represents the region selected in a study of the diffuse PWN emission around IGR J18490-0000 using *XMM-Newton* MOS 1&2 data.

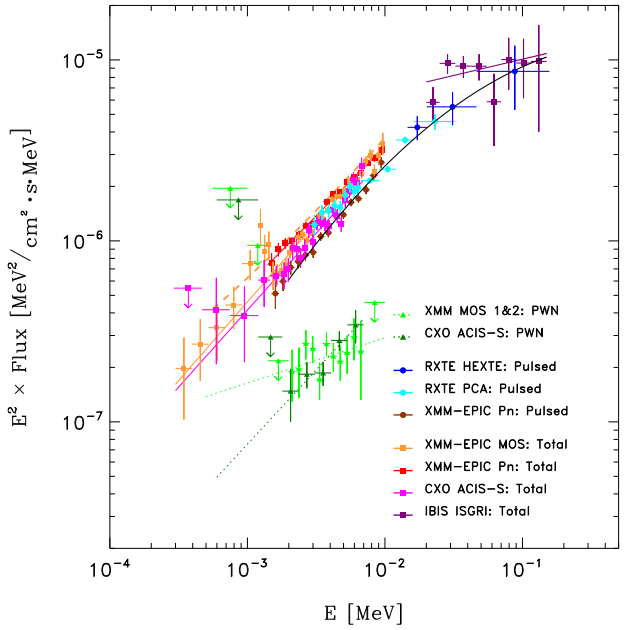

Figure 22. PSR J1849-0001; unabsorbed ($N_H = 4.5\times 10^{22}$ cm^{-2}) total and pulsed spectra from 0.3-150 keV combining data from *RXTE* PCA and HEXTE (pulsed), *INTEGRAL* ISGRI (total), *Chandra* ACIS-S (total), *XMM-Newton* EPIC pn (pulsed & total) and MOS (total). Total flux measurements have filled square symbols, while pulsed fluxes have filled circles. A fit ("curved" power-law model) through all pulsed flux measurements is shown as black solid line. The emission of IGR J18490-0000 is highly pulsed with a pulsed fraction of about 80%. The spectrum of the diffuse emission is also shown below that of the pulsar (a) lime triangles ACIS-S; $150''\times 65''$ extraction box minus $5''$ circular source region; 2) green triangles *XMM-Newton* EPIC MOS 1+2; annulus of $75''$ inner- and $150''$ outer radius).

projection of the 2d-imaging information into a radial event distribution ($0\farcs25$ binsize) is shown in the right panel of Fig. 20 with superposed the point source model for IGR J18490-0000 with 406 source counts on top of the local background, estimated in an annulus with $10''$ inner- and $25''$ outer radius. The latter background value is fully consistent with that derived from the 2d-ML method fitting the background and source simultaneously. No significant deviations between measured distribution and model can be found, indicating that there is no evidence for structured extended emission in the near environment of IGR J18490-0000.

Our second *Chandra* observation (CXO observation id. 13291) with IGR J18490-0000 at the aim point of the back-illuminated ACIS-S3 chip was performed on Nov. 16, 2012 for 25.6 ks yielding an effective exposure of 22.7 ks. A Gaussian smoothed and logarithmically scaled (to emphasize diffuse emission) ACIS-S3 map for energies in the range 2–10 keV is shown in Fig. 21. Diffuse emission is now clearly visible confined more or less in a "rectangular" region of size $75''\times 37\farcs5$ (small yellow solid rectangle/box) around IGR J18490-0000. A similar map for events with energies in the range 0.5–2 keV does not show evidence for diffuse emission, consistent with the HRC-S findings, while the point source emission from IGR J18490-0000 is still detected.

More quantitatively, we produced a Maximum Likelihood ratio map selecting events with energies within 0.5–10 keV for a $2'\times 2'$ region centered on IGR J18490-0000 to search for point sources in the near environment of IGR J18490-0000, polluting the determination of the genuine diffuse emission. This method assigns 2359 ± 49 counts to the point source IGR J18490-0000 in this band, yielding a source count rate $C_R^{0.5\text{-}10\,\mathrm{keV}}$ of 0.104 ± 0.002 c/s. In addition, five sources are popping-up with detection significances $>5\sigma$ of which three (with relatively high significances in the range $6.7-15.2\sigma$) cluster in a small region at about $\sim 60''$ from IGR J18490-0000 (see Fig.21, just outside the large dashed yellow box). In the estimation of the spectrum of the diffuse emission we chose an extraction region for the diffuse emission excluding these sources. In fact, these sources clearly polluted the diffuse spectrum derived from *XMM-Newton* EPIC data by Gotthelf et al. (2011), who used an annulus of $30''$ inner- and $150''$ outer radius centered on IGR J18490-0000 as extraction region (see also Fig. 2 of Terrier et al. 2008).

We used two rectangular extraction regions encompassing IGR J18490-0000, excluding a circular region of $5''$ radial extend centered on IGR J18490-0000, to evaluate the spectrum of the diffuse emission: 1) a $75''\times 37\farcs5$ box (small yellow box in Fig.21) and 2) a $150''\times 65''$ box (large yellow box in Fig.21). We also carefully chose two $60''$ circular background regions, free of sources, in the vicinity of IGR J18490-0000 (see also Fig.21; the two white dashed circles). The background subtracted count spectrum (0.6–7 keV band), properly taking into account the area difference of the diffuse- and background extraction regions, has been fitted in a forward folding procedure adopting an absorbed power-law model with a fixed Hydrogen column density of N_H of 4.5×10^{22} cm^{-2} (see further this section) and proper response information. We found for the large extraction box a photon index of -1.18 ± 0.05 and an unabsorbed 2–10 keV flux of $(7.1\pm 0.5)\times 10^{-13}$ erg/cm^{2}s

(see Fig. 22 for the ACIS-S PWN fluxes and fit; lime coloured), about 5–6 times smaller than that of the IGR J18490-0000 point source. For the smaller extraction box we found a similar photon index of -1.13 ± 0.06 and a ~ 1.6 times lower flux. Thus, our CXO ACIS-S derived spectrum of the diffuse emission is much harder than that derived by Gotthelf et al. (2011) using *XMM-Newton* EPIC data, while our flux estimates are compatible given the different extraction regions and methods used.

Next, we derived the total ACIS-S (point source) count spectrum of IGR J18490-0000 by fitting simultaneously a point-source model and a flat background model to the spatial event distribution (using the ML-method adopting Poissonian statistics) for each chosen energy band between 0.3 and 7 keV. These spatial event distributions have been sampled in a $5''$ circular region centered on IGR J18490-0000 in $0\farcs5 \times 0\farcs5$ bins. The resulting source counts per energy slice have subsequently been converted to photon flux values using proper energy response information and an effective exposure value of 22.67 ks adopting an absorbed power-law model. A model fit with N_H free yielded a column density of $(4.30 \pm 0.16) \times 10^{22}$ cm^{-2} and a photon index of -1.08 ± 0.02. Fixing N_H to 4.5×10^{22} cm^{-2} resulted in a slightly softer photon index of -1.15 ± 0.02 and an unabsorbed 2–10 keV flux of $(4.11 \pm 0.09) \times 10^{-12}$ erg/cm^{2}s. These flux measurements are shown in Fig. 22 as magenta data points.

We studied the effects of pile-up on the spectral parameter estimation for this CXO ACIS-S observation, because the measured count rate (0.5-10 keV) per 3.2 s frame time is ~ 0.33 cnts/frame which is sufficiently large for a moderate pile-up impact (see e.g. the middle panel of Fig. 3 of "The *Chandra* ABC Guide to pileup" which is referenced from *http://cxc.harvard.edu/ciao/ahelp/acis_pileup.html*).

The pile-up fraction f_f (i.e. the fraction of frames that have detected events containing two or more events) is about 15%, while the total fraction f_t of events lost, either through grade or energy migration, with respect to the expect rate is about 28%. To study the impact of pile-up on our spectral results in more detail we simulated spectra using *webspec* adopting different pile-up model parameters (no pile-up, pile-up with grade migration parameter $\alpha = (0, 0.5, 1)$ for an input photon flux model with photon-index -1.08 and normalization at 1 keV of 4×10^{-4} ph/cm^{2}s keV absorbed by a Hydrogen column of 4.5×10^{22} cm^{-2}. We found for all the three different pile-up models a photon flux reduction of about 22% with respect to the unpiled case. The pile-up impact on the reconstructed photon index was marginal and its size is about 0.1.

XMM-Newton has observed IGR J18490-0000 for a second time on March 23-24, 2011 for about 54 ks. EPIC MOS operated in Prime Full Window mode using a medium filter for an effective exposure of 52.635 ks and 52.664 ks for MOS 1 and MOS 2, respectively. EPIC pn operated in Small Window mode (medium filter) for an effective exposure of 37.76 ks allowing studies of the pulsed signal given the ~ 5.7 ms time resolution in this mode. These *XMM-Newton* observations do not suffer from pile-up effects, and allow us to reconstruct the unpiled total (MOS 1 & 2,pn) and pulsed (pn, only) spectrum of the source.

To extract the total emission spectrum of IGR J18490-0000 (MOS 1 & 2; pn) we applied a similar procedure as used for the ACIS-S, now sorting the events with energy between 0.3-10 keV and within $60''$ from the IGR J18490-0000 centroid in $2'' \times 2''$ spatial bins for each energy band. For MOS 1 & 2 we derived, adopting an absorbed power-law model, an Hydrogen column density N_H of $(4.51 \pm 0.10) \times 10^{22}$ cm^{-2} and a photon index Γ of -1.13 ± 0.01 ($\chi^2_{r,35-3} = 1.20$). For the pn we found for N_H a value of $(4.54 \pm 0.10) \times 10^{22}$ cm^{-2} and for the photon index -1.23 ± 0.01, somewhat softer than determined from MOS 1 & 2 data ($\chi^2_{r,17-3} = 0.86$; 1.42-10 keV). The derived Hydrogen column density is consistent with the value found by Gotthelf et al. (2011), and in all further spectral analysis of X-ray data we fixed N_H to 4.5×10^{22} cm^{-2}. The unabsorbed 2–10 keV total flux of IGR J18490-0000 is $(4.72 \pm 0.05) \times 10^{-12}$ and $(4.92 \pm 0.05) \times 10^{-12}$ erg/cm^2 s, for MOS 1 & 2 and pn, respectively, about 17% higher than the ACIS-S estimate, which suffered from pile-up effects. The flux measurements are shown in Fig. 22 as red (EPIC-pn) and orange (MOS 1 & 2) datapoints.

We also studied the diffuse emission around IGR J18490-0000 using MOS 1 & 2 data. We chose a source region consisting of an annulus with an inner radius of $75''$ (just outside the regions studied using ACIS-S data) and an outer radius of $150''$ (purple annulus in Fig. 21), well outside the "source cluster" at an angular distance of about $60''$ from IGR J18490-0000. The background region consisted of an annular region with $150''$ inner and $225''$ outer radius. The difference count spectrum, taking into account the difference in area of the source- and background extraction regions, has been fitted with an absorbed power-law model (N_H fixed to a value of 4.5×10^{22} cm^{-2}) utilizing response functions produced for the annular source region. The fit yielded an unabsorbed 2–10 keV energy flux of $(6.23 \pm 0.42) \times 10^{-13}$ erg/cm^{2}s and a photon index of -1.75 ± 0.05, considerably softer than found by the ACIS-S for the inner PWN region. This can best be explained as a manifestation of Synchrotron cooling, which makes the outskirts of a PWN softer than the inner parts. The MOS 1 & 2 PWN flux measurements are shown in Fig. 22 as green datapoints.

We also performed a timing analysis of the EPIC-pn data, which, sampled in Small Window Mode, has a time resolution of ~ 5.7 ms, amply sufficient to study the 38.5 ms pulsed signal. For this purpose we selected barycentered events within $15''$ from the IGR J18490-0000 centroid. A restricted period search around the predicted pulsed period extrapolating the timing parameters of the IGR J18490-0000 entry listed in Table 1 yielded a very significant peak in the periodogram exactly atop the prediction. Subsequent phase folding adopting again the timing model listed in Table 1 for IGR J18490-0000 yielded significant pulsed emission down to about 1 keV.

To derive the pulsed spectrum we first applied for each selected energy band, adopting Poissonian statistics, a Maximum Likelihood template fit procedure consisting of optimizing the number of pulsed excess counts and unpulsed (flat) level simultaneously assuming that the pulse shape is described by the pulse profile (=template) as shown in Fig. 19.

These excess counts are converted to flux values in a forward folding procedure adopting an absorbed power-law model ($N_H \equiv 4.5 \times 10^{22}$ cm^{-2}) using instrument response functions determined for the $15''$ extraction radius. We derived an unabsorbed 2–10 keV pulsed flux of $(3.65 \pm 0.06) \times 10^{-12}$ erg/cm^{-2}s and a photon index of -1.14 ± 0.01. The pulsed flux measurements by EPIC-pn are shown as dark-red datapoints in Fig. 22. Given the total and pulsed 2–10 keV (XMM) fluxes we determined a pulsed fraction of 0.76 ± 0.02 for the 2–10 keV band, in full agreement with the HRC-S estimate for its integral energy band and the PCA based value.

The sky region near IGR J18490-0000 was also frequently in the field of view of the soft γ-ray imager ISGRI (15-300 keV) aboard the *INTEGRAL* satellite. A deep image centered on rotation-powered pulsar PSR J1846-0258 (see Section 5.14) and enclosing IGR J18490-0000 has been shown by Kuiper & Hermsen (2009).

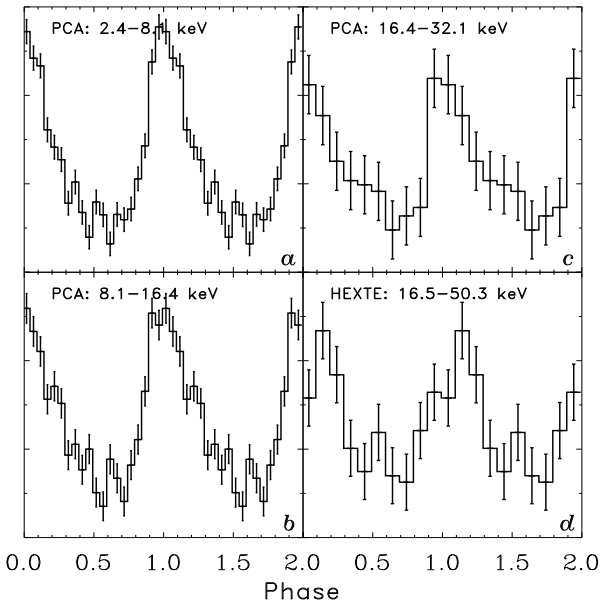

Figure 23. PSR J1930+1852; pulse profiles in various energy bands for *RXTE* PCA (panels a–c) and *RXTE* HEXTE (panel d). Pulsed emission has been detected up to ~ 50 keV (4.5σ; panel d).

The total spectrum of IGR J18490-0000 for the 20-300 keV band has been derived from maps produced in 10 logarithmically binned energy bands covering the 20-300 keV window. The selected *INTEGRAL* observations covered *INTEGRAL* revolutions 49 – 603 (March 10, 2003 – Sept. 23, 2007) and represent a total GTI exposure of 7.35 Ms. For more details we refer to Section 3.1 of Kuiper & Hermsen (2009). Fitting a power-law model we derived a photon index of -1.82 ± 0.14 and a 20–100 keV energy flux of $(2.25 \pm 0.16) \times 10^{-11}$ erg/cm^{2}s, consistent with the values determined by Terrier et al. (2008), who used less *INTEGRAL* exposure time. These ISGRI flux measurements (sum of pulsed/unpulsed emission from the pulsar and the diffuse emission) and best fit are shown in Fig. 22 as purple data points and solid line, respectively. Finally, in the GeV γ-ray band no pulsed emission from IGR J18490-0000 has been detected by *Fermi* LAT (Abdo et al. 2013).

In summary, we found hard pulsed emission for IGR J18490-0000 from $\sim$ 1 keV to $\sim$ 60 keV, which represents about 80% of the total emission. The diffuse emission, 5–6 times weaker than the point source emission of IGR J18490-0000, is also hard and softens towards the outer parts of the PWN. This is characteristic for Synchrotron cooling.

5.16 PSR J1930+1852

Seward et al. (1989) reported the detection of the Crab-like SNR G54.1+0.3 at X-rays using *Einstein* IPC (0.5-4 keV) data from an observation performed on May 7, 1980 collecting about 50 photons, too faint to determine accurate spectral information. More detailed X-ray spectral information was obtained by Lu et al. (2001) using data from the *ROSAT* PSPC (0.1-2.5 keV; $\sim$ 20 ks) and the *ASCA* GIS (16.5 ks) and SIS ($\sim$ 20 ks) detectors, both operating in the 0.5-10 keV range. Spatially resolved spectral analysis in the X-ray band became possible using the superb imaging quality of the *Chandra* ACIS instrument, revealing in a 30.9 ks exposure a central bright hard point-source - the putative pulsar - and several diffuse structures surrounding it (Lu et al. 2002).

Targeting at the central source Camilo et al. (2002) discovered the energetic pulsar PSR J1930+1852 at radio frequencies. Its period of $\sim$ 136 ms was also detected at soft X-rays in the archival *ASCA* GIS data. Lu et al. (2007) showed, analysing additional *Chandra* ACIS-I data taken on June 30, 2003 for a total exposure time of 58.4 ks in CC-mode, that the pulsed emission is hard with a photon-index Γ of $1.2(2)$ and that the source has a high pulsed fraction of $71 \pm 5\%$. The absorbed pulsed flux in the 2–10 keV band was 1.2×10^{-12} erg/cm^{2}s, which translates to an unabsorbed flux of $\sim 1.33 \times 10^{-12}$ erg/cm^{2}s in the same band taking into account the 1.6×10^{22} cm^{-2} absorbing Hydrogen column. These authors also analyzed data from a $\sim$ 80 ks *RXTE* observation taken during September 12–14 and December 23–25, 2002, but only for timing purposes.

Guided by the available radio ephemeris (Camilo et al. 2002) we generated a phase coherent ephemeris based on these X-ray data for the 2002 September 12 – December 25 period, listed in Table 1. We re-analysed the *RXTE* PCA and HEXTE data using template fitting to obtain the pulsed emission spectrum over a much broader bandpass than *Chandra*. Pulse profiles for various energy bands are shown in Fig.23 and pulsed emission has been detected up to $\sim$ 50 keV (see Fig. 23d). The reconstructed photon spectrum of the pulsed emission across the 2.8-32.1 keV range, adopting a Hydrogen column density N_H of 1.6×10^{22} cm^{-2} (see Lu et al. 2002), has a power-law index of -1.30 ± 0.02 and an unabsorbed 2-10 keV flux of $(1.57 \pm 0.07) \times 10^{-12}$ erg/cm^{2}s, slightly higher than the value obtained by Lu et al. (2007) who used *Chandra* ACIS data. Using *Chandra* ACIS-S data of observations performed over the period 8–15 July 2008, totaling 290.77 ks of exposure time, Temim et al. (2010) derived for the total pulsar spectrum a photon index of -1.44 ± 0.04 and an unabsorbed 0.3-10 keV flux of 3.26×10^{-12} erg/cm^{2}s, which translates to a 2-10 keV flux of 2.25×10^{-12} erg/cm^{2}s. From this total 2–10 keV flux value and our pulsed 2-10 keV flux we derive a pulsed fraction of $\sim 70\%$, consistent with the value derived by using only *Chandra* data. The pulsed (*RXTE* PCA and HEXTE) and total (*Chandra*; Temim et al. 2010) emission spectra of PSR J1930+1852 are shown in Fig. 24.

Soft γ-ray emission in the 20-60 keV band from a location consistent with PSR J1930+1852 has also been detected in an imaging study of ISGRI data (Segreto et al. 2010).

PSR J1930+1852 is not listed as high-energy γ-ray pulsar in the *Fermi* second pulsar catalogue (Abdo et al. 2013), however, at TeV energies a pointlike source, VER J1930+188, has been detected by the VERITAS ground-based gamma-ray observatory from the direction of SNR G54.1+0.3 with an integral flux above 1 TeV of 2.5% of the Crab nebula, very likely the PWN associated with PSR J1930+1852 (Acciari et al. 2010).

5.17 PSR J2022+3842

PSR J2022+3842 was discovered at 1.95 GHz with the GBT SPIGOT spectrometer targeting at the point source detected in the X-ray band at the center of SNR G76.9+1.0 (see e.g. Wendker et al. 1991; Landecker et al. 1993) in a 54 ks *Chandra* ACIS observation (Arzoumanian et al. 2011). The radio pulsations of PSR J2022+3842 are severely affected by dispersion (DM $= 429.1 \pm 0.5$) and scattering in the interstellar medium, and these effects explain the non-detections of pulsed emission in targeted searches at lower radio frequencies, 618 and 1170 MHz, with the GMRT (Marthi et al. 2011). Subsequent radio-observations with

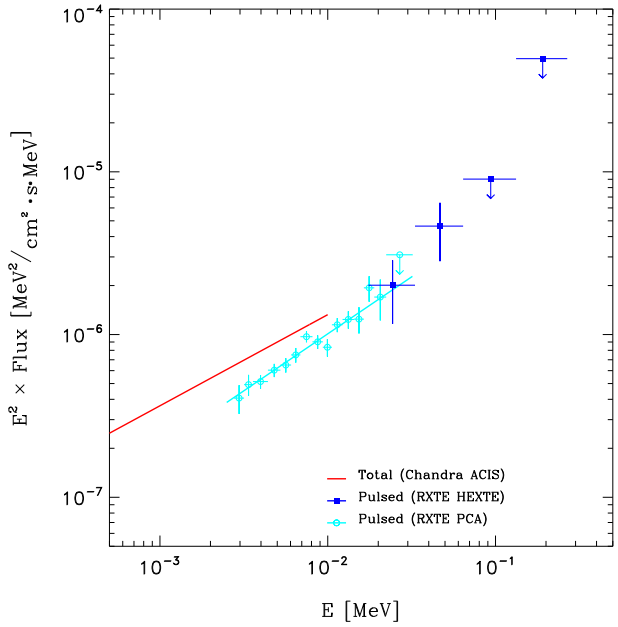

Figure 24. PSR J1930+1852; high-energy (0.5-250 keV) total and pulsed spectra as derived from measurements by *Chandra* ACIS (total pulsar 0.5-10 keV; solid red; Temim et al. (2010)), *RXTE* PCA (pulsed 2.5-30 keV and best fit; aqua; this work) and *RXTE* HEXTE (pulsed 15-250 keV; blue; this work).

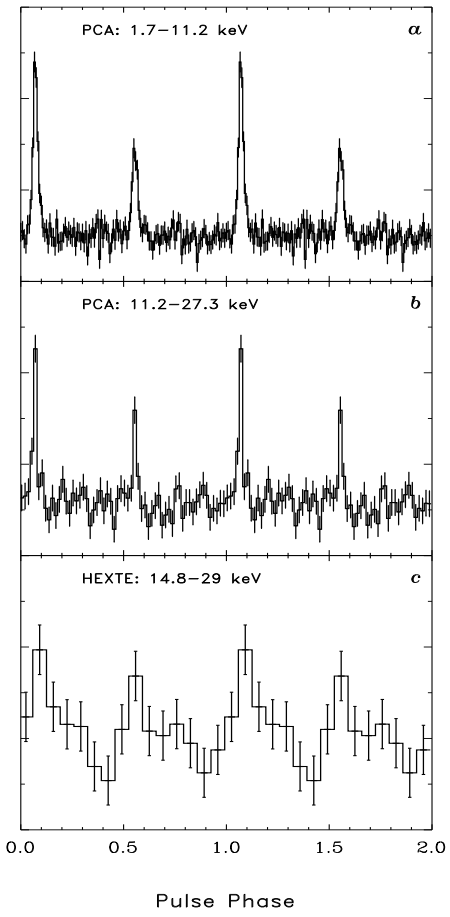

Figure 25. PSR J2022+3842; pulse profiles for *RXTE* PCA (panels a & b) and *RXTE* HEXTE (panel c). Pulsed emission has been detected up to ~ 30 keV. Note the sharpness of the pulses of about 1.2 ms (FWHM).

the GBT of this weak pulsar (60 μJy at 2 GHz with a very flat spectrum, index $\alpha = -0.33$) settled the timing properties of PSR J2022+3842 (Arzoumanian et al. 2011). A spin-up glitch occuring between MJD 54400 and 54950 was also evident in these radio observations.

Dedicated *RXTE* monitoring observations performed between Jan. 27, 2010 and Febr. 4, 2010 revealed the pulsed signal (a single sharp pulse at pulse period 24.3 ms) also in the 2-20 keV PCA band (Arzoumanian et al. 2011). These authors found a hard spectral index of -1.1 ± 0.2 and an absorbed 2–10 keV pulsed flux of 5.4×10^{-13} erg/cm^{2}s, which is comparable to the total measured absorbed 2–10 keV flux by *Chandra*, indicating a pulsed fraction of $\sim 100\%$.

An *XMM-Newton* observation of PSR J2022+3842 of 116 ks performed on April 14, 2011 revealed that the pulse period is actually twice (48.6 ms) the initially found period due to the presence of an interpulse at about ~ 0.5 phase separation of the main pulse (Arumugasamy et al. 2014). The adapted spin-down luminosity and characteristic age are now: $\dot{E}_{sd} \sim 2.97 \times 10^{37}$ and 8.9 kyr, respectively.

We re-analyzed the *RXTE* PCA data (88.73 ks of screened PCU-2 exposure) in order to deal with this "change" from single peaked to double peaked nature and to better characterize the hard X-ray spectrum by including all PCA detection layers, being more sensitive to photons with energies in excess of ~ 10 keV. We also analyzed the HEXTE data. A high-statistics template pulse profile (double peaked) was used in the correlation analysis to derive the pulse time-of-arrivals from which we constructed a phase coherent timing model (see Table 1). This ephemeris has subsequently been used in a folding procedure creating the event distributions as a function of pulse phase and energy for both the PCA and HEXTE. Pulsed emission has been detected up to ~ 30 keV (see Fig. 25 panels a & b for the PCA 1.7-11.2 (28.2σ) and 11.2–27.3 keV (10.8σ) and panel c for the HEXTE 14.8-29 keV (3.4σ) lightcurves, respectively).

The broad-band PCA pulse profile can satisfactorily be fitted by a model composed of two Gaussians plus background yielding a pulse phase separation of 0.484 ± 0.001 between main- and interpulse and pulse widths (FWHM) of 0.0254 ± 0.0014 (main pulse) and 0.0273 ± 0.0024 (interpulse). The X-ray pulse profile of PSR J2022+3842 bears strong similarities with the pulse profile of PSR J0205+6449 (see e.g. Kuiper et al. 2010).

The pulsed excess counts for the main pulse (P1), interpulse (P2) and its sum (total pulsed; TP=P1+P2) have been determined across the 2.5-32 keV PCA band (for which a proper energy calibration exists) through fitting the measured pulse profiles for various differential energy bands in terms of the previously derived best Gaussian models (fixed position and shape) and background. Subsequently, these excess counts have been converted to pulsed fluxes in a forward folding spectral fitting procedure assuming a power-law model and adopting an absorbing Hydrogen column density N_H of 1.7×10^{22} cm^{-2} (Arzoumanian et al. 2011).

We found for the 2.5-32 keV band a photon index of -1.31 ± 0.02, -1.04 ± 0.03 and -1.20 ± 0.014 for the main pulse, inter pulse and total pulse, respectively. The corresponding unabsorbed 2–10 keV band fluxes are $(3.60 \pm 0.12) \times 10^{-13}$, $(1.91 \pm 0.11) \times 10^{-13}$ and $(5.50 \pm 0.17) \times 10^{-13}$ erg/cm^{2}s, for P1, P2 and TP, respectively. The main pulse thus comprises $\sim 65\%$ of the total pulsed flux. The absorbed/unabsorbed 2–10 keV total pulsed flux of

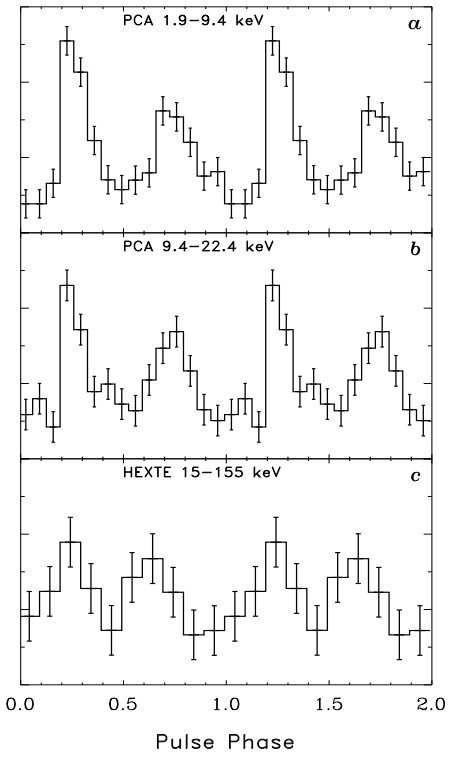

Figure 26. PSR J2229+6114; pulse profiles in various energy bands for *RXTE* PCA (panels a–b), *RXTE* HEXTE (panels c). Pulsed emission has been detected up to $\sim$ 22 keV.

$(4.94\pm0.37)\times10^{-13}/(5.50\pm0.17)\times10^{-13}$ erg/cm^{2}s is somewhat less than found by Arzoumanian et al. (2011), but is still comparable (93 %) to the total absorbed 2–10 keV flux of the point source derived from *Chandra* (imaging) data.

PSR J2022+3842 is not listed as high-energy γ-ray pulsar in the *Fermi* second pulsar catalogue (Abdo et al. 2013), however, the *Fermi* LAT second source catalogue (Nolan et al. 2012) reports on a 10σ γ-ray source, 2FGL J2022.8+3843c, positionally consistent with G76.9+1.0. At TeV energies (100 GeV - 50 TeV) the VERITAS survey of the Cygnus region, reaching a VHE sensitivity of $\sim$ 4% of the Crab nebula flux for an energy threshold of 200 GeV, did not result in a detection of a TeV source at the location of PSR J2022+3842/ G76.6+1.0 (Ward et al. 2010).

5.18 PSR J2229+6114

PSR J2229+6114 was discovered at radio frequencies in the error region of the unidentified EGRET source 3EG J2227+612 after the end of the *CGRO* mission (Halpern et al. 2001b). The pulsed signal ($P \sim 51.6$ ms) was also detected in the X-ray band using archival *ASCA* GIS (0.7-10 keV) data, taken 1.6 year before the detection of the radio pulsations, showing 2 pulses separated about 0.5 in phase.

A non-thermal incomplete radio shell, G106.6+2.9, surrounds PSR J2229+6114. This compact radio nebula of size $\sim 3'$, called the "Boomerang", has a flat spectrum and is polarized at a level of $\sim 25\%$, and represents the PWN associated with PSR J2229+6114. It is located at the northeastern tip of the radio continuum source G106.3+2.7 of size $0.^\circ5 \times 1^\circ$ which is classified as the remnant of a supernova (see e.g. Kothes et al. 2006), that gave birth to PSR J2229+6114. Diffuse emission from the near field of PSR J2229+6114 has also been clearly detected at X-rays by Ng & Romani (2004) in a 95 ks *Chandra* ACIS-S observation (taken March 15, 2002), who fitted the observed morphology with their pulsar wind torus model.

In recent years the pulsed fingerprint of PSR J2229+6114 has also securely been found in *AGILE* and *Fermi* LAT data at energies above 100 MeV (Pellizzoni et al. 2009; Abdo et al. 2009b), showing a single asymmetric peak at a phase separation of 0.49 from the (single) radio pulse. At TeV energies Acciari et al. (2009) reported the detection of extended emission from G106.3+2.7, as measured by VERITAS.

We analyzed the - so far unpublished - *RXTE* PCA and HEXTE data from *RXTE* observation runs 60130 and 80092 (performed on Dec. 7–8, 2001 and Nov. 25–29, 2003 for 90.4 ks and 129.8 ks, respectively) in order to characterize the pulsed emission spectrum of PSR J2229+6114 over the 3–250 keV band. In both observation runs the pulsed signal could easily be detected in the PCA $\sim$ 2–10 keV band (PHA range 4–27) taking into account the phase smearing due to the frequency derivative by including the $\dot{\nu}$ value of $-2.92006(5) \times 10^{-11}$ Hz/s, found at radio frequencies for a later epoch. The event cubes (2d distribution of events versus pulse phase (60 bins) and energy (PHA; 256 bins)) for both runs have been made and combined after applying an appropriate phase shift to align both distributions in phase. The combined (cleaned) exposure for PCU-2 amounts 220.144 ks. Similar folding and alignment (with known phase shift) procedures have been followed for HEXTE data. The pulse profiles of PSR J2229+6114 obtained for the PCA bands 1.9-9.4 keV (PHA 5–22) and 9.4-22.4 keV (PHA 23–53) are shown in Fig. 26a (12.3σ) and b (8.3σ), respectively. The double peaked morphology, already visible in the *ASCA* GIS data for the 0.8-10 keV band (Halpern et al. 2001b), is evident, now also for energies above 10 keV. Pulsed emission has been detected up to $\sim$ 22 keV. In HEXTE data we found only indications for the pulsed signal for energies above $\sim$ 15 keV (see Fig. 26c; 2.4σ).

We also analyzed archival *ASCA* GIS (Ohashi et al. 1996) data obtained during an observation run (57038000) on August 4–7, 1999 with an effective exposure of about 113.8 ks. We confirmed the findings of Halpern et al. (2001b), but derived a more significant pulse profile for the GIS 0.8-10 keV range with a more pronounced double peak morphology by using $2'$ as optimum extraction radius instead of $4'$. We fitted this lightcurve with 2 symmetric Lorentzians on top of a flat background and derived a phase separations of 0.49 ± 0.02. The individual Lorentzian profile shapes are subsequently used as templates in the derivation of the pulsed excess counts for both *ASCA* GIS and *RXTE* PCA pulse profiles for user defined energy bands. Applying proper response information, (effective) exposure times, correction factors for the missing fraction of the PSF (*ASCA* GIS; the extraction region was a circular aperture of $2'$, which covers about 57% of the PSF) these pulsed excess counts have been converted to pulsed fluxes in a forward folding spectral analysis procedure, adopting an absorbed power-law model assuming an absorbing Hydrogen column N_H of 6.3×10^{21} cm^{-2} (Halpern et al. 2001a).

For the PCA 2.8-32.2 keV band the pulsed emission (sum of the two pulses) is properly described by a power-law with (hard) photon index of -1.11 ± 0.03 and an unabsorbed 2–10 keV flux of $(5.2 \pm 0.3) \times 10^{-13}$ erg/cm^{2}s, consistent with the value derived by Halpern et al. (2002) using *ASCA* GIS data. We found no evidence for different spectral behaviour of the pulses in the X-ray band. However, between $\sim$ 20 keV and 100 MeV the pulse morphology drastically changes from a double peaked to an asymmetric single peaked profile (Abdo et al. 2009b), indicating different spectral behaviour as a function of pulse phase. Unfortunately, there are no

sensitive measurements in this energy band to further constrain the pulsed emission properties. The total pulsed emission spectrum of PSR J2229+6114 from soft X-rays to high-energy γ-rays is shown in Fig. 28 including *ASCA* GIS (0.8-10 keV), *RXTE* PCA (2.7-32 keV) and *Fermi* LAT measurements as orange data points/symbols and hatched region.

6 CANDIDATE SOFT γ-RAY PULSARS

The sample size of detected soft γ-ray pulsars is still small, despite efforts to increase this sample by searching for timing signatures for energies above 20 keV from very promising candidate RPPs. Such strong candidates for detection at hard X-rays are *Fermi* LAT detected very young ($\lesssim$ 15 kyr) energetic ($L_{sd} \gtrsim 10^{36}$ erg/cm^2 s) pulsars, often coincident with a TeV source, but also similarly young and energetic pulsars which are *not* detected by the LAT. In this section we will discuss the status (from literature and our work) for the candidate soft γ-ray pulsars as defined above.

6.1 PSR J1833-1034 in SNR G21.5-0.9

An interesting example is the weak ($S_{1400} = 71 \mu Jy$) radio-loud and *Fermi* LAT pulsar PSR J1833-1034 ($\tau \simeq 4.8$ kyr; $L_{\rm sd} \simeq 3.4 \times 10^{37}$ erg/s) at the centre of SNR G21.5-0.9, associated with TeV source HESS J1833-105 (Djannati-Ataï et al. 2008), which has a bright *INTEGRAL* soft γ-ray counterpart (De Rosa et al. 2009). Therefore, it evidently is a soft γ-ray pulsar candidate. However, deep timing searches in *NuSTAR* data (3–79 keV) did not reveal a pulsed signal from this pulsar (Nynka et al. 2014). This suggests that the soft γ-ray beams are for this pulsar not pointed in the observer's direction, contrary to the high-energy γ-ray beams.

6.2 PSR J1119-6127, PSR J1124-5916 and PSR J1357-6429

Other puzzling examples are the three, very young, energetic pulsars PSR J1119-6127 ($\tau \simeq 1.6$ kyr; $L_{\rm sd} \simeq 2.3 \times 10^{36}$ erg/s), PSR J1124-5916 ($\tau \simeq 2.8$ kyr; $L_{\rm sd} \simeq 1.2 \times 10^{37}$ erg/s) and PSR J1357-6429 ($\tau \simeq 7.3$ kyr; $L_{\rm sd} \simeq 3.1 \times 10^{36}$ erg/s), all radio and *Fermi* LAT pulsars associated with SNRs. From these pulsars, pulsed *thermal* X-ray emission has been detected (well below 2 keV and with a broad single pulse), but not the expected strong non-thermal ($\gtrsim$ 2 keV) pulsed emission (see e.g. Gonzalez et al. 2005; Hughes et al. 2003; Chang et al. 2012, respectively). For two of the three pulsars also TeV counterparts have been identified, HESS J1119-614 for PSR J1119-6127 and HESS J1356-645 for PSR J1357-6429.

6.3 PSR J1420-6048 and PSR J1418-6058 in the Kookaburra

Two other potential soft γ-ray pulsars are located in the "Kookaburra" radio complex (Roberts et al. 1999), coindicent with *CGRO* EGRET source 3EG 1420-6038 (and GeV J1417-6100). Within this complex, encompassing an area of about $1^\circ \times 1^\circ$, two young and energetic pulsars have been detected at an angular separation of only $16\farcm5$. One, PSR J1420-6048 ($\tau \simeq 13.5$ kyr; $L_{\rm sd} \simeq 1.0 \times 10^{37}$ erg/s) is located in the North-Eastern wing as radio pulsar (D'Amico et al. 2001) and is later also detected as high-energy γ-ray pulsar (Weltevrede et al. 2010). The other, PSR J1418-6058 ($\tau \simeq 10.2$ kyr; $L_{\rm sd} \simeq 5.0 \times 10^{36}$ erg/s) is in the South-Western wing, coincident with a bright radio nebula called the "rabbit", and is detected in a blind search at high-energy γ-rays (Abdo et al. 2009d).

Moreover, Aharonian et al. (2006b) detected TeV counterparts for both pulsars, HESS J1420-607 and HESS J1418-609, while Hoffmann et al. (2007) reported on a soft γ-ray source positionally consistent with PSR J1420-6048 (see also Fiocchi et al. 2010).

A (very) hard X-ray point source, embedded in a weak diffuse nebula, has been identified for PSR J1420-6048 within the (radio) K3 nebula (Roberts et al. 1999) by Ng et al. (2005) who found for a 10 ks *Chandra* ACIS-S observation only 26 counts within an aperture of $1''$ around PSR J1420-6048. Further spectral analysis yielded a photon index Γ of ~ -1 with a very large uncertainty due to the poor source statistics. We analysed a 90.7 ks on-axis *Chandra* ACIS-I observation performed on December 8, 2010 (obs.id. 12545; unpublished so far) to determine the (total) spectrum of the pulsar. Adopting an absorbed power-law model and using a Maximum Likelihood (energy resolved) PSF fit method to extract the source counts (now 233 counts for the 1.5–10 keV range), we derived a photon index Γ of -0.46 ± 0.07, an unabsorbed/absorbed 2–10 keV (total) flux of $(1.33 \pm 0.10) \cdot 10^{-13}$ / $(1.14 \pm 0.30) \cdot 10^{-13}$ erg/cm^{2}s and a Hydrogen column density $N_{\rm H}$ of $(3.35^{+0.74}_{-0.51}) \times 10^{22}$ cm^{-2}, which is slightly larger than the Galactic column of $(1.58 - 2.13) \times 10^{22}$ cm^{-2}. This confirms the hardness and weakness of the source with greatly improved accuracy. Our derived column density is also consistent with earlier X-ray derived values, using different instruments aboard *XMM-Newton* and *Suzaku* and adopting much larger extraction radii, and thus including also the softer diffuse nebula emission (see e.g. Van Etten & Romani 2010; Marelli et al. 2011; Kishishita et al. 2012).

However, so far in the canonical X-ray band (0.3-10 keV) pulsed emission has *not* been securely detected yet from PSR J1420-6048 (Ng et al. 2005) in spite of some weak indications in *ASCA* GIS data (Roberts et al. 2001). Given the hardness of the source spectrum and encouraging results from W3PIMMS concerning its detectability in *RXTE* PCA data[9] we searched for the non-thermal pulsed component of PSR J1420-6048 above $\sim$ 2 keV analysing a 66.4 ks on-axis *RXTE* PCA observation (obs.id. 80088) performed in the period August 4–6, 2003. The pulsar was observed in a post-glitch episode with valid (radio) ephemerides before and after the glitch (Yu et al. 2013), thereby considerably narrowing the period search window. However, also now for the 2–30 keV PCA band the non-thermal pulsed emission component could not be detected within the predicted period search window.

The region around the other pulsar, PSR J1418-6058, within the "Rabbit" nebula has been resolved by *Chandra* (obs.id. 2794; 10.1 ks; September 22, 2002; Ng et al. 2005) into two unresolved point sources , denoted R1 and R2, and an extended source North of these sources. In a later *Chandra* observation (obs.id. 7640; 71.1 ks; June 14, 2007) source R2 was undetectable and is likely associated with an AGN, while the other source R1 and the extended source behaved as steady sources. Updated positional information for PSR J1418-6058 from Fermi LAT timing analysis (see the TEMPO parameter file in the supplementary material provided in Abdo et al. 2013) yielded a position consistent with R1 (see also Section on PSR J1418-6058 in Ray et al. 2011b). Searches

[9] Assuming a pulsed fraction of 100% for PSR J1420-6048 the measured *Chandra* spectrum predicts for the *RXTE* PCA with 3 PCU's operating a 5σ (3σ) detection for a total observing time of 125 (45) ks in the PCA 2-22 keV band.

for pulsed X-ray emission from PSR J1418-6058 so far focussed on source R2 (ACIS in Continuous Clocking mode and XMM-EPIC pn in Small Window Mode; Ng et al. 2005), while the extended source North to R1 and R2 was favoured as counterpart in Marelli (2012) (see Chapter 4 page 154–157), who performed a spectral analysis on this proposed counterpart subsequently.

We performed a period search using EPIC-pn Small Window Mode data from a long 125.2 ks *XMM-Newton* observation performed on Februari 21–23, 2009 (obs.id. 0555700101) selecting events from a $15''$ aperture centered on R1. We could *not* detect pulsed emission in the expected (a Fermi LAT based ephemeris overlapping the XMM observation period is available) period range, neither in the 0.3-2 keV nor in the 2–10 keV band.

6.4 The Fermi blind-search pulsars PSR J1023-5746, PSR J1838-0537 and PSR J1826-1256

PSR J1023-5746, detected in a blind search in (*Fermi*) LAT data, is located near star forming region RCW 49 and its OB association Westerlund 2. It has a characteristic age of only 4.6 kyr and spin-down luminosity of 1.1×10^{37} erg/s (Saz Parkinson et al. 2010). Archival off-axis *Chandra* ACIS observations revealed a hard X-ray source, CXOU J102302.84-574606.9, coincident with the Fermi LAT timing position with a typical (hard) pulsar-like power-law spectrum with a photon index Γ of -1.2 ± 0.2 and unabsorbed flux of $(1.2 \pm 0.3) \times 10^{-13}$ erg/cm^{2}s (Saz Parkinson et al. 2010). The detection was later confirmed in an on-axis 9.9 ks *Chandra* ACIS observation within the *Chandra* Pulsar Survey (ChaPS) project (Kargaltsev et al. 2012b). The pulsar location is also positionally consistent with TeV source HESS J1023-575 (H.E.S.S. Collaboration et al. 2011). Unfortunately, the current (hard) X-ray archive does not contain suitable observations to perform period searches in order to reveal the possible/expected pulsed fingerprint of the pulsar.

PSR J1838-0537 ($\tau \simeq 5$ kyr; $L_{\rm sd} \simeq 5.9 \times 10^{36}$ erg/s) was discovered by Pletsch et al. (2012) as *Fermi* LAT blind-search pulsar applying a novel data-analysis search technique. Its sky position coincides with the extended TeV source HESS J1841-055, which is likely composed of multiple sources. Recently, a 43.3 ks on-axis *XMM-Newton* observation (obs.id. 0720750201; Oct. 14, 2013) has been performed. The EPIC-pn exposure was split in two chunks of 24.7 and 12.5 ks, while it was operating in Full Frame mode (time resolution 73.4 ms, which is just too low to catch the 145.77 ms timing signal). The second chunk was heavily contaminated by soft proton flares (only 3.7 ks of exposure left after screening) and subsequently ignored in our further analysis. The first exposure part, however, was unpolluted, and has an effective exposure of 22.1 ks. In this exposure we detected at a 6σ level in the 2–10 keV band a (very) weak source positionally consistent with PSR J1838-0537. We found 61 ± 13 counts for the source in the 2–10 keV band, while below 2 keV no detection could be claimed. The count rate, however, is too low to determine and constrain the X-ray spectral characteristics of the pulsar. Unfortunately, there are no further suitable X-ray observations in the (HEASARC) archive providing sufficient time resolution to search for a possible timing signal of this pulsar.

Another *Fermi* LAT blind-search pulsar is PSR J1826-1256 ($\tau \simeq 14.4$ kyr; $L_{\rm sd} \simeq 3.6 \times 10^{36}$ erg/s; Abdo et al. 2009d), not to be confused with the nearby energetic pulsar PSR J1826-1334 (PSR B1823-13; $\tau \simeq 21$ kyr; $L_{\rm sd} \simeq 2.8 \times 10^{36}$ erg/s) about $38'$ away, which has not been detected (yet) as high-energy γ-ray pulsar contrary to its PWN (Grondin et al. 2011). PSR J1826-1256 coincides with the Northern extension of the extended TeV source HESS J1825-137 (Aharonian et al. 2006c). This TeV structure is positionally consistent with *CGRO* EGRET source (> 1 GeV) GeV J1825-1310 (also 3EG J1826-1302; see Roberts et al. 2001b). A plausible soft X-ray counterpart is *ASCA* GIS source AX J1826.1-1257 located within the error contours of GeV J1825-1310. The X-ray source region was later resolved by *Chandra* (obs.id. 3851; 15.2 ks; ACIS-I; Feb. 17, 2003) in a point-like component, positionally consistent with the pulsar, with a faint, $\sim 4'$ long trail of hard (> 2 keV) X-ray emission, resembling an "Eel" (Roberts et al. 2007). Using data from a much deeper more recent *Chandra* ACIS-I observation (obs.id. 7641; 74.8 ks; July 26, 2007) the spectral characteristics of the counterpart could be determined yielding a (very hard) photon index Γ of -0.79 ± 0.39 and an unabsorbed 0.3-10 keV flux of $(1.12 \pm 0.25) \times 10^{-13}$ erg/cm^{2}s absorbed through a Hydrogen column N_H of $(1.26^{+0.53}_{-0.46}) \times 10^{22}$ cm^{-2} (see Chapter 4, page 202–204 of Marelli 2012). In the X-ray archive we found a 92.9 ks *RXTE* observation (obs.id. 90069; Nov. 24–29, 2004) with PSR J1826-1256 $5'.7$ off-axis. A subsequent search for a possible timing signal in the 2–30 keV band yielded a negative result, not surprising given the source flux and its prediction for the PCA instrument requiring observation times in the range 450–650 ks for a 5σ detection. A decisive answer about the X-ray timing properties will be given soon from the data analysis of a 140 ks *XMM-Newton* observation performed on Oct. 11, 2014.

6.5 Young and energetic pulsars not detected by *Fermi* LAT: PSR J1301-6305, PSR J1341-6220, PSR J1614-5048, PSR J1803-2137 and PSR J1856+0245

Table 13 of Abdo et al. (2013) lists 28 pulsars not detected by the LAT with spin-down powers exceeding 10^{36} erg/s. Apart from PSR J1747-2809 (in G0.9+0.1) all top 12 pulsars listed in this table, those with the highest spin-down power, *are* detected as soft γ-ray pulsars (note: PSR B0540-69 has now been detected also as *Fermi* pulsar; Martin et al. 2014). Of the additional 15 pulsars we consider those pulsars which are young and/or associated with TeV counterparts the best candidates to detect as soft γ-ray pulsars.

In particular, PSR J1301-6305 ($\tau \simeq 11$ kyr; $L_{\rm sd} \simeq 1.7 \times 10^{36}$ erg/s), associated with HESS J1303-631 (Aharonian et al. 2005c; H.E.S.S. Collaboration et al. 2012b), and PSR J1341-6220 (PSR B1338-62; $\tau \simeq 12.1$ kyr; $L_{\rm sd} \simeq 1.4 \times 10^{36}$ erg/s), associated with SNR G308.7+0.0/G308.8-0.1 (Caswell et al. 1992; Kaspi et al. 1992) are good candidates to harbour a soft γ-ray pulsar. For the latter pulsar, a frequent glitcher, now also a weak X-ray counterpart is visible (this work) in archival XMM Newton data (obs.id. 0301740101; July 26, 2005, 37.8 ks).

Other interesting candidates are the 7.4 kyr old pulsar PSR J1614-5048 (PSR B1610-50; $L_{\rm sd} \simeq 1.6 \times 10^{36}$ erg/s) showing weak > 2 keV X-ray emission in *ASCA* GIS images (Kawai & Tamura 1996; Brinkmann et al. 1999), but doubted by Pivovaroff et al. (2000), and PSR J1803-2137 (PSR B1800-21; $\tau \simeq 15.8$ kyr; $L_{\rm sd} \simeq 2.2 \times 10^{36}$ erg/s) possibly associated with HESS J1804-216 (Kargaltsev et al. 2007b; Lin et al. 2013). For the latter pulsar Kargaltsev et al. (2007a) detected weak, but hard pulsar emission in a 30.2 ks *Chandra* ACIS observation.

Noteworthy is also the 81 ms pulsar PSR J1856+0245 ($\tau \simeq 21$ kyr; $L_{\rm sd} \simeq 4.6 \times 10^{36}$ erg/s) discovered in the Arecibo PALFA survey (Hessels et al. 2008) coincident with TeV source HESS J1857+026. At X-rays the pulsar was clearly detected in a 39 ks *Chandra* ACIS-I observation (obs.id. 12557; Feb. 28, 2011 Rousseau et al. 2012), but the low number of source counts prevented an accurate spectral characterisation of the pulsar at X-rays.

Table 2. Rotation powered (non-recycled) pulsars with (securely detected) pulsed emission in the hard X-ray band ($\gtrsim$ 20 keV).

name	period (ms)	age (kyr)	$^{10}\log(L_{\rm sd})$	S_{1400} (mJy)	pulse shape	photon index	*Fermi* LAT/Pulsed	TeV PWN/Pulsed
PSR J0205+6449 (3C58)	65.7	5.4	37.43	0.045^{1}	two sharp pulses	-1.1(1)	yes	yes
PSR J0534+2200/B0531+21 (Crab)	33.5	1.23	38.66	14	two pulses	curved	yes	yes/yes
PSR J0537-6910 (N157B in LMC)	16.1	4.9	38.69	$< 0.06^{2}$	single, sharp	-1.57(1)	no	yes
PSR J0540-6919/B0540-69 (N158A in LMC)	50.5	1.7	38.18	0.106^{3}	structured broad	curved	yes	...
PSR J0835-4510/B0833-45 (Vela)	89	11	36.84	1100	multiple sharp	-1.1	yes	yes/yes
PSR J1400-6325 IGR J14003-6326	31.2	12.7	37.71	0.242	single, broad	-1.95(4)	no	no
PSR J1513-5908/B1509-58 (MSH 15-52)	150	1.6	37.26	0.94	single broad	curved	yes	yes
PSR J1617-5055	69.0	8.0	37.20	0.5^{4}	single, broad	-1.42(2)	no	?
PSR J1640-4631 (G338.3-0.0)	206	3.4	36.64	$< 1.0^{5}$	single	-1.3	no	yes
PSR J1811-1925 (G11.2-0.3)	65.0	24.0	36.81	$< 0.07^{2}$	single, broad	-1.11(1)	no	no
PSR J1813-1246	48.1	43.0	36.80	$< 0.017^{6}$	two pulses	-0.85(3)	yes	...
PSR J1813-1749 (G12.82-0.02)	44.7	5.6	37.75	$< 0.01^{7}$	single, broad	-1.30(3)	no	yes
PSR J1838-0655 AX J1838.0-0655	70.5	23.0	36.75	< 2	structured broad	-1.12(1)	no	yes
PSR J1846-0258 (Kes 75)	324	0.72	36.91	$< 0.027^{8}$	single, broad	-1.20(1)	no	yes
PSR J1849-0001 IGR J18490-0000	38.5	42.8	36.99	$< 0.853^{9}$	single, broad	-1.37(1)	no	yes
PSR J1930+1852 (G54.1+0.3)	136	2.9	37.08	0.045^{1}	single, broad	-1.21(1)	no	yes
PSR J2022+3842 (G76.9+1.0)	48.6	8.9	37.47	0.067^{10}	two sharp pulses	-1.20(2)	no	no
PSR J2229+6114 (G106.6+2.9)	51.6	10.5	37.34	0.25	two pulses	-1.11(3)	yes	yes

Notes.
Column 1 gives source name(s) and associated SNR or PWN (between brackets), when applicable.
Column 3 gives the characteristic age ($\tau = -0.5\nu/\dot{\nu}$)
Column 4 the spin-down power ($L_{\rm sd} = 4\pi^2 I \nu\dot{\nu}$), in erg/s.
Column 5 gives the radio flux density (or upper limit) at 1400 MHz (S_{1400}; see Section 6), taken from the ATNF database except for the noted entries, where: (1) Camilo et al. (2002), (2) Crawford et al. (1998), (3) Manchester et al. (1993),(4) Kaspi et al. (1998), (5) Castelletti et al. (2011), (6) Ray et al. (2011b), (7) Halpern et al. (2012), (8) Archibald et al. (2008), (9) Pandey et al. (2006), (10) Arzoumanian et al. (2011).
Columns 6 and 7 give for the 2–150 keV band a description of the pulse shape and the energy spectrum (power-law photon index or curved spectrum).
Column 8 indicates whether the *Fermi* LAT detected a pulsed signal.
Finally, column 9 indicates whether a PWN and pulsed emission have been detected at TeV energies.

Data from an archival 55.3 ks *XMM-Newton* observation (obs. id. 0505920101; March 27, 2008) have been analysed in this work applying our Maximum Likelihood source fitting method per energy band to disentangle the source contributions from the pulsar and an unrelated source at an angular distance of about $20''$, rendering about 300 pulsar counts above 2 keV for further spectral analysis. Adopting an absorbed power-law model we obtained a very hard photon index Γ of -0.34 ± 0.08 absorbed through a Hydrogen column N_H of $(1.8^{+1.2}_{-0.7}) \times 10^{22}$ cm^{-2}, consistent with the Galactic value of (1.5–1.8)$\times 10^{22}$ cm^{-2}. The unabsorbed 2–10 keV flux was $(9.52^{+0.91}_{-0.80}) \times 10^{-14}$ erg/cm^{2}s, consistent with the value given in Rousseau et al. (2012). Our results are, however, somewhat different from those reported by Nice et al. (2013), who found a softer photon index and a somewhat lower unabsorbed 2–10 keV flux, mainly due to the higher absorbing Hydrogen column density N_H of $(4.9^{+3.2}_{-2.4}) \times 10^{22}$ cm^{-2} that they derived.

6.6 Another soft γ-ray pulsar candidate: IGR J11014-6103

A puzzling soft γ-ray pulsar candidate is *INTEGRAL* source IGR J11014-6103 (Bird et al. 2010), studied in detail by Pavan et al. (2011) using all available archival X-ray data of the region. These authors concluded that the source is probably a PWN surrounding an energetic pulsar given the morphology of the source composed of two distinct sources separated by $\sim 22''$ and a dimmer elongated structure (tail) of $\sim 4'$ size.

A subsequent *Chandra* observation shed light on the spatial structure of the emission components, and showed that the putative pulsar moves away from SNR MSH 11-61A, located $11'$away from IGR J11014-6103 (Pavan et al. 2014). The modulated main jet and counter jet structures are perpendicularly oriented with respect to the propagation direction away from the SNR. Spectral analysis yielded for the pulsar counterpart, adopting an absorbed power-law model, a hard photon index Γ of -1.1 ± 0.2 with a 2–10 keV flux of $(6.1 \pm 0.6) \times 10^{-13}$ erg/cm^{2}s.

The putative pulsar has been detected recently by Halpern et al. (2014), who found 62.8 ms pulsations in two different *XMM-Newton* observations performed on July 21, 2013 and June 8, 2014. From the timing characteristics they deduced a spin-down luminosity $L_{\rm sd}$ of $\simeq 1.36 \times 10^{36}$ erg/s and a characteristic age τ of 116 kyr, rather old for such a system. These values should be taken with some care, because it had been assumed that no glitch or glitches had occured between the two observations.

In this work we have also determined the pulsed spectrum of IGR J11014-6103 (analoguous to the method outlined for PSR J1813-1749 in Sect. 5.12), employing EPIC-pn data from the two *XMM-Newton* observations. We found for spectrum of the pulsed emission a photon index Γ of -1.13 ± 0.11 and an unabsorbed 2–10 keV flux of $(3.93 \pm 0.35) \times 10^{-13}$ erg/cm^{2}s, ab-

sorbed through an Hydrogen column N_H of $(0.95^{+0.38}_{-0.25}) \times 10^{22}$ cm^{-2}. The latter value is consistent with the column density derived by Pavan et al. (2014), who used *Chandra* ACIS-I data, for the total pulsar emission. From the pulsed and total (unabsorbed) 2–10 keV fluxes we derived a pulsed fraction of about 64%. This demonstrates that IGR J11014-6103 is an excellent candidate to show up as soft γ-ray pulsar in the future, given its spectral hardness and the already established soft γ-ray nature for its total source emission.

7 SUMMARY & DISCUSSION

In section 5 we presented in detail the multi-wavelengths characteristics of the currently 18 members of the soft γ-ray pulsar population, and provided for 14 of them new high-energy results from this work. For PSR B0531+21 (PSR J0534+2200), PSR B0540-69 (PSR J0540-6919), PSR J0205+6449 and PSR J1846-0258 we reviewed the current status at high energies referring to up-to-date literature.

For all of them the pulse profiles have been detected significantly above 20 keV and the spectral shapes of the pulsed-emission spectra have been determined (curved or power-law shapes). However, these pulsars are weak emitters in the hard X-ray window, with PSR J0534+2200 (the Crab pulsar) and PSR J1513-5908 being the exceptions. By exploiting the extensive *RXTE* and *INTEGRAL* archives for accumulating sufficient exposures on these pulsars at hard X-rays, we could achieve this major progress. Phase-coherent ephemerides were required to find the hard X-ray pulsed signals for all observations used. An extreme example is the case of PSR J0537-6910 for which we derived and used 30 ephemerides spread over 7.7 years to arrive at a $\sim 10\sigma$ detection of the pulse profile between 15 and 50 keV, in this case in *RXTE* HEXTE data. In several cases we also obtained new or statistically improved results at lower X-ray energies using archival *XMM-Newton* data.

An interesting example is PSR J0835-4510 (the Vela pulsar), for which we present in Fig. 4 pulse profiles from the radio to the high-energy γ-ray band. High statistics *INTEGRAL* ISGRI, *RXTE* PCA and *XMM-Newton* EPIC-pn data reveal a plethora of sharp pulses, which have counterparts at lower energies in the radio, optical and/or UV bands as well as at the high-energy γ-rays. One can identify five, possibly more sharp pulses, exhibiting very different variations in shape and intensity over the electromagnetic spectrum. This complexity has not yet been addressed in theoretical works, and it is beyond this paper to address this unique behaviour of the Vela pulsar.

A pulsar, for which we present an extensive study is PSR J1849-0001, discovered as *INTEGRAL* source IGR J18490-0000 and associated with the TeV source HESS J1849-000. The latter association suggested the pulsar to be located in a PWN. Using again archival *RXTE* PCA and *XMM-Newton* data, we derived a new high-statistics spectrum for the pulsed emission (2-10 keV) that can be well described with a power-law shape with index of -1.37 ± 0.01 and pulsed flux of $(4.21 \pm 0.08) \times 10^{-12}$ erg/cm^{2}s. The latter flux is a factor about four higher than reported by Gotthelf et al. (2011). This pulsed spectrum could be extended up to 60 keV by analysing *RXTE* HEXTE data. Using *INTEGRAL* ISGRI data, we obtained a new spectrum for the total emission in the energy band 20-300 keV with a softer spectral index of -1.82 ± 0.14. Taking the latter spectrum into account, the spectrum of the pulsed emission is better described with a curved spectral shape from 2 keV up to $\sim$ 300 keV (see Fig. 22). We applied for CXO observations (with the HRC-S for timing and the ACIS-S for spatially resolved spectral analysis) to resolve the contributions from the point source and the PWN. These HRC-S and the *RXTE* PCA observations both give a pulsed fraction of $\sim 80\%$, about three times the value published by Gotthelf et al. (2011). The ACIS-S observation reveals for energies 2-10 keV structured diffuse emission in a rectangular region ($75'' \times 37\farcs5$ box in Fig.21) around the point source with a photon spectral index of -1.13 ± 0.06, to be compared with an index of -1.75 ± 0.05 that we measured with XMM for a more extended region. This difference we explain as Synchrotron cooling towards the outskirts of the PWN.

7.1 Characteristics of the soft γ-ray pulsar population

In the following we will summarize and discuss the characteristics of the population of soft γ-ray pulsars in comparison with those of the sample of non-recycled pulsars in the *Fermi* LAT second pulsar catalogue. Table 2 summarizes the main characteristics of the 18 soft γ-ray pulsars. They are all fast rotators with spin-periods ($P = 1/\nu$) between 16.1 ms and 324 ms, most of them (14) even spinning well below 100 ms (see column 2 of Table 2). The characteristic ages ($\tau = -0.5\nu/\dot{\nu}$) of this pulsar sample range from 1.23 kyr (PSR B0531+21) up to 43 kyr (PSR J1813-1246), thus representing a very young population, well below 50 kyr. Moreover, the population is very energetic with spin-down powers ($L_{\rm sd} = 4\pi^2 I \nu \dot{\nu}$; I is the moment of inertia of the neutron star assumed to be 10^{45} g cm^2) above 4.4×10^{36} erg/s (the lowest value measured for PSR J1640-4631).

The radio flux densities (or upper limits) at 1400 MHz (S_{1400}) are shown in column 5 of Table 2, taken from the ATNF Pulsar Catalog, except for the noted entries. When there are no published values at 1400 MHz, we extrapolated to S_{1400} from measurements/upper limits at other frequencies, assuming $S_\nu \propto \nu^\alpha$ with $\alpha = -1.7$ or using a published α value for a particular pulsar. For 8 members no radio pulsations have yet been detected, however, two (PSR J1640-4631 and PSR J1849-0001) have upper limits at 1400 MHz as high as $\sim$ 1 mJy. Abdo et al. (2013) defined for the *Fermi* LAT catalogue a pulsar as "radio-loud" if $S_{1400} > 30\mu Jy$, and "radio-quiet" if the measured radio flux density is lower. In their sample of 77 young non-recycled pulsars 41 (53%) are radio-loud, and the fraction of radio-loud pulsars increases with increasing $L_{\rm sd}$ (consistent with 100% for $L_{\rm sd} > 10^{37}$ erg/s). Adopting that definition, in Table 2 there are three radio-quiet pulsars PSR J1813-1246, PSR J1813-1749 and PSR J1846-0258 with upper limits below $30\mu Jy$. There are also three weak radio-loud pulsars listed with flux densities $30\mu Jy < S_{1400} < 100\mu Jy$ and two with upper limits in that range. Only the Vela and Crab pulsars have flux densities above 1 mJy (11%). The sample of LAT radio-loud non-recycled pulsars has only three entries below $100\mu Jy$ and 18 (44%) above 1 mJy (see Fig. 3 of Abdo et al. (2013)). This indicates that the radio-loud soft γ-ray pulsars appear to be on average weaker radio pulsars than their LAT counterparts. However, the fraction of radio-loud pulsars of the energetic ($L_{\rm sd} > 4.4 \times 10^{36}$ erg/s) soft γ-ray sample is similar to that fraction of the LAT pulsars, namely in the range 56 % to 83%, depending on how many of the so far not detected pulsars are radio-quiet, and seems to agree with the trent reported above for the *Fermi* LAT pulsars.

Another noteworthy finding is that only 7 of the 18 members of the soft γ-ray pulsar population are detected as γ-ray pulsars in the hard γ-ray band above 100 MeV (see column 8, with as latest addition the Fermi detection of PSR J0540-6919, the twin

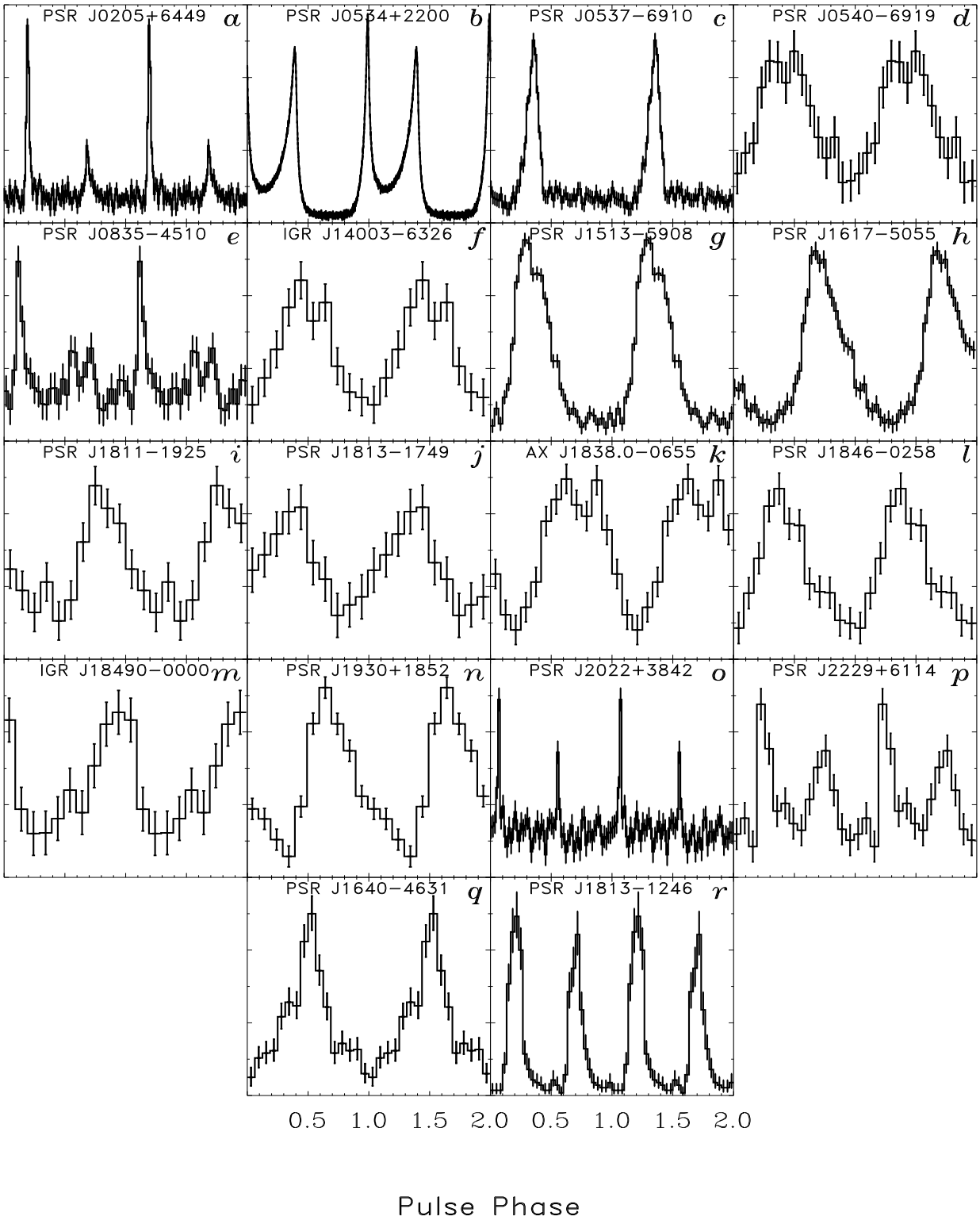

Figure 27. The pulse shapes of the soft γ-ray pulsar population members: *a)* PSR J0205+6449, PCA 8.2–27.8 keV, *b)* PSR J0534+2200/B0531+21, ISGRI 20–300 keV, *c)* PSR J0537-6910, PCA $\gtrsim$ 10 keV, *d)* PSR J0540-6919/B0540-69, HEXTE 12–48 keV, *e)* PSR J0835-4510/B0833-45, ISGRI 20–300 keV, *f)* IGR J14003-6326, PCA 7.6–32.2 keV, *g)* PSR J1513-5908/B1509-58, ISGRI 20–300 keV, *h)* PSR J1617-5055, PCA 8.2–32.0 keV, *i)* PSR J1811-1925, ISGRI 15–135 keV, *j)* PSR J1813-1749, PCA 8.1–27.5 keV, *k)* AX J1838.0-0655, ISGRI 20–150 keV, *l)* PSR J1846-0258, ISGRI 20–150 keV, *m)* IGR J18490-0000/PSR J1849-0001, HEXTE 14–150 keV, *n)* PSR J1930+1852, PCA 8.2–32.1 keV, *o)* PSR J2022+3842, PCA 11.2–27.3 keV, *p)* PSR J2229+6114, PCA 9.4–22.4 keV, and the recently reported hard X-ray pulsars *q)* PSR J1640-4631, *NuSTAR* 3–25 keV, *r)* PSR J1813-1246, XMM EPIC-pn 8–12 keV (significantly smeared due to the rather coarse time resolution of ~ 5.7 ms given its period of 48.1 ms; see also Fig. 12).

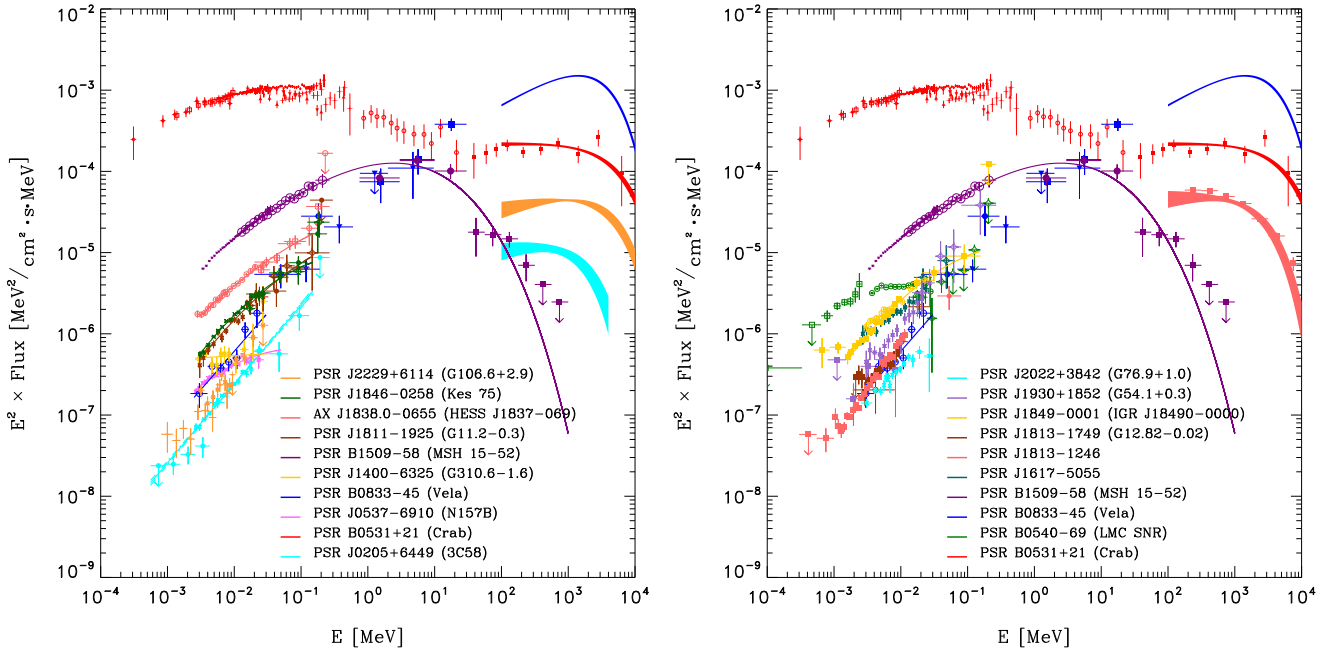

Figure 28. The high-energy *pulsed* emission spectra for 17 of the 18 soft γ-ray pulsar population members from 0.1 keV – 10 GeV spread across two panels. The spectra of PSR B0531+21 (Crab), PSR B0833-45 (Vela) and PSR B1509-58 are shown in both panels for reference purposes. The names of the soft γ-ray pulsar members, ordered according to their right ascension increasing from bottom to top, are indicated in the plots along with color coding. Symbols/data points are for flux measurements and solid lines (filled regions for the Fermi passband) for the model fits. The pulsed spectrum of PSR J1640-4631 is not shown in either of the panels, because only its total spectrum has been reported on.

of the Crab pulsar in the LMC; Martin et al. 2014). Furthermore, Abdo et al. (2013) list in their Table 13 28 rotation-powered pulsars which are not (yet) detected by *Fermi* despite of their high spin-down powers (above 10^{36} erg/s). Of the top 12 in that table, those with the highest spin-down power, 11 are listed in Table 2 of this paper. Interestingly, those most energetic pulsars missed by the LAT, are reported by us to be soft γ-ray pulsars.

In the last column of Table 2 one can see that at least 12 members do have, often bright, TeV counterparts, associated with the TeV emission from their PWNe. For three of these pulsars (PSR J1813-1749 , PSR J1838-0655 and PSR J1849-0001) we present in this paper the total (PWN+pulsar) source spectra as measured with the imaging instrument *INTEGRAL* ISGRI from 20 keV up to $\sim$ 150 keV, together with the pulsed-emission spectra. The difference between these two spectra gives an estimate of the PWN spectrum at hard X-rays. This PWN spectrum is shown for PSR J1838-0655 in Fig.18 for energies between 3 and $\sim$ 60 keV, and suggests a break/bend around 50 keV. For PSR J1617-5055 and PSR J1811-1925 the latter located in SNR G11.2-0.3, we also present the pulsed and total-emission spectra, but these pulsars are not detected at TeV energies, so far. In only two cases, PSR J0534+2200 (Crab) and PSR J0835-4510 (Vela), pulsed TeV emission has been detected.

The variation in morphology of the pulse profiles (described in column 6 of Table 2) in the hard X-ray band can be seen in Fig. 27. This figure shows that the large majority (11 members) has broad/structured single pulses, and one (PSR J0537-6910) has a sharper single pulse, making the fraction with single pulses 67%. These are all, except the canonical soft γ-ray pulsar PSR J1513-5908 and PSR J0540-6919, *not* detected at high-energy γ-rays ($>$ 100 MeV) by *Fermi* LAT. The remaining 6 (33%) have double or even multiple (PSR J0835-4510; Vela pulsar) pulses, of which 5 *are* detected at high-energy γ-rays (except so far PSR J2022+3842). It is interesting to note that of the 77 non-recycled pulsars in the second *Fermi* pulsar catalogue 58 (or 75%) show two strong, caustic peaks significantly separated, thus a very much larger fraction than for the soft γ-sample. In fact, 91% (10/11) of the soft γ-ray pulsars which are *not* detected by *Fermi* LAT show a single, mostly broad/structured pulse.

Finally, column 7 of Table 2 gives information about the spectral shape at hard X-rays. All members, except PSR J0534+2200, PSR J0540-6919 and PSR J1400-6325, show very hard spectra in the soft γ-ray band with photon indices in the range -0.85 – -1.57. Fig. 28 shows in two panels the spectral energy distributions over the high-energy band from $\sim$ 2 keV up to 10 GeV of the pulsed emissions of the soft γ-ray pulsars. The preliminary *Fermi* spectrum of PSR J0540-6919 (Martin et al. 2014) is not included, but the pulsed spectrum over the total 1 keV - 10 GeV band mimics the shape of that of PSR J0534+2200. Also PSR J1640-4631 is not included, because spectral information on the pulsed emission has not yet been reported for energies above 10 keV. For reference, the high-energy pulsed spectra of PSR J0534+2200, PSR J0835-4510 and PSR J1513-5908 are shown in both panels. PSR J0835-4510 exhibits a pulsed spectrum that is 'typical' for the *Fermi* LAT-detected pulsars with maximal luminosity at GeV energies. PSR J1513-5908 has also been (weakly) detected by *Fermi* above 100 MeV, but reaches its maximum luminosity at MeV energies. It is clear from this figure that the pulsed emission spectra of the soft γ-ray pulsar population, given the hardness of the spectra at hard X-rays/soft γ-rays and the non-detections above 100 MeV (11 members) or the detections as soft *Fermi* LAT pulsars (5 members), also reach maximum luminosities in the MeV range. This is thus remarkably different from the typical spectral characteristics of the *Fermi* LAT-detected pulsars. Note, that PSR J0835-4510 has been

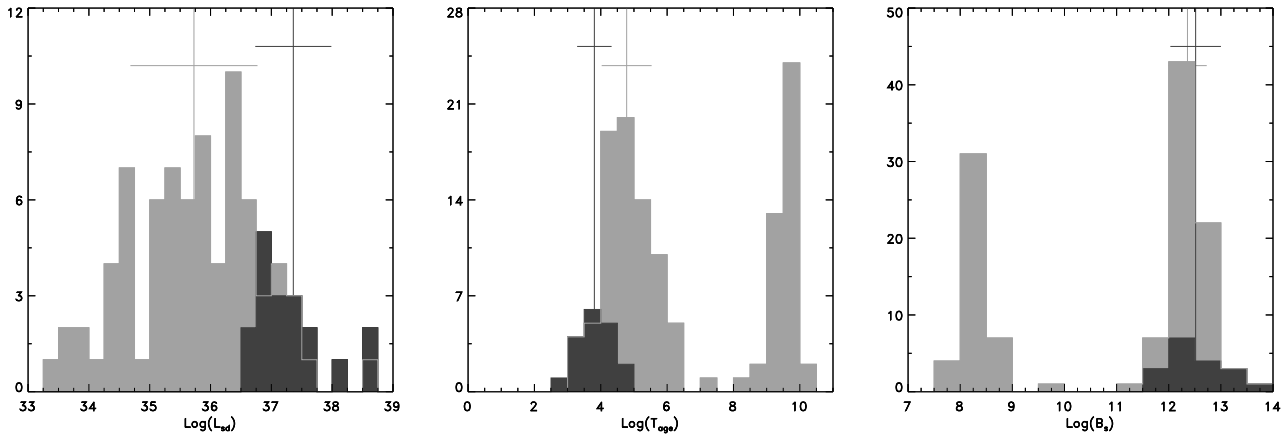

Figure 29. The distributions of the soft γ-ray (dark grey; 18 members) and hard γ-ray (light grey, *Fermi* LAT) pulsar populations as a function of spin-down luminosity (left panel; including only non-recycled *Fermi* LAT pulsars; 77 members), characteristic age (middle panel) and surface (dipole) magnetic field strength (right panel). The means (vertical) and standard deviations (horizontal) for both populations are indicated by the solid lines. The recycled pulsar subset (43 members) of the *Fermi* LAT population has been ignored in the estimation of these numbers. The soft γ-ray pulsar population is on average ~ 50 times more luminous (left panel) and ~ 10 times younger than the *Fermi* LAT pulsar population, while the B_S distributions are comparable.

detected in the soft γ-ray band, only, because its distance is ~ 290 pc.

We also compared the distributions of the spin-down power, characteristic age and surface magnetic field strength at the pole ($B_{\rm s} \simeq 3.2 \times 10^{19} \sqrt{-\dot{\nu}/\nu^3}$ G) of the soft- and hard γ-ray pulsar populations. The results are shown in the three panels of Fig. 29 for spin-down power (left), characteristic age (middle) and surface magnetic field strength (right). The averages (vertical lines) and standard deviations (horizontal lines) of the $^{10}\log$ of the spin-down powers for the *Fermi* LAT non-recycled (77 members; light grey histogram left panel Fig. 29) and soft γ-ray (18 members; dark grey histogram left panel Fig. 29) pulsar population are 35.73 ± 1.04 and 37.36 ± 0.63, respectively. Thus the latter is on average $\sim 43\times$ more energetic than the *Fermi* LAT population. The averages and standard deviations of the $^{10}\log$ of the characteristic ages are 4.78 ± 0.75 and 3.81 ± 0.52 for the non-recycled *Fermi* LAT pulsar- and soft γ-ray pulsar population, respectively. This indicates that the soft γ-ray pulsar population is on average $\sim 9.3\times$ younger than the non-recycled *Fermi* LAT pulsar population. Finally, the right panel of Fig. 29 shows that the distributions of the surface magnetic field strengths are comparable with averages $^{10}\log B_{\rm s}$ of 12.36 ± 0.37 and 12.52 ± 0.49 for the non-recycled *Fermi* LAT pulsar- and soft γ-ray pulsar population, respectively.

7.2 Too many young luminous γ-ray pulsars?

The advent of the *Fermi* launch and the milestone later achieved with the release of the second *Fermi* pulsar catalogue triggered studies of the collective properties of the pulsar population for comparisons with predictions from competing γ-ray pulsar models, constraining the birth properties, beaming and evolution (Gonthier et al. 2007; Watters & Romani 2011; Takata et al. 2011; Pierbattista et al. 2012). One of the conclusions from these studies is that (one-pole) outer-gap type models and slot-gap type models can reproduce many of the average radio and high-energy γ-ray characteristics. However, significant differences in properties between the simulated and the observed *Fermi* LAT populations are also noted. The sample of soft γ-ray pulsars is too small for a similar study, and the peculiar characteristics of the young and energetic pulsars *not* detected at soft γ-ray energies does not make it a fully coherent picture. Nevertheless, it is interesting to shortly address how this sample fits in the general picture emerging from the theoretical studies of the *Fermi* population of young non-recycled pulsars.

In Table 2, we are dealing with very young energetic pulsars, which are mostly *not* detected by *Fermi* LAT because they reach their maximum luminosities in the MeV band and become too weak for detection above 100 MeV. All high-energy emission models propose contributions to the non-thermal pulsar spectrum of synchrotron radiation produced deeper in the magnetosphere, reaching its maximum luminosity at MeV energies, and of higher-energy curvature radiation and inverse Compton radiation produced higher-up in the magnetosphere, closer to the light cylinder. Apparently, the contribution from synchrotron emission is in our sample dominating in the shape of the measured average spectrum over the components produced closer to the light cylinder. These curvature and inverse Compton components appear to be too weak for detection by *Fermi* LAT. Some of these pulsars will likely be detected by *Fermi* after the accumulated exposures have been sufficiently increased over the coming years (a first example is the recently reported detection of PSR B0540-69). This is particularly interesting because Pierbattista et al. (2012) conclude that their simulations for all models (Polar Cap, Slot Gap, Outer Gap and One Pole Caustic) under predict the detected number of LAT pulsars with high $L_{\rm sd}$. Our sample of soft γ-ray pulsars increases even further the number of pulsars with the highest $L_{\rm sd}$ that emit non-thermal gamma-ray radiation, thus increases the found discrepancy.

In section 6 we discussed a sample of young luminous pulsars which are not yet detected in the soft γ-ray band, but are excellent candidates for detection in dedicated observations with X-ray instruments with large sensitive areas and operating in modes with sufficient time resolution. *NuSTAR* (in the 3–80 keV band) and *XMM-Newton* (2–12 keV band) are currently the only observatories, which can provide the required capabilities. An increase of the size of the detected soft γ-ray pulsar population and, in particular, a more detailed measurement of the timing and spectral characteristics of individual pulsars and the sample in the soft γ-band up to MeV energies will give important constraints for the above mentioned comparisons between the different models aiming at explaining the production of high-energy radiation in the pulsar mag-

netospheres. It is therefore unfortunate that no future space missions are currently planned to bridge the observational gap between 100 keV and 100 MeV.

ACKNOWLEDGMENTS

This research has made extensive use of data and/or software provided by the High Energy Astrophysics Science Archive Research Center (HEASARC), which is a service of the Astrophysics Science Division at NASA/GSFC and the High Energy Astrophysics Division of the Smithsonian Astrophysical Observatory. We also acknowledge the use of NASA's Astrophysics Data System (ADS) and of the SIMBAD database, operated at CDS, Strasbourg, France. In this work we analysed observations performed with *INTEGRAL*, an ESA project with instruments and science data centre funded by ESA member states (especially the PI countries: Denmark, France, Germany, Italy, Switzerland, Spain) and with the participation of Russia and the USA, and we also analysed observations obtained with *XMM-Newton*, an ESA science mission with instruments and contributions directly funded by ESA Member States and the USA (NASA). Moreover, this research has made use of data obtained from the *Chandra* Data Archive.

REFERENCES

Abdo A. A., et al., 2009a, ApJ 699, L102
Abdo A. A., et al., 2009b, ApJ 706, 1331
Abdo A. A., et al., 2009c, ApJ 696, 1084
Abdo A. A., et al., 2009d, Sci 325, 840
Abdo A. A., et al., 2010a, ApJS 187, 460
Abdo A. A., et al., 2010b, ApJ 714, 927
Abdo A. A., et al., 2010c, ApJ 708, 1254
Abdo A. A., et al., 2010d, ApJ 713, 154
Abdo A. A., et al., 2011, Sci 331, 739
Abdo A. A., et al., 2013, ApJS 208, 17
Abramowski A., et al., 2014, ApJ 794, L1
Acciari V. A., et al., 2009, ApJ 703, L6
Acciari V. A., et al., 2010, ApJ 719, L69
Aharonian F., et al., 2005, Sci 307, 1938
Aharonian F., et al., 2005b, A&A 435, L17
Aharonian F., et al., 2005c, A&A 439, 1013
Aharonian F., et al., 2006, ApJ 636, 777
Aharonian F., et al., 2006, A&A 456, 245
Aharonian F., et al., 2006, A&A 460, 365
Aharonian F., et al., 2007, A&A 472, 489
Aleksić E., et al., 2011, ApJ 742, 43
Aleksić E., et al., 2014, A&A submitted, (arXiv:1405.6074v1)
Aleksić E., et al., 2014, A&A 565, L12
Aliu E., et al., 2008, Sci 322, 1221
Aliu E., et al., 2011, Sci 334, 69
Anada T. et al., 2009, PASJ 61, S183
Aoki T., Dotani T. and Mitsuda K., 1992, IAUC Circ. 5588
Archibald A. M., et al., 2008, ApJ 688, 550
Arzoumanian, Z. et al ., 2011, ApJ 739, 39
Arumugasamy, P., Pavlov G.G. & Kargaltsev, O., 2014, ApJ 790, 103
Arumugasamy, P., et al., 2014b, Conference "Physics of Neutron Stars - 2014", St. Petersburg, Russia, July 28 - August 1, 2014
Bai X-N & Spitkovsky A., 2010a, ApJ 715, 1270
Bai X-N & Spitkovsky A., 2010b, ApJ 715, 1282
Becker W., Aschenbach B., 2002, in Proc. 270, WE-Heraeus Seminar on Neutron Stars, Pulsars and Supernova Remnants, ed. W. Becker, H. Lesch & J. Trümper, MPE Report 278, 63
Bird A. J., et al., 2007, ApJS 170, 175
Bird A. J., et al., 2010, ApJS 186, 1
Bennett K., et al., 1977, A&A 61, 279
Brinkmann W., et al., 1999, A&A 346, 599
Brogan C.L., et al., 2005, ApJ 629, L105
Buccheri R., et al., 1983, A&A 128, 245
Camilo F., et al., 2002, ApJ 574, L71
Campana R., et al., 2008, MNRAS 389, 691
Caraveo P., et al., 2001, ApJ 561, 930
Castelletti G., et al., 2011, A&A 536, 98
Caswell J.L., et al., 1992, ApJ 399, L151
Chang C., et al., 2012, ApJ 744, 81
Chaves R.C.G., et al., 2008, in AIP Conf. Proc. 1085, Proc. 4th International Meeting on High Energy Gamma-ray Astronomy, eds. F.A. Aharonian, W. Hoffmann, & F. Rieger, 219
Chaves R.C.G., et al., 2009, in Proc. of the 31st International Cosmic Ray Conference, Łódź, Poland, 2009, 1 (arXiv:0907.0768v1)
Cheng K.S., Ho C., Ruderman M., 1986, ApJ 300, 500
Cheng K.S., Ruderman, M., Zhang L., 2000, ApJ 537, 964
Crawford F., et al., 1998, in Proc. of the Elba Workshop: Neutron Stars and Supernova Remnants, Mem. Soc. Astron. Italiana, 69, 951
Cusumano G., et al., 1998a, IAU Circ. 6814
Cusumano G., et al., 1998b, A&A 333, L55
Cusumano G., et al., 2003, A&A 402, 647
D'Amico N., et al., 2001, ApJ 552, L45
Dean A. J., et al., 2008, MNRAS 384, 29
Deeter J.E., et al., 1999, ApJ 512, 300
den Hartog P.R., et al., 2014, ApJ in prep.
de Luca A., et al., 2000, A&A 354, 1011
de Plaa J., Kuiper L., Hermsen W., 2003, A&A 400, 1013
De Rosa A., et al., 2009, MNRAS 393,527
Djannati-Ataï A., et al., 2008, in Proc. of the 30th International Cosmic Ray Conference 2007, Mérida, México, Vol. 2 (OG part 1), 823
Dodson R., et al., 2003, ApJ 596, 1137
Durant M., et al., 2013, ApJ 763, 72
Dyks J. & Rudak, B., 2003, ApJ 598, 1201
Falanga, M., Kuiper, L., Poutanen, J., et al. 2005, A&A, 444, 15
Falanga, M., Kuiper, L., Poutanen, J., et al. 2011, A&A, 529, 68
Fierro J.M., et al., 1998, ApJ 494, 734
Finley J.P., et al., 1993, ApJ 410, 323
Fiocchi M., et al., 2010, ApJ 720, 987
Fishman G.J., et al., 1993, A&AS 97, 17
Funk S., et al., 2007, A&A 470, 249
Funk S., et al., 2007b, ApJ 662, 517
Gaensler B.M., et al., 2002, ApJ 569, 878
Garmire G.P., et al., 2003, SPIE Proc. 4851, 28
Gavriil F.P., et al., 2008, Science 319, 1802
Gonzalez M.E., et al., 2005, ApJ 630, 489
Gonthier P.L., et al., 2007, Ap&SS 309, 245
Gotthelf E.V., et al., 2000, ApJ 542, L37
Gotthelf E.V. & Wang Q.D., 2000, ApJ 532, L117
Gotthelf E.V., et al., 2008, ATEL #1392
Gotthelf E.V. & Halpern, J.P., 2009, ApJ 700, L158
Gotthelf E.V., et al., 2011, ApJ 729, L16
Gotthelf E.V., et al., 2014, ApJ 788, 155
Gouiffes C., 1998, Proc. Neutron Stars and Pulsars: 30 years af-

ter the discovery, Eds. N. Shibazaki,N. Kawai, S. Shibata and T. Kifune, P. 363, Universal Academic Press
Grebenev S.A., et al., 2013, MNRAS 428, 50
Grenier I.A., et al., 1988, A&A 204, 117
Grondin M.-H., et al., 2011, ApJ 738, 42
Halpern, J.P., et al., 2001a, ApJ 547, 323
Halpern, J.P., et al., 2001b, ApJ 552, L125
Halpern, J.P., et al., 2002, Neutron Stars in Supernova Remnants, ASP Conference Series, 271, 199
Halpern, J.P., et al., 2012, ApJ 753, L14
Halpern, J.P., et al., 2014, ApJ 795, L27
Harding A. K., et al., 2002, ApJ 576, 376
Harding A. K., Usov V.V., Muslimov A.G., 2005, ApJ 622, 531
Harding A. K., et al., 2007, Ap&SS 309, 221
Harnden Jr. F.R., et al., 1972, ApJ 172, L91
Harnden F.R., et al., 1985, ApJ 299, 828
Helfand, D., et al., 2001, ApJ 556, 380
Helfand, D., et al., 2003, ApJ 582, 783
Helfand, D., et al., 2007, ApJ 665, 1297
Hermsen, W., Bloemen, H., Kuiper, L., et al., 1993, in AIP Conf. Proc. 280, *Compton Gamma-Ray Observatory*, eds. M. Friedlander, N. Gehrels, & D.J. Macomb (New York: AIP), 204
Hermsen, W., Kuiper, L., et al., 1994, ApJS 92, 559
Hermsen, W., Hessels, J.W.T., Kuiper, L., et al., 2013, Sci 339, 436
Hertz P., et al., 1995, ApJ 445, 351
H.E.S.S. Collaboration, et al., 2011, A&A 525, 46
H.E.S.S. Collaboration, et al., 2012, A&A 545, L2
H.E.S.S. Collaboration, et al., 2012b, A&A 548, 46
H.E.S.S. Collaboration, et al., 2014, MNRAS 439, 2828
Hessels J.W.T., et al., 2004, ApJ 612, 389
Hessels J.W.T., et al., 2008, ApJ 682, L41
Hirayama M., et al., 2002, MNRAS 333, 603
Hirotani K., 2015, ApJ 798, L40
Hoffmann A.I.D., et al., 2007, Ap&SS 309, 215
Hughes J.P., et al., 2003, ApJ 591, L139
Humensky B., et al., 2009, in Proc. of the 31st International Cosmic Ray Conference, Łódź, Poland, 2009, 1 (arXiv:0907.5020v1)
Jahoda, K., Swank, J.H., Giles, A.B., et al. 1996, Proc. SPIE, 2808, 59
Johnston S., et al., 2001, ApJ 549, L101
Kaaret P., et al., 2001, ApJ 546, 1159
Kalapotharakos C., et al., 2012a, ApJ 749, 2
Kalapotharakos C., et al., 2012b, ApJL 754, 1
Kanbach G., et al., 1980, A&A 90, 163
Kanbach G., et al., 1994, A&A 289, 855
Kargaltsev O. & Pavlov G.G., 2007, Ap&SS 308, 287
Kargaltsev O. et al., 2007a, ApJ 660, 1413
Kargaltsev O. et al., 2007b, ApJ 670, 643
Kargaltsev O., Pavlov G.G., Wong J.A, 2009, ApJ 690, 891
Kargaltsev O., et al., 2012, ApJ 745, 99
Kargaltsev O., et al., 2012b, ApJS 201, 37
Kaspi V.M., et al., 1992, ApJ 399, L155
Kaspi V.M., et al., 1998, ApJ 503, L161
Kaspi V.M., et al., 2001, ApJ 560, 371
Kawai N., Okayasu R., Brinkmann W., et al., 1991, ApJ 383, L65
Kawai N. & Tamura K., et al., 1996, ASP Conference Series 105, 367
Keek S., Kuiper L. and Hermsen W., 2006, ATEL #810
Keith M.J, et al., 2011, MNRAS 416, 346
Kishishita T., et al., 2012, ApJ 750, 162
Knight F.K., et al., 1982, ApJ 260, 553
Komin N., et al., 2012, ICRC 2011, Beijing (arXiv:1201.0639v1)
Krivonos R., et al., 2012, A&A 545, 27
Kothes R., et al., 2006, ApJ 638, 225
Krishnamohan S. & Downs G.S., 1983, ApJ 265, 372
Kuiper L., et al., 1998, in Proc. of the NATO Study Institute on "The many faces of Neutron Stars", NATO ASI Series 515, 195, eds. R. Buccheri, J. van Paradijs & M.A. Alpar
Kuiper L., et al., 1999, A&A 351, 119
Kuiper L., et al., 2001, A&A 378, 918
Kuiper L., et al., 2002, ApJ 577, 917
Kuiper L., et al., 2003, A&A 411, L31
Kuiper L. & Hermsen W., 2003a, Conference proceedings 4th *AGILE* Science Workshop "X-ray and Gamma-ray Astrophysics of Galactic Sources", Roma - June 11-13 2003, (arXiv:0312204v1)
Kuiper L., et al., 2004, AdSpR 33, 507
Kuiper L., et al., 2008, ATEL #1405
Kuiper L. & Hermsen W., 2009, A&A 501, 1031
Kuiper L., et al., 2010, A&A 515, 34
Kuiper L. & Hermsen W., 2010a, ATEL #2446
Kumar H.S. & Safi-Harb, S., 2008, ApJ 678, L43
Lande J., et al., 2012, ApJ 756, 5
Landecker T.L., et al., 1993, A&A 276, 522
Landi R., et al., 2007, MNRAS 380, 926
Large M.I., Vaughan A.E. & Mills B.Y., 1968, Nat 220, 340
Lasker B.M., 1976, ApJ 203, 193
Lebrun, F., Leray, J. P., Lavocat, P., et al. 2003, A&A, 411, L141
Lemiere A., et al., 2009, ApJ 706, 1269
Lemoine-Goumard M., et al., 2014, ApJ submitted (arXiv:1409.4994v1)
Li J., et al., 2012, ApJ 746, 60
Lin D., et al., 2013, ApJ 776, 29
Lin L.C.C., et al., 2013, ApJ 770, L9
Lin L.C.C., et al., 2014, ApJ submitted (arXiv:1408.4741v1)
Livingstone M., et al., 2005, ApJ 633, 1095
Livingstone M., et al., 2006, ApJ 647, 1286
Livingstone M., et al., 2009, ApJ 706, 1163
Lu F., et al., 2001, A&A 370, 570
Lu F., et al., 2002, ApJ 568, L49
Lu F., et al., 2007, ApJ 663, 315
Lund, N., Budtz-Jørgensen, C., Westergaard, N.J., et al. 2003, A&A, 411, L231
Malizia A., et al., 2005, ApJ 630, L157
Manchester R.N., et al., 1980, MNRAS 190, 9
Manchester R.N., et al., 1982, ApJ 262, L31
Manchester R.N., et al., 1993, ApJ 560, 742
Manzali A., et al., 2007, ApJ 669, 570
Marelli M., et al., 2011, ApJ 733, 82
Marelli M., 2012, PHD thesis (arXiv:1205.1748v1)
Marelli M., et al., 2014, ApJ 790, 51
Marelli M., et al., 2014b, ApJ 795, 168
Marshall F. E., et al., 1998a, IAU Circ. 6810
Marshall F. E., et al., 1998b, ApJ 499, L179
Marshall F. E., et al., 2004, ApJ 603, 682
Marthi V.R., et al., 2011, MNRAS 416, 2560
Martin P., et al., 2014, Fifth International *Fermi* symposium, 20–24 October 2014, Nagoya University - Nagoya, Japan
Matsumoto H., et al., 2007, PASJ 59, 199
Matz S.M., Ulmer M.P., Grabelsky D.A., et al. 1994, ApJ 434, 288
McBride V.A., et al., 2008, A&A 477, 249
Middleditch J. & Pennypacker C., 1985, Nat 313, 659

Middleditch J., et al., 2006, ApJ 652, 1531
Mignani R., et al., 2007, A&A 473, 891
Mineo T., et al., 1999, A&A 348, 519
Molkov A., et al., 2004, Astron. Lett., 30, 534
Murray S.S., et al., 2000, SPIE Proc. 4012, 68
Murray S.S., et al., 2002, ApJ 568, 226
Muslimov A.G. & Harding A.K., 2004, ApJ 606, 1143
Nagase F., et al., 1990, ApJ 351, L13
Nakamori T., et al., 2008, ApJ 677, 297
Nasuti F. P., et al., 1997, A&A 323, 839
Ng C.-Y. and Romani R.W., 2004, ApJ 601, 479
Ng C.-Y., et al., 2005, ApJ 627, 904
Nice D.J., et al., 2013, ApJ 772, 50
Nolan P.L. et al., 2012, ApJS 199, 31
Nynka M., et al., 2014, ApJ submitted, (arXiv:1405.3239v1)
Ögelman H., et al., 1983, Nat. 361, 136
Ögelman H. & Zimmermann H.-U., 1989, A&A 214, 179
Ohashi T., et al., 1996, PASJ 48, 157
Pancrazi B., et al., 2012, A&A 544, A108
Pandey M., et al., 2006, A&A 453, 83
Parent D., et al., 2011, ApJ 743, 170
Pavan L., et al., 2011, A&A 533, A74
Pavan L., et al., 2014, A&A 562, A122
Pavlov G.G., et al., 2001a, ApJ 552, L129
Pavlov G.G., et al., 2001b, ApJ 554, L189
Pavlov G.G., et al., 2003, ApJ 591, 1157
Pellizzoni A., et al., 2009, ApJ 695, L115
Pétri J., 2012a, MNRAS 424, 2023
Pétri J., 2012b, MNRAS 424, 605
Pierbattista, M., et al., 2012, A&A 545, A42
Pilia M., et al., 2010, ApJ 723, 707
Pivovaroff M.J., et al., 2000, ApJ 528, 436
Pletsch H.J., et al., 2012, ApJ 755, L20
Ray P. S., et al., 2011a, Astrophysics and Space Science Proc., 37
Ray P. S., et al., 2011b, ApJS 194, 17
Ratti E., et al., 2010, MNRAS 408, 1866
Renaud M., et al., 2010, ApJ 716, 663
Ridley J.P., et al., 2013, MNRAS 433, 138
Roberts M., et al., 1999, ApJ 515, 712
Roberts M., et al., 2001, ApJ 561, L187
Roberts M., et al., 2001b, ApJS, 451
Roberts M., et al., 2003, ApJ 588, 992
Roberts M., et al., 2004, AIP Conf. Proc., Vol. 714, 306
Roberts M., et al., 2007, Proceedings of the 363 WE-Heraeus Seminar on Neutron Stars and Pulsars 40 years after the discovery. Edited by W. Becker and H. H. Huang. MPE-Report 291, 2007, p.24
Rodriguez J., et al., 2008, A&A 482, 731
Romani R.W., 1996, ApJ 470, 469
Romani R. W. & Yadigaroglu I.-A., 1995, ApJ 438, 314
Romani R., et al., 2005, ApJ 627, 383
Romani R.W. & Watters K.P., 2010, ApJ 714, 810
Rothschild, R.E., Blanco, P.R., Gruber, D.E., et al. 1998, ApJ, 496, 538
Rousseau R., et al., 2012, A&A 544, A3
Sacco B., 1990, ApJ 349, L21
Saz Parkinson P.M., 2010, ApJ 725, 571
Schönfelder V., et al., 1993, ApJS 86, 657
Segreto A., et al., 2010, 8^{th} *INTEGRAL* workshop "The restless Gamma-ray Universe", September 27-30 2010, Dublin Castle, Dublin, Ireland
Serafimovich N.I., et al., 2004, A&A 425, 1041
Seward F.D & Harnden Jr., F.R., 1982, ApJ 256, L45
Seward F.D., 1984, ApJ 287, L19
Seward F.D., 1989, AJ 97, 481
Seward F.D., 2000, ApJ 536, 948
Shibanov Yu. A., 2003, A&A 406, 645
Slane P., 2010, ApJ 720, 266
Staelin D.H. & Reifenstein E. C., 1968, Sci 162, 1481
Stegmann C. & H.E.S.S. collaboration, 2014, "Astroparticle Physics 2014" A joint TeVPA/iDM conference, June 2014, Amsterdam
Strickman M.S., et al., 1996, ApJ 460, 735
Strickman M.S., et al., 1999, ApJ 524, 373
Strüder L., et al., 2001, A&A 365, L18
Sugizaki M., et al., 2001, ApJS 134, 77
Swanepoel J.W.H., et al., 1996, ApJ 467, 261
Takata, J., et al., 2011, ApJ 726, 44
Tavani M., et al., 2011, Sci 331, 736
Temim T., et al., 2010, ApJ 710, 309
Terrier R., et al., 2008, in Aharonian F. A., Hofmann W., Rieger F., eds, AIP Conf. Ser. Vol. 1085, High Energy Gamma-Ray Astronomy. Am. Inst. Phys., New York, p. 312
Thompson D.J., et al., 1975, ApJ 200, L79
Thompson D.J., et al., 1977, ApJ 214, L17
Tomsick J.A., et al., 2009, ApJ 701, 811
Torii K., et al., 1997, ApJ 489, L145
Torii K., et al., 1998, ApJ 494, L207
Torii K., et al., 1999, ApJ 523, L69
Torii K., et al., 2000, ApJ 534, L71
Townsley L.K., et al., 2006, AJ 131, 2164
Tümer O.T., et al., 1984, Nat. 310, 214
Ubertini, P., Lebrun, F., Di Cocco, G., et al. 2003, A&A, 411, L131
Ubertini P., et al., 2005, ApJ 629, L109
Ulmer M.P., Matz S.M., Wilson R.B., et al., 1993, ApJ 417, 738
Van Etten A. & Romani R.W., 2010, ApJ 711, 1168
Vasisht G., et al., 1996, ApJ 456, 59
Vedrenne, G., Roques, J.-P. , Schönfelder, V., et al. 2003, A&A, 411, L63
Wallace P.T., et al., 1977, Nat. 266, 692
Wang D.Q. & Gotthelf E.V., 1998, ApJ 509, L109
Wang D.Q., et al., 2001, ApJ 559, 275
Wang R. & Hirotani K., 2011, ApJ 736, 127
Ward J.E., et al., 2010, 8^{th} *INTEGRAL* workshop "The restless Gamma-ray Universe", September 27-30 2010, Dublin Castle, Dublin, Ireland
Watters K.P., et al., 2009, ApJ 695, 1289
Watters, K.P. & Romani, R.W., 2011, ApJ 727, 123
Weisskopf M.C., et al., 2000, SPIE Proc. 4012, 2
Weltevrede P., et al., 2010, ApJ 708, 1426
Wendker H.J., et al., 1991, A&A 241, 551
Wilson R.B., Finger M.H., Pendleton G.N., et al., 1993a, p. 257, in "Isolated Pulsars", Taos, New Mexico, Eds. Van Riper K.A. and Ho C., Cambridge Univ. Press
Wilson R.B., Fishman G.J., Finger M.H., et al., 1993b, AIP Conf. Proc. 280, p. 291, Eds. Friedlander M., Gehrels N. and Macomb D.
Wilson-Hodge C.A., et al., 2011, ApJ 727, L40
Winkler, C., Courvoisier, T. J.-L., Di Cocco, G., et al. 2003, A&A, 411, L1
Yu M., et al., 2013, MNRAS 429, 688
Zyuzin D., et al., 2013, ApJ 775, 101

This paper has been typeset from a TEX/ LATEX file prepared by the author.